University of Alberta

T cell-mediated inflammation is stereotyped:
mouse delayed-type hypersensitivity reaction and mouse T cell-mediated rejection of renal allografts share common molecular mechanisms

by

Jeffery M. Venner

A thesis submitted to the Faculty of Graduate Studies and Research
in partial fulfillment of the requirements for the degree of

Master of Science

in

Experimental Medicine

Department of Medicine

Fall 2011
Edmonton, Alberta

Dedicated to those who have inspired me:

My family and friends, my teachers and mentors.

You laid the foundation – my success is guaranteed

ABSTRACT

Genome-wide gene expression analysis of diseases has revealed large-scale changes in the expression of thousands of genes (transcripts) representing biological processes. The processes that occur during T cell-mediated rejection (TCMR) of renal allografts in mice and humans have been previously delineated, and they appear to be independent of cytotoxic mechanisms; thus, TCMR is analogous to delayed-type hypersensitivity (DTH). Since TCMR and DTH involve similar mechanisms, we hypothesized the molecular changes in TCMR are stereotyped; thus, they are qualitatively the same as those in DTH. Using microarrays to compare the transcript expression changes of both diseases in mice, we found they share the same processes: T cell and macrophage infiltration, IFNG-effects, alternative macrophage activation, and a coordinated injury-repair response of the tissue parenchyma. Additional analysis revealed IFNG is vital for stabilizing the injury-repair response in TCMR and DTH. We conclude the molecular changes in TCMR and DTH involve stereotyped, coordinated processes.

TABLE OF CONTENTS

LIST OF TABLES

CHAPTER 2: MATERIALS AND METHODS **PAGE**

CHAPTER 3: COMPARISON OF THE MOLECULAR CHANGES IN MOUSE CONTACT HYPERSENSITIVITY AND T CELL MEDIATED REJECTION IN MOUSE RENAL ALLOGRAFTS

LIST OF FIGURES

CHAPTER 3: COMPARISON OF THE MOLECULAR CHANGES IN MOUSE CONTACT HYPERSENSITIVITY AND T CELL MEDIATED REJECTION IN MOUSE RENAL ALLOGRAFTS **PAGE**

LIST OF ABBREVIATIONS

ABMR..... antibody-mediated rejection

AMA..... alternative macrophage activation

AMATs..... alternative macrophage activation-associated transcripts

CD ..... cluster of differentiation

CHS..... contact hypersensitivity

CMA ..... classical macrophage activation

DTH..... delayed-type hypersensitivity

ESRD ..... end-stage renal disease

ETC ..... effector T cell

GKO ..... interferon-gamma deficient mouse (*Ifng*$^{-/-}$)

GO..... gene ontology

GRITs..... interferon-gamma- and rejection-induced transcripts

GRKO..... interferon-gamma receptor 1 deficient mouse (*Ifngr1*$^{-/-}$)

GSTs ..... gamma-interferon-suppressed transcripts

IFNG..... interferon-gamma

IRITs..... injury- and repair-induced transcripts (kidney- or skin-selective, *injury-up*)

KTs..... kidney-associated transcripts (kidney-selective, *injury-down*)

MHC ..... major histocompatibility complex

mRNA..... messenger ribonucleic acid

PBT ..... pathogenesis-based transcript set

PMN ..... polymorphonuclear cell

QCAT ..... quantitative cytotoxic T cell-associated transcripts

QCMAT ..... quantitative constitutive macrophage-associated transcripts

STs..... skin-associated transcripts (skin-selective, *injury-down*)

TCMR..... T cell-mediated rejection

CHAPTER 1

INTRODUCTION

1.1 BACKGROUND

Tissue injury and antigenic insult induces a large-scale, coordinated cascade of changes; ultimately leading to a state of inflammation and injury-repair processes. The cardinal signs of inflammation, described as stereotyped gross pathological changes, were first recorded by Celsus in ancient Rome as; *calor* (heat), *dolor* (pain), *tumor* (swelling), and *rubor* (redness) (1). Later, *functio laesa* (loss of function) was added by Virchow, or debatably, Galen (2). Since these descriptions, efforts have largely been focussed on picking apart the individual genetic and molecular differences between various inflammatory diseases or disease states. With the advent of genome-wide gene expression microarrays, it has been revealed that transcript expression changes behave in concerted, stereotyped 'herd-movements' that correspond to major biological processes (3-5). This has changed our interpretation of diseases and disease processes: instead of describing tissue abnormalities through the expression of single molecules such as messenger RNA (mRNA) transcripts, the tip of the iceberg; microarrays are able to reveal concerted changes in transcript expression involving hundreds of transcripts related to specific biological processes. Our laboratory has been particularly interested in studying the genome-wide molecular changes that occur during organ transplant rejection, with kidney transplant rejection as the focus of our past studies (recently reviewed in (6,7)).

To simplify by excluding other conditions such as de novo diseases or recurrent primary disease, transplanted organs can fall to one of, or combination of two diseases; T cell-mediated rejection (TCMR) and antibody-mediated rejection (ABMR). Using microarray expression data we have annotated changes in transcript expression in

mouse and human renal allograft rejection that correspond with biological processes, such as T cell and macrophage infiltration, as pathogenesis-based transcript sets (PBTs) (6-8). Our PBTs demonstrate that hundreds of transcripts experience expression changes in TCMR and ABMR as a highly stereotyped, concerted pattern. These changes are not disease specific qualitatively, but rather differentiation of TCMR and ABMR can be demonstrated quantitatively: TCMR, as T cell- and macrophage-associated transcripts (9); ABMR, as NK- and endothelial-associated transcripts (10,11); with strong interferon-gamma (IFNG)-effects (12), and an active injury-repair response (13,14) in both TCMR and ABMR.

Mouse models of kidney transplantation have revealed that mice largely develop TCMR and do not manifest ABMR (15). Rejection of kidney transplants in nonimmunosuppressed mice across full major histocompatibility complex (MHC) and minor disparities is T cell-dependent, and involves the development of histological lesions seen in TCMR of kidney transplants in humans (described below) (15). Therefore, mouse models of transplantation have permitted us to explore TCMR, independent of ABMR mechanisms. Indeed, through various knockout mouse models our laboratory found that TCMR is independent of cytotoxic mechanisms (16), which has led to the theory that TCMR mechanisms are analogous to a delayed-type hypersensitivity (DTH) reaction involving the contact-dependent communications of T cells and macrophages. Applying our understanding of transcript expression changes as herd-movements, we hypothesize the molecular changes that occur during a mouse model of DTH would resemble those changes seen in TCMR of mouse renal allografts.

1.2 TRANSPLANTION AND ALLOGRAFT REJECTION OVERVIEW

1.2.1 Transplantation in the real world. For patients with end-stage renal disease (ESRD), kidney transplantation offers an improved quality-of-life and reduced risk of

cardiovascular disease and mortality compared to long-term dialysis. In 2009 there were 1,222 kidney transplants in Canada; however, by the end of 2009 there were approximately 3,200 still on the waitlist. The waitlist is exponentially larger in the United States, where upwards of 90,000 patients are waiting for a kidney transplant (17). As demand for donor kidneys outstrips supply, in addition to increasing the donor pool, it is important that steps are taken to ensure long-term graft survival in transplant recipients.

Transplantation can either be xenogeneic, allogeneic, or syngeneic. In xenotransplantation, grafts are transplanted between species, and thus, they offer a route towards increasing the donor pool. However, xenotransplantation is currently impractical due to species-specific growth factor receptors, immunological disparities, and a fear of zoonosis (18,19). Allogeneic and syngeneic transplantation is between individuals of the same species; the former between genetically non-identical individuals, and the latter involving genetically identical individuals (such as monozygotic twins). The first successful human organ transplant was a kidney transplant performed between monozygotic twins in 1954 by Joseph Murray. Thus there was no immunological (alloimmune) barrier to overcome. Nonetheless, identical twins are scarce; leaving allogeneic transplantation as the only viable option. The synergistic development of efficacious immunosuppressive regimens along with an improved immunological knowledge base has made allogeneic transplantation a realistic therapy for ESRD.

1.2.2 Non-specific graft injury. Surgical-mediated disruptions from nephrectomy and anastomosis, and ischemia/reperfusion cause non-specific injury to grafts. Necrosis and ischemia/reperfusion injury results in the release of endogenous damage-associated molecular patterns which bind to various, putative pattern-recognition receptors largely found on resident epithelial cells, polymorphonuclear (PMN) leukocytes, or myeloid cells (macrophages and dendritic cells) (20). One, example includes the release of DNA as a result of loss of cell and membrane integrity during necrosis; free endogenous DNA sections are able to bind to Toll-like receptor (TLR)-9. Subsequent intracellular signalling

from TLRs leads to the translocation of transcription factors, such as nuclear factor (NF)-κB and interferon-regulatory factor (IRF) proteins, into the nucleus where transcription of cytokines and chemokines begins (21). In particular, expression of IFNG can lead to increased antigen processing, subsequent MHC surface expression and lymphocyte chemotaxis (22,23). While these processes evoke a non-specific, alloimmune-independent inflammatory response, they foster the development of adaptive immune responses by inducing the expression of MHC, co-stimulatory molecules, and the diapedesis-supporting selectins and integrins on the host parenchyma and microvascular endothelium (22,24); and thus, conceivably promote an alloimmune response against the allograft. However, this is counterintuitive to the observation that a kidney allograft recipient who 5 years post-transplant (who would have recovered from any surgical and ischemia/reperfusion injury), can begin to reject the graft at any time, particularly if they discontinue the immunosuppressive drugs.

1.2.3 Generating the alloimmune response. Activation of naïve cognate T cells occurs within secondary lymphoid organs. The T cell receptor (TCR) recognises donor antigen on the surface of dendritic cells and triggers “signal 1” through the CD3 complex. CD80 or CD86 on the surface of dendritic cells then ligate with CD28 on T cells, providing “signal 2.” Together, these two signals activate three signal transduction pathways within T cells (25): the calcium-calcineurin pathway, the RAS-mitogen-activated protein (MAP) kinase pathway, and the NF-κB pathway. Consequently, the transcription of numerous molecules is initiated, including interleukin (*Il*)-2, *Cd*154 and *Cd*25. IL-2 provides “signal 3,” activating the mammalian target of rapamycin (mTOR) pathway, and subsequent T cell proliferation and differentiation. This activation process also involves the increased expression of chemokine receptors, such as CXCR3 and CXCR6, so activated effector T cells (ETCs) can home to local sites of inflammation. Alternatively, naïve T cells can differentiate to become central and effector memory T cells, identified by the respective presence or absence of surface L-selectin and CCR7 (26).

Through CXCR3 and CXCR6, ETCs home to sites of inflammation releasing the chemokine ligands, CXCL9/10/11 and CCL16 for the above receptors, respectively. Interestingly, without killing the activated donor endothelium, ETCs then migrate across the microvascular endothelium. ETCs express P-selectin glycoprotein ligand 1 (PSGL-1) which binds to E- or P-selectin on the endothelium, and they also express the integrins VLA-4 that binds VCAM-1, and LFA-1 that binds ICAM-1 and -2 (24). Characteristic of TCMR, entry of ETCs and other mononuclear cells (largely macrophages) into the interstitial space presents itself histologically as interstitial inflammation (8). Over time, or by days 7-14 post-transplant in mouse renal allografts, ETCs then enter the tubular epithelium, termed tubulitis (8). Marked interstitial inflammation with tubulitis are associated with a clinical loss in renal function; indicated by rising serum creatinine or decreasing glomerular filtration rate (GFR) (27). Interstitial inflammation and tubulitis are prototypical histological lesions for diagnosing TCMR (8); and in mouse renal allografts, interstitial inflammation develops at approximately day 5 post-transplant, with mild tubulitis at day 7 and becoming severe by day 21 post-transplant (28).

1.2.4 Potential effector mechanisms of TCMR. Although tubulitis is the principal histological diagnostic lesion for TCMR, the cellular mechanisms required for tubulitis and associated allograft deterioration are not completely understood. In mouse renal allografts, tubulitis is T cell-dependent; it is absent in nude (*nu*/*nu*, athymic) mice which lack T cells, but develops in hosts lacking B cells and antibody (*Igh-6* deficient) (15). As well, because nude mice failed to develop TCMR lesions, this rules out a potential role of NK cells. Nonetheless, both CD4 and CD8 ETCs express a plethora of cytotoxic mediators (29), including; granzymes (*Gzma*/*b*), perforin (*Prf1*), Fas (*Fas*) and Fas-ligand (*Fasl*). Expression of *Gzma*/*b* and *Prf1* has been detected in mouse and human renal allografts with TCMR (30,31), and FAS and FASL mediated cytotoxicity has been demonstrated *in vitro* (32). Additionally, because integrin CD103 (*Itgae*) is commonly found on intestinal intraepithelial lymphocytes, and is also expressed within renal

allografts; it has also been considered a mediator for T cell entry into the tubular epithelium (33,34), possibly leading to epithelial injury.

Perforin, which is structurally related to the complement C9 protein is released with granzymes from secretory granules on NK cells and ETCs into the leukocyte-target cell synapse. Perforin forms a pore on target cells which allows for the passage of granzymes into the target cells (35). Granzymes are serine proteases that once inside the target cell cytosol, they activate caspases and BID; ultimately leading to the release of cytochrome C from the mitochondria, DNA fragmentation and apoptosis (36). Ligation of FASL (CD95) on ETCs and NK cells to FAS on target cells induces recruitment of FADD proteins to the cytosolic FAS death domains, which in turn leads to caspase activation and cytochrome C release within the target cell (37). Interestingly, neither of these molecules, host *Perf* and/or *Gzma*/*b*, and/or donor *Fas* are required for the development of tubulitis or allograft deterioration, in mouse renal allografts (16,28,38).

CD103 (*Itgae*) which forms a heterodimer with ITGB7, and binds to E-cadherin, is highly expressed on intestinal intraepithelial T cells and $CD8^+$ T cells within rejecting human renal allografts (33,34). The ITGAE/B7 dimers on T cells ligate to E-cadherin between epithelial cells; however the exact function of this interaction is yet to be determined, as entry and retention of intestinal intraepithelial T cells in mucosal tissues is not dependent of *Cd103* (39). Likewise, *Cd103* is not required for tubulitis and renal allograft dysfunction (16).

Unlike B cells and NK cells, the myeloid cells are present in all human and mouse TCMR of renal allografts (9), and their presence is quantitatively associated with poor allograft function (9). However, determining a functional significance for these cells has been difficult, as there are no robust depletion mechanisms for macrophage or dendritic cells. Nonetheless, one study demonstrated that interstitial infiltration and tubulitis were significantly attenuated in a rat model of renal allograft rejection, after a 70% monocyte and macrophage depletion via liposomal-clodronate treatment (40). Therefore, the lack for a direct necessity of cytotoxic mechanisms in the development of

TCMR has led to the proposal that the dominant effector function in TCMR involves interactions between alloantigen-specific T cells and antigen presenting cells (macrophages and dendritic cells); thus TCMR is analogous to the mechanism of DTH.

1.2.5 IFNG prevents cytotoxic mechanisms in TCMR. While the need for IFNG within renal allografts may appear counterintuitive due to its pro-inflammatory effects, namely MHC class I induction (22,23); various mouse models of renal allograft rejection would suggest IFNG is more of a necessity rather than a burden. In mouse renal allografts where the graft is unable to receive IFNG, for example, *Ifng* deficient (GKO) hosts with wild type allografts or wild type hosts with *Ifngr1* deficient (GRKO) allografts; these grafts develop severe necrosis and microvasculature congestion by day 5 to 7 post-transplant (41). A similar phenotype is seen in *Tap* or *B2m* deficient allografts (which are unable to express MHC class I on the cell surface) in wild type hosts; furthermore the necrotic phenotype is dependent on host perforin and granzymes A and B (41). Interestingly, alternative macrophage activation and injury-repair processes are highly induced in the above deficient allografts. AMA and the injury-repair response are discussed in more detail below.

It has yet to be shown, but one explanation for the above observations entails: IFNG induced MHC class I surface expression on the donor allograft microvascular endothelium. T cells then receive an inhibitory signal from binding class I products on the endothelium; perceivably this is carried out via class Ib products binding the inhibitory heterodimer NKG2A/CD94. In separate experiments, it has been shown that programmed death ligand-1 (PDL-1) and CD80-dependent interactions may also play a key role in allograft stabilization and subsequent prevention of necrosis (42). Consequently, these interactions may allow microvascular sparing and subsequent T cell diapedesis into the interstitium (41). When IFNG is unable to induce MHC class I expression or other co-inhibitory molecules, or the graft is deficient in these molecules, the utilization of cytotoxic mechanisms on T cells is not prevented.

1.2.6 Antibody-mediated rejection (ABMR). ABMR is not a focus of this thesis; therefore it will not be discussed in detail. In brief, ABMR is histologically characterized by microcirculation inflammation (glomerulitis and peritubular capillaritis), and variable vasculitis (7). Immunologically, ABMR is mediated through donor specific antibodies (DSA) that ligate to donor human leukocyte antigens (HLA) on the graft endothelial vasculature and microcirculation (43). Subsequent ligation is associated with complement cascade activation, and it is associated with positive C4d staining (a split product of the C4 component) (44). In brief, complement components C3a and C5a can act as neutrophil, monocyte, and macrophage chemotactins; as well, they can bind to receptors on endothelial cells, inducing endothelial activation (43). Endothelial activation promotes thrombus formation and diapedesis of leukocytes. Additionally, components C5b through C9 form the membrane attack complex which can cause lyses of targeted cells (45). A form of C4d negative ABMR has also been reported (43); in these cases it has been proposed that complement is not a likely agent of injury, but rather antibody-dependent cell-mediated cytotoxicity is the putative effector mechanism. Cells that express Fc receptors, such as monocytes and NK cells are capable of binding to antibody-coated target cells and releasing the cytotoxic granules, perforin and granzymes (43).

1.3 REVEALING THE HERD-MOVEMENT IN TCMR OF RENAL ALLOGRAFTS

To better understand the biology of rejecting renal allografts in humans and mouse models our laboratory has studied the changes in expression of thousands of mRNA transcripts (6). What we found is a stereotyped pattern that exists across all diseases, such as TCMR, ABMR or ischemia/reperfusion injury; thus, there is no single molecule specific for rejection. Nonetheless, we can demonstrate disease specificity

through the quantitative assessment of stereotyped biological processes annotated through our PBTs (6).

Presented below is a brief description of the PBTs relevant to this thesis, how they were derived, the biological processes they asses, and how they have built upon our understanding of disease processes. In brief, members of each PBT were chosen on the basis of microarray assessed expression within (or absent from); healthy nephrectomised kidneys, various cell cultures, transplant animal models using select knock outs, and/or other cell types based on literature searches. Depending on the species, the transcripts are translated from human to mouse, or vice versa. (For detailed instructions on their exact derivation, please see the indicated references.)

1.3.1 Quantitative cytotoxic T cell-associated transcripts (QCATs) (31). Referred to as cytotoxic T cell-associated transcripts from herein; the transcript members of this PBT were: one, had a higher signal intensity in cultured human primary $CD8^+$ T cells than nephrectomy, B cells, and macrophages; two, had a low signal intensity (<200) in nephrectomy, B cells, macrophages, and IFNG-treated macrophages; and three, had a high signal intensity (>1000) when the $CD8^+$ T cell mRNA was spiked with nephrectomy mRNA, and correlated ≥0.98 (Pearson correlation coefficient) between the signal intensity and dilution ratio.

The cytotoxic T cell-associated transcripts are expressed in mouse renal allografts by day 1 post-transplant (6); therefore, a T cell burden is established before tubulitis lesions appear on day 7 post-transplant or later. Because most of the cytotoxic T cell-associated transcripts are not $CD8^+$ T cell specific, such as *Gzmb* or *Klrd1 (Cd94*), they can represent a plethora of cytotoxic-cell phenotypes homing to the allograft, including ETCs, memory T cells and NK cells. Furthermore, as discussed above, the presence of certain transcripts, such as *Prf1* or *Gzma*/*b*, does not necessitate the utilization of select mechanisms. Regardless, the cytotoxic T cell associated transcript set can robustly quantify TCMR of human and mouse renal allografts (31).

1.3.2 Quantitative constitutive macrophage-associated transcripts (QCMATs) (9). Referred to as macrophage-associated transcripts from herein; this transcript set was selected in a similar manner to that of the cytotoxic T cell-associated transcripts. Probesets had to have: one, a higher signal intensity in human primary macrophages than nephrectomy, $CD4^+$ and $CD8^+$ T cells, B cells, and NK cells; two, a low signal intensity (<200) in the same excluding cells; and three, a high signal intensity (>1000) of spiked macrophage mRNA with nephrectomy mRNA, with a ≥0.98 Pearson correlation coefficient between the raw signal and dilution ratio.

Expression of the macrophage-associated transcripts is strongly associated with TCMR of human and mouse renal allografts (9). Moreover, increased expression of the macrophage-associated transcript, *Cd68*, corresponds with CD68 protein expression within rejecting renal allografts (46). Thus, an indication that macrophages are involved in the process of TCMR.

1.3.3 IFNG- and rejection-induced transcripts (GRITs) (47). Herein referred to as IFNG-induced transcripts or IFNG-effects; probeset members of this PBT had to: one, increase signal intensity in native kidneys within mice treated with recombinant-IFNG intravenously ("IFNG-induced"); two, increase in mouse renal allorgrafts day 5 post-transplant compared to normal kidneys ("rejection-induced"); and three, be rejection-induced and have a decreased signal intensity (compared to normal kidneys) in wild type renal allografts within *Ifng* knock out hosts on day 5 post-transplant.

Some of the IFNG-induced transcripts included *B2m*, *Cd74* (class II invariant chain), *Tapbp* (tapasin), *Cxcl9* and various transcripts that code for H2 or HLA molecules (depending on the species being analysed). Therefore, IFNG-effects largely reflect antigen processing, antigen presentation, and chemotaxis.

1.3.4 Alternative macrophage activation-associated transcripts (AMATs) (48). Referred to AMA-associated transcripts from herein; this PBT represents the macrophage phenotype of AMA. Analogously to the Th1/Th2 paradigm, macrophages can be skewed to a classical macrophage activation (CMA) phenotype or an AMA phenotype. The division of CMA and AMA has become cloudy, as features of AMA can be found on dendritic cells, or features of both CMA and AMA can co-exist in various inflammatory compartments (46,49,50). In brief, cytokines such as IL-1, TNF and IFNG can induce a CMA phenotype, which characteristically leads to the production of TNF, IL-6 and nitric oxide. These molecules have been associated with DTH reactions, and they can activate the endothelium to express MHC and adhesion molecules to promote diapedesis (50). Not mutually exclusive from CMA, AMA is induced via IL-4/13 and potentially activin A (46,50). Alternatively activated macrophages express the C-type lectin mannose receptor, MRC1 (CD206); and furthermore, IL-4/13 can inhibit IFNG-induced nitric oxide production by utilizing arginase (*Arg1*) which promotes L-ornithine formation from L-arginine; this is a step used in collagen production for extracellular matrix repair (50).

In addition to *Mrc1* and *Arg1*, the AMA-associated transcripts also include *Thbs1* (thrombospondin) and the chitinase-like molecule *Chi3l3*. Together, the IFNG-induced transcripts and the AMA-associated transcripts are the two PBTs that can most robustly quantify TCMR in human renal allografts. Thus, AMA is a feature of TCMR, despite the strong IFNG-effects.

1.3.5 Injury-repair response (injury-up): injury- and repair-induced transcripts (IRITs) (13). The IRITs were defined in mouse renal isografts; that is, they represent the increased expression of transcripts involved in reversible injury (“injury-up”), in the parenchyma, stroma and endothelium. More specifically, IRITs represent a number of preprogrammed processes, including; collagen and extracellular matrix remodelling,

promotion of secondary inflammation, and the expression of embryonic genes signifying dedifferentiation.

1.3.6 Injury-repair response (injury-down): kidney-associated transcripts (KTs) (14). The counter-arm to the IRITs (injury-up), are the KTs (injury-down). This PBT was defined by probesets that had: a signal intensity (>50) in normal mouse kidneys, but also had a signal intensity that was 5x higher that the signal intensity in mixed lymphocyte reactions, $CD8^+$ T cells, B cells, thioglycolate-induced macrophages and fibroblasts and had no overlapping members with the IRITs.

These transcripts represented the functional aspect of the kidney parenchyma, which is largely transporter activity and basic metabolic activities. During a disease state (for example, ischemia/reperfusion or TCMR), KTs will decrease expression; this represents a programmed loss of function (14). Histologically, loss of function can be demonstrated by reduced Ksp-cadherin and E-cadherin staining on tubular epithelium during TCMR (16).

1.3.7 Gamma-interferon-suppressed transcripts (GSTs) (48). Also referred to as IFNG-suppressed transcripts or effects; this PBT represented those transcripts putatively suppressed by IFNG-effects. The IFNG-suppressed transcript set was derived from our GKO and GRKO renal allograft experiments described above. In brief, probesets were increased in GRKO allografts into wild type hosts and in wild type allografts into GKO hosts, at both days 5 and 7 post-transplant, compared to wild type allograft controls.

As mentioned above, renal allografts unable to receive IFNG undergo sever necrosis, hence many of the IFNG-suppressed transcripts share overlapping membership with the IRITs. Interestingly, IFNG-suppressed transcripts also have members associated with AMA. What is even more perplexing, is that AMA still develops in GRKO allografts in *Prf1* or *Gzma*/*b* deficient hosts (non-necrotic grafts) and in *B2m* or *Tap* deficient allografts

in wild type hosts (necrotic grafts) (41). In other words, the necrosis phenotype or deficient IFNG-signaling is not required for AMA.

1.4 DELAYED-TYPE HYPERSENSITIVITY (DTH)

DTH, also known by the Coombs and Gell classification as type IV hypersensitivity, received these labels due to its relative "delayed" immunological cellular-dependent response to specific antigen; as supposed types I, II and III which are "immediate" humoral (antibody)-dependent immunological responses. DTH is a T cell-mediated inflammatory reaction and is typically modelled in the skin; because it appears to involve a similar pathology of clinical allergic contact dermatitis, such as the reaction to urushiol from poison ivy. Similar to TCMR of renal allografts, DTH is T cell-dependent and B cell-independent as DTH reactions are unable to be elicited in SCID mice reconstituted with B cells or antibody depleted T cells (51-54). There are three subtypes of DTH; all of which involve two phases; a sensitization phase, followed by an elicitation or challenge phase.

1.4.1 DTH subtypes. Three types or models of DTH are differentiated based on the type of antigen, or antigen source: one, classical DTH (the tuberculin reaction); two, protein-adjuvant reactions; and three, contact hypersensitivity (CHS). Classical DTH was first described by Robert Koch in 1882, who discovered the tubercule bacillus when he attempted to use the killed tuberculin as a vaccine (55). The protein-adjuvant reaction involves the administration of a protein that is not normally immunogenic, such as ovalbumin, along with an immunogenic protein (the adjuvant). Subsequently, the individual becomes sensitized to the "nonimmunogenic" protein. In CHS, chemical haptens are applied to the surface of the skin where they are absorbed into the tissue and subsequently covalently bind to carrier self-proteins (56). The target carrier proteins

are typically cell surface proteins, or even intracellular proteins which bind to the hapten after it is diffuses through the cell membrane (56). Examples of haptens include trinitrochlorobenzene, oxazolone, or urushiol from poison ivy. The end result is that the modified self-proteins are treated as any foreign antigen; thus they are capable of inducing a T cell-mediated response. Despite reports on minor difference in the ratio of infiltrating PMNs (basophils versus neutrophils), in the three subtypes (57); there is no conclusive report that the types of antigens used induce disparate ratios of $CD4^+$ or $CD8^+$ T cell infiltrates (57,58). It is likely that both $CD4^+$ and $CD8^+$ T cells have some effector mechanisms.

1.4.2 Mechanism of DTH. Sensitization involves the cutaneous or subcutaneous exposure to antigen. Antigen can be quickly carried by the afferent lymphatic vessels to secondary lymphoid organs, where dendritic cells then take up the antigen (59). Alternatively, antigen at the site of exposure can be processed by local Langerhans ($CD207^+$, $EPCAM^+$, $CD11b/c^+$) or dendritic cells ($CD207^{+/-}$, $EPCAM^-$, $CD11b/c^+$). These antigen presenting cells undergo maturation, marked by the increased surface expression of MHC class I and II and CCR7, and migration to secondary lymphoid organs follows (60). As described above, antigen is presented to naïve T cells, and subsequent proliferation and differentiation would occur.

The mechanisms of the elicitation phase of DTH are poorly understood. Upon antigenic-challenge it is likely that Langerhans cells do not act as a local antigen presenting effector cell with cognate ETCs or effector memory T cells; as Langerhans leave the skin and home to lymphoid organs when they encounter antigen (61). Instead, resident dendritic epidermal cells ($CD11b^+$ and $CD206^+$) and/or macrophages ($CD68^+$ and $CD206^+$) may be involved in the elicitation phase (62). Resident dermal T cells of gamma-delta TCR lineage may be involved in DTH reactions, but their involvement may be more mediative through their involvement in dermal wound repair by releasing keratinocyte growth factor-1, or enhancing the immunosurveillance of local cells by

secreting IFNG (63). In a mouse model of psoriasis using skin xenografts, it has been shown that alpha-beta memory T cells ($CD45RO^+$) will home to the epidermis by translocating across the collagen IV rich epithelial basement membrane in a VLA-1 (ITGA1B1)-dependent fashion (64). Despite the shortcomings in our understanding of DTH mechanisms, it is known that within DTH reactions and TCMR of renal allografts, IFNG and tumor necrosis factor (TNF) are capable of activating macrophages, which are a prominent component of TCMR and DTH (65,66). Activated macrophages could then putatively trigger a parenchymal and stromal injury-repair response, including parenchymal dedifferentiation and the promotion of secondary inflammation (6). Additional studies are needed on the mechanisms of DTH, including ones that test the employment of cytotoxic mechanisms (*Prf1* and *Gzmalb*). Indeed, one study showed PRF1 and GZMB expression were associated with allergic contact dermatitis lesions in humans (67), however; we know from our renal allograft studies that despite transcript expression (16), these mechanisms are not necessary for allograft rejection.

1.5 PROJECT SYNOPSIS AND JUSTIFICATION

Renal allograft rejection in mice mirrors the histological and molecular changes seen in TCMR of human renal allografts; thus, mouse renal allograft rejection serves as an excellent experimental model for which the mechanisms of TCMR can be studied. The large-scale, coordinated molecular changes that occur in TCMR, of both human and mouse renal allografts, has been well characterized: T cell and macrophage infiltration, IFNG-effects with the development of AMA, and a preprogrammed injury-repair response. The injury-repair response involves: one, increased expression of transcripts involved in tissue remodeling, secondary inflammation, and embryonic transcripts; and two, decreased expression of tubular epithelium solute carriers, manifesting as a loss of function and dedifferentiation. Since the mechanisms of TCMR appear to resemble those

of DTH, we hypothesized that the molecular changes seen in TCMR of mouse renal allografts would be stereotyped to DTH. We also hypothesized that IFNG would act on a local tissue compartment with DTH as it does in TCMR; that is, we predicted we would observe an increased injury-repair response with increased AMA when DTH is induced in mice with deficient IFNG-signaling. The aims of this study was: one, to compare the transcriptome of DTH to the transcriptome of renal TCMR, to determine if there is a stereotyped response of the epithelium to inflammation caused by these different stimuli; and two, to characterize the IFNG-dependent molecular changes of DTH.

CHAPTER 2

MATERIALS AND METHODS

2.1 OVERVIEW

In the following project, we used microarrays to study and compare large, coordinated changes in gene expression within hapten-induced T cell mediated inflammation and TCMR of kidney allografts in mice. We further characterized the IFNG-dependent gene expression changes in hapten-induced inflammation. The material sources, experimental methods, and the analyses performed are described in the following sections.

In brief, we established a working model of hapten-induced cutaneous inflammation in wild type and *Ifngr1*$^{-/-}$ mice, and utilized a previously established model of mouse kidney transplantation. We furthered the study by challenging with hapten, *Ifngr1*$^{-/-}$ skin isografts onto wild type hosts. Changes in gene expression were analysed by real time RT-PCR and microarrays. Further histological analyses were performed by hematoxylin and eosin staining and immunohistochemistry.

2.2 MICE

2.2.1 Mouse strains. CBA/J (H-2^{k}, abbreviated CBA), C57BL/6J (H-2^{b}, abbreviated B6), and B6.129S7-Ifngr^{tm1Agt}/J (*Ifngr1*-deficient B6, abbreviated B6.GRKO) mice were purchased from the Jackson Laboratory (Bar Harbor, ME). All mice used in this project were male between 9 – 12 weeks of age. Mouse maintenance and experiments were approved by the Animal Care and Use Committee for the Health Sciences at the University of Alberta.

2.3 MOUSE EXPERIMENTS

I gratefully acknowledge Dr. Lin-Fu Zhu for performing the mouse transplants. I performed all other experiments discussed within this section. In addition to the descriptions below, the mouse experiments are also summarized in **Table 2.1** and **Table 2.2**.

2.3.1 Mouse renal transplantation. Details of the mouse model for renal transplantation has been described previously (15). Briefly, donor kidneys were anastomosed heterotopically to the vena cava and abdominal aorta of recipient mice. In order to study the natural course of rejection, the left kidney in recipient mice is not removed and immunosuppressive therapy is not used. The kidney allografts were examined histologically, and those with evidence of infection or surgical complications were precluded from the study.

2.3.2 Contact hypersensitivity. Naïve B6 and B6.GRKO mice were sensitized and challenged with the hapten, oxazolone (4-ethoxymethylene-2-phenyl-2-oxazolin-5-one; Sigma-Aldrich, Canada), as previously described (68). Oxazolone was chosen as a suitable hapten because of our laboratory's previous experience with the chemical (69). In brief, mice were sensitized epicutaneously on the shaved abdomen with 100 µL of 3% oxazolone suspended in 100% ethanol on day 0. On day 5, primed mice were challenged epicutaneously on the shaved back (or shaved isografts) with 50 µL of 1.5% oxazolone. Control naïve B6 and B6.GRKO mice were sham-treated on days 0 and 5 using the ethanol vehicle only.

2.3.3 Mouse skin transplantation. To study the pure injury-repair response in skin, as we had in kidney isografts (13), B6 recipients received B6 full thickness skin isografts as

described below, but received no oxazolone or sham treatments. To mirror the oxazolone time course, these isografts were harvested on day 6 post-transplant.

Mouse skin grafting was performed based on the technique previously reported (70). Donor isografts were prepared by recovering full thickness dorsal flank skin from B6 donors, which were fitted to recipient graft beds approximately 1 cm^2. Each recipient received two B6 isografts that were placed into contralateral dorsal flank graft beds. The mice were housed individually and the grafts were bandaged until day 6 post-transplant to aid in graft healing.

2.3.4 Mouse tissue harvesting. At the time of harvesting, mice were sacrificed by cervical-dislocation after isoflurane (Halocarbon Laboratories, NJ, USA) anesthetisation.

Sections of native skin and skin isografts approximately 1 cm^2, were harvested and then divided into thirds. One third was preprocessed for RNA extraction by further sectioning the skin, quickly, into fine pieces (approximately 2 mm^2) and the pieces were immediately placed into a 14 mL polypropylene tube which was snap frozen in liquid nitrogen and stored at -70°C prior to RNA extraction. If the skin was not preprocessed, the Polytron (described below) was not able to efficiently homogenize the fibrous skin tissue and the RNA would degrade. Another one third-section was snap frozen in Optimal Cutting Temperature (OCT) compound and stored at -70°C prior to frozen sectioning on a microtome. The last one third-section was formalin fixed and embedded in paraffin.

Normal kidneys and kidney allografts were harvested and also divided into thirds. However, because kidneys are much more tender than skin, they did not require the further sectioning. As such, one third-section was snap frozen in liquid nitrogen and stored at -70°C prior to RNA extraction, another was snap frozen in OCT compound and stored at -70°C prior to frozen sectioning on a microtome, and the last third-section was formalin fixed and embedded in paraffin.

2.4 TISSUE RNA EXTRACTION AND RNA EXPRESSION ANALYSES

2.4.1 RNA extraction. Tissue (skin and kidney) RNA was extracted using TRIzol (Invitrogen, Burlington, ON, Canada) according to the manufacturer's directions. Briefly, frozen tissue sections were suspended in 1mL (for kidney) and 2mL (for skin) of TRIzol and were immediately homogenized using a Polytron, while simultaneously keeping the polypropylene tube contained in an ice bath. Immediately after homogenization, sample RNA was extracted using the RNAse Easy Micro kit (Qiagen, Toronto, ON, Canada) as per the manufacturer's directions. Briefly, the aqueous phase of each sample was transferred to a fresh 1.5 mL tube where 100% ethanol was used to precipitate the RNA. The contents of each sample were transferred to Qiagen columns where they underwent washes with RW1 and RPE buffers and 80% ethanol. The purified RNA was collected in a fresh RNAse free 1.5 mL tube by diluting each sample in 15 mL of molecular grade RNAse free water.

RNA yield and purity was assessed by UV absorbance using the absorbance ratio between absorbance at 260 nm and 280 nm, respectively, using a NanoDrop (Thermo Scientific, Wilmington, DE). RNA quality was assessed using an Agilent 2100 Bioanalyzer (Agilent Technologies, Palo Alto, CA). Total RNA was stored at -70°C until needed.

2.4.2 Reverse transcriptase polymerase chain reaction (RT-PCR). 2 µg of RNA (0.2 µg/µL) were reverse transcribed in a 20 µL reaction containing 4 µL 5x first strand buffer, 1 µL 10x dNTPs, 0.2 µL BSA (10 mg/mL), 2 µL DTT (0.1 M), 0.8 µL RNAsin RNase inhibitor (Invitrogen), 0.15 µL random primers (3 µg/µL), and 1 µL M-MLV reverse transcriptase (200 U/µL; Invitrogen). The reaction was held at 37 °C for 60 minutes, after which it was heated to 95 °C for 5 minutes. Each cDNA preparation was diluted to 10 ng/µL by adding 180 µL of RNAse-free water (Qiagen).

2.4.3 Real time polymerase chain reaction (real time RT-PCR). The resulting cDNA was amplified and detected in triplicates using forward and reverse gene-specific primers and labeled probes (**Table 2.3**), on an ABI PRISM 7900HT Sequence Detector (AB Applied Biosystems, Foster City, CA). Each 10 µL reaction consisted of 20 ng cDNA template, TaqMan quantification probe and forward and reverse primers at their optimized concentrations. The PCR amplification conditions were as follows: 50 °C for two minutes, 95 °C for 10 minutes, then 40 cycles of 95 °C for 15 seconds and 60 °C for one minute. Amplification plots were constructed using ABI 7900HT Sequence Detection System version 2.2.2 (AB Applied Biosystems). Threshold cycle numbers (Ct) were determined and transformed using the ddCt method as described by the manufacturer, using the murine glyceraldehyde 3-phosphate dehydrogenase (Gapdh) as the internal reference. To calculate the relative amount of mRNA as a fold change, the following equation was used to derive ddCt values: $2^{-[(Ct\ target\ gene_x - Ct\ Gapdh_x) - (Ct\ target\ gene_{calibr} - Ct\ Gapdh_{calibr})]}$ where 'calibr' refers to the values obtained from the control sample in the experiment. Alternately, relative amounts of mRNA were expressed as a percentage of Gapdh transcript expression (%Gapdh): $[2^{-[(Ct\ target\ gene_x - Ct\ Gapdh_x)}][100]$.

Statistical analysis of the real time RT-PCR data was performed using SPSS software (SPSS Incorporated, Chicago, IL), that used an Analysis of variance (ANOVA) with a Bonferroni correction. Statistical analyses of the real time RT-PCR data used the dCt values to calculate significance between groups expressed as relative %Gapdh transcript expression; unless comparing the fold change, in which case ddCt values were used.

2.4.4 Microarray sample preparation. I gratefully acknowledge Anna Hutton and Karyn Berry-Wynne for preparing and processing the RNA samples for microarray analysis. The Agilent 2100 Bioanalyzer (Agilent Technologies) was used to assess RNA quality; only those samples with an RNA integrity number equal to or greater than seven were used. Mouse kidney and skin RNA was prepared for labeling and hybridization to

MM9_EXP_HX12 12x135K Arrays (Roche NimbleGen, Madison, WI) according to the manufacturer's directions (www.nimblegen.com).

2.4.5 Microarray data analysis. NimbleGen .NDF files were preprocessed (normalized) by Robust Multi-array Average (RMA) in Nimblescan version 2.5. Kidney and skin samples were preprocessed as two separate batches. The non-specific filtering, interquartile range (IQR<0.5; $\log_2$ units), was used to remove genes with little or no variation across the kidney or skin samples. The data was imported into Partek (St. Louis, Missouri) Genomics Suite version 6.5, here gene expression was calculated as fold change relative to the control samples in the experiment, and the significance was tested by a one-way ANOVA with false discovery rate (FDR) set to 0.05. Unlike a standard t-test which relies solely on transcript-specific variance, the Bayes t-test combines transcript-specific variance with the variances over all transcripts. This reduces type-I error, which may be misleadingly small by chance alone given the small sample size seen in most microarray analysis.

2.4.6 PBT analysis of microarrays. PBTs provide a convenient method to assess the molecular changes associated with inflammation and injury-repair processes. As such, we applied our transcript sets to the microarray data to reflect the following biological processes: cytotoxic t cell infiltration, IFNG-effects, macrophage infiltration and the injury-repair response. To assess these biological processes in TCMR of kidney allografts and oxazolone-induced inflammation, we used the following PBTs (**Table 2.4**): quantitative cytotoxic T cell-associated (QCATs); IFNG induced (GRITs); IFNG suppressed (GSTs); quantitative macrophage-associated (QCMATs); alternative macrophage activation-associated (AMATs); and epithelial injury-repair induced (IRITs) and deterioration (KTs, STs). All of the PBTs, with the exception of the skin-derived injury-repair transcript sets (**Table 2.4**), were previously derived on the Affymetrix platform. Therefore, we identified the PBT members on the NimbleGen platform using a combination of the Entrez gene

name and GenBank ID, in order to obtain the greatest number of transferred members from the Affymetrix platform to the NimbleGen platform.

To summarize the burden of biological processes present in tissue, a transcript set score is calculated for each PBT. The transcript set (PBT) score is the geometric mean of the normalized signal across all IQR filtered members of a PBT. Significance of difference in transcript set scores between experimental conditions or an experimental condition and respective control was tested by the two-tailed Welch t-test. Enrichment of unique transcripts, using the GenBank ID, in gene ontology (GO) categories was estimated by DAVID Analysis Wizard (DAVID Bioinformatics Resources 6.7, http://david.abcc.ncifcrf.gov/).

2.5 MOUSE HISTOLOGY AND IMMUNOHISTOCHEMISTRY

Paraffin embedded tissue sections (2 μm) were stained with Hematoxylin and Eosin (H&E) and periodic acid-Schiff and subject to histologic analysis as described previously (15). Briefly, in kidneys interstitial inflammation and tubulitis were assessed and scored as the rejection lesions following the Banff criteria for diagnosing TCMR in human renal allografts (71). Skin inflammation was scored semi-quantitatively on a scale from 0 through 4: 0, no infiltrate; 1, mild focal mononuclear dermal infiltrate; 2, moderate dermal infiltrate; 3, dermal infiltrate with focal epithelial ulcerations; and 4, multiple erosive epithelial ulcerations.

Immunohistochemistry was performed as previously described (46). Briefly, previously frozen sections of skin and kidney in OCT were cut to 4 μm using a microtome. The cut sections of skin and kidney were fixed and stained using rat-anti-mouse CD68 (clone FA-11, Serotec, Raleigh, NC) and MRC1 (clone MR5D3, Serotec) antibodies. The total number of positive cells for each marker in kidney peritubular interstitium were counted in 5 ocular grid areas at 400x (=0.5 mm^2 total). Because the

skin had a higher density of positive cells for each marker, this made it harder to distinguish the cells at 400x; as such, the dermis was counted in 10 ocular grid areas at 600x (=0.67 mm^2 total).

2.6 TABLES

Table 2.1: Summary of mice used in the contact hypersensitivity experiments.

Donor strain(s)	Host strain (Number used)	Time of oxazolone sensitization and challenge	Time of skin or isograft harvest
-*	Naïve B6 skin (4)	No treatment given	N/A
-	B6 (6)	Sham-treated, day 0 and day 5	Day 6
-	B6 (6)	Oxazolone-treated, day 0 and day 5	Day 6
-	B6.GRKO (6)	Sham-treated, day 0 and day 5	Day 6
-	B6.GRKO (6)	Oxazolone-treated, day 0 and day 5	Day 6
B6 + B6 contralateral	B6 (6)	No treatment given	Day 6 post-transplant

*-, not applicable

Table 2.2: Summary of mice used in the kidney allograft experiments.

Donor strain(s)	Host strain (Number used)	Time of kidney allograft harvest (post-transplant)
-*	Naïve CBA (2)	N/A
CBA	B6 (6)	Day 7

*-, not applicable

Table 2.3: Mouse gene-specific primers and probes used in real time RT-PCR, using an ABI PRISM 7900 Sequence Detector.

Gene Name	Sequence (5'-3')	
Aif1	Applied Biosystems, Assay on Demand Mm00479862_g1, RefSeq: NM_019467.2	
Arg1	Applied Biosystems, Assay on Demand Mm00475988_m1, RefSeq: NM_007482.3	
Cd68	fwd	ATGGCGGTGGAATACAATGTG
	rev	GGAGCTCTCGAAGAGATGAATTCT
	probe	AGGCAGCACAGTGGACATTCATGGC
Chi3l3	Applied Biosystems, Assay on Demand Mm0657889_mH, RefSeq: NM_009892.2	
Cxcl9	fwd	CCTTTTGGGCATCATCTTCCT
	rev	AGGAGCATCGTGCATTCCTT
	probe	AGCAGTGTGGAGTTCGAGGAACCCTAGTG
Gapdh	Applied Biosystems, Assay on Demand 4352932E, RefSeq: NM_008084.2	
Ifng	fwd	AGCAACAGCAAGGCGAAAAA
	rev	AGCTCATTGAATGCTTGGCG
	probe	ATTGCCAAGTTTGAGGTCAACAACCCACA
Il4	fwd	GGCATTTTGAACGAGGTCACA
	rev	AGGACGTTTGGCACATCCA
	probe	AGAAGGGACGCCATGCACGGAG
Inhba	Applied Biosystems, Assay on Demand Mm00434339_m1, RefSeq: NM_008380.1	
Mrc1	Applied Biosystems, Assay on Demand Mm00485148_m1, RefSeq: NM_008625.2	
Ubd	fwd	GCAGACACAAGGATCTTTTCTTATTCA
	rev	GGTCATTAACCGCCATTGGT
	probe	TGTCCGCACCTGTGTTGTCCGTTCA

Table 2.4: Pathogenesis-based transcript sets (PBTs).

Inflammatory and Interferon-gamma PBTs			
Acronym (# unique members)	**PBT Name**	**Biological Description**	**References**
QCATs (21)	Quantitative Cytotoxic T cell-associated	**Burden of effector/effector-memory T cells**	(31)
GRITs (47)	Interferon-gamma-induced	**Interferon-gamma-effects on the tissue and inflammatory cells**	(47)
GSTs (185)	Gamma-interferon-suppressed	**Tissue and inflammatory cell transcripts suppressed by interferon-gamma**	(48)
QCMATs (46)	Quantitative constitutive macrophage-associated	**Burden of macrophages**	(9)
AMATs (20)	Alternative macrophage activation-associated	**Alternatively activated macrophages**	(48)
Active Injury-Repair Response PBTs			
Acronym (# unique members	**PBT Name**	**Biological Description**	**References**
(K)IRITs (509)	Injury- and repair-induced (kidney-selective)	**Active injury-repair response** (*injury-up*): Increased in kidney isografts, peaking day 3 or day 5	(13)
(S)IRITs (691)	Injury- and repair-induced (skin-selective)	**Active injury-repair response** (*injury-up*): Increased in skin-isografts on day 6	This paper
KTs (610)	Kidney-associated	**Active injury-repair response** (*injury-down*): Kidney parenchymal transcripts	(14)
STs (465)	Skin-associated	**Active injury-repair response** (*injury-down*): Skin parenchymal transcripts	This paper

CHAPTER 3

COMPARISON OF THE MOLECULAR CHANGES IN MOUSE CONTACT HYPERSENSITIVITY AND T CELL MEDIATED REJECTION IN MOUSE RENAL ALLOGRAFTS

3.1 OVERVIEW

The evolution of the molecular changes within rejecting human and mouse renal allografts has been well described (6,7), especially those changes which occur within the specific disease, TCMR (8). However, these molecular changes are likely not restricted to the immunological processes of renal allograft rejection. The purpose of this study was to compare the molecular changes of TCMR of mouse renal allografts to the molecular changes of a T cell mediated disease outside the kidney and allograft compartment. Therefore, we compared the molecular changes of CHS, a model of DTH, to the molecular changes of TCMR in mouse renal allografts. First, histology and real time RT-PCR were used to verify our induction of CHS by testing the efficacy of oxazolone to induce cutaneous inflammation. Second, we used microarrays to study the genome wide gene expression changes within: oxazolone-challenged mouse skin compared to sham-controls; and mouse renal allografts with TCMR compared to normal kidneys. For each of these two comparisons, we annotated the differentially expressed transcripts belonging to our PBTs, and qualitatively compared overlapping PBT memberships in order to assess the sharing of the following biological processes: one, the inflammatory burden, including T cell and macrophage infiltration, alternative macrophage activation and IFNG-effects; and two, the active injury-repair response within the local parenchymal and stromal cells.

3.2 ESTABLISHMENT OF THE CHS MODEL

To reiterate, sham-treated (control) B6 skin was sham "sensitized" and sham "challenged" with 100% ethanol on days 0 and 5. Oxazolone-challenged (experimental) B6 skin was sensitized to oxazolone in an ethanol vehicle on day 0, and was challenged on day 5. All skin samples, sham-treated and oxazolone-challenged were harvested for analysis on day 6.

3.2.1 Mouse histology. Sham-treated (control) B6 skin displayed normal gross appearance and histology. Oxazolone-challenged B6 skin showed evidence of edematous dermatosis with ulceration and sloughing of the epidermis, as previously described (72). This resulted in a higher histological score depicted by greater dermal inflammation than was seen in the sham-controls (p<0.0001, **Figures 3.1-3.2**). Therefore, challenge with the hapten oxazolone led to mononuclear infiltration of the dermis and epithelial ulceration.

3.2.2 Molecular assessment of oxazolone-induced cutaneous inflammation by real time RT-PCR. We compared transcript expression in sham-treated skin to oxazolone-challenged B6 skin samples by quantitative real time RT-PCR as a preliminary assessment of the inflammatory molecular changes occurring within the skin. We measured the relative expression levels of the following transcripts that represented prominent biological processes in inflammation (46,47): *Ifng* and IFNG-effects (*Cxcl9*, *Aif1* and *Ubd*); macrophage burden (*Cd68*); and AMA burden (*Mrc1*, *Il4*, *Arg1*, and *Chi3l3*).

Ifng transcript expression was significantly increased in oxazolone-challenged skin compared to respective sham-controls (p<0.05, **Figure 3.3A**). In agreement with an increased expression of *Ifng*, expression of the IFNG inducible transcripts *Cxcl9*, *Aif1* and *Ubd* also increased in oxazolone-challenged skin (p<0.05, **Figure 3.3B-D**).

Transcript expression of the macrophage marker, *Cd68*, and the marker of AMA, *Mrc1*, both increased in oxazolone-challenged skin ($p<0.05$, **Figure 3.4A-B**), indicating an overall influx of macrophages and AMA, respectively. There was also an increased expression of *Il4* and *Chi3l3* in the oxazolone-challenged skin ($p<0.05$, **Figure 3.5A-B**). Expression of *Arg1* did not significantly change in the oxazolone-challenged skin over the sham-treated controls ($p>0.05$, **Figure 3.5C**).

The histological and real time RT-PCR data suggest that we successfully induced an inflammatory reaction or compartment within the skin. Thus, we were ready to further examine the histological and molecular changes of oxazolone-challenged skin, and compare these changes to those seen in rejecting mouse allografts with TCMR.

3.3 THE INFLAMMATORY PHENOTYPE IS SHARED BETWEEN CHS AND RENAL ALLOGRAFTS WITH TCMR.

3.3.1 Mouse histology. Control (CBA) kidneys displayed normal histology with no inflammation, while all CBA allografts into B6 hosts at day 7 had diffuse interstitial mononuclear infiltration with edema and focal tubulitis, representing the features of TCMR (**Table 3.1**). The histology of the mouse skin was described above (**section 3.2.1**).

3.3.2 Comparison of the genome wide gene expression changes in oxazolone-induced cutaneous inflammation in mice to that of TCMR of mouse renal allografts. We used Roche NimbleGen MM9_EXP_HX12 12x135K Arrays to compare the genome wide gene expression in oxazolone-challenged B6 skin to sham-treated controls. Analysis with Partek Genomics Suite revealed 4192 unique transcripts (IQR>0.5, FDR<0.05) to be differentially expressed (from 15997 unique transcripts pre-IQR and statistical filtering). Using our inflammatory PBTs, of these 4192 transcripts nine (of 21)

were annotated as cytotoxic T cell-associated, 27 (of 47) as IFNG-induced, 21 (of 47) as macrophage-associated, and seven (of 20) as AMA-associated transcripts (**Figure 3.6A**). The unique members of the inflammatory PBTs above were all increased in the oxazolone-challenged skin compared to the sham-treated controls (fold change >1.0; FDR<0.05), except for the cytotoxic T cell-associated transcript *Nell2* (fold change 0.39; FDR=0.04). Although highly expressed in cultured T cells, as was defined by our cytotoxic T cell-associated transcripts (31), *Nell2* is not T cell specific (73). The expression of the *NELL2* transcript in the human skin diseases, atopic dermatitis and psoriasis, differs greatly; and additionally, its transcript expression level can depend on specific local cytokine milieus (74). Therefore, *Nell2* may not be a reliable transcript marker for T cell mediated inflammation. Furthermore, the raw signal for the *Nell2* probeset in the sham-treated skin was very weak (<50, **Table 3.2**), which makes it difficult to assess a meaningful decrease of expression in the oxazolone-challenged skin, thus *Nell2* may not be a good cytotoxic T cell-associated transcript.

Similar to the oxazolone-challenged and sham-treated skin, we compared the genome wide gene expression of TCMR in day 7 CBA into B6 renal allografts to that of kidney-controls (normal CBA kidneys) and found 10276 differentially expressed unique transcripts (IQR>0.5, FDR<0.05). Next, we wanted to compare the transcripts that were differentially expressed in both TCMR of renal allografts and oxazolone-challenged skin. Of the 10276 differentially expressed transcripts in TCMR and the 4192 differentially expressed transcripts in oxazolone-challenged skin, 1770 of these transcripts overlapped (**Figure 3.6B**). These skin-kidney overlapping transcripts contained many members belonging to our inflammatory PBTs, representing T cell and macrophage infiltration, IFNG-effects and AMA. In total there were: nine overlapping (of 21) cytotoxic T cell-associated, 26 overlapping (of 47) IFNG-induced, 20 overlapping (of 46) macrophage-associated, and seven overlapping (of 20) AMA-associated transcripts (**Figure 3.6B**). Therefore, all of the differentially expressed transcripts belonging to the inflammatory

PBTs found in oxazolone-challenged skin versus sham-treated controls were also found in renal allografts with TCMR.

3.3.3 T cells and IFNG-effects. Nine of the 21 cytotoxic T cell-associated transcripts which were differentially expressed in both oxazolone-challenged skin and TCMR of renal allografts included increased expression of common T cell markers, *Tcra*, *Cd8a*, and *Cxcr6* (**Table 3.2**). Thus, both oxazolone-challenged skin and TCMR of renal allografts have a similar molecular phenotype indicating the presence of cytotoxic-potentiating T cells.

There were 26 of 47 IFNG-induced transcripts that were found in both oxazolone-challenged skin and TCMR of renal allografts; these included increased expression of *Cxcl9*/*10*, *Psmb8*/*9*, and *Tapbp* (Tapasin) (**Table 3.3**). Hence, IFNG acts in a similar manner in both inflamed skin and rejecting kidneys.

3.3.4 Macrophage burden and features of alternative macrophage activation (AMA). There were 20 unique transcripts identified within our macrophage-associated transcripts (n=46) which were differentially expressed in both oxazolone-challenged skin and TCMR of renal allografts. Some of these differentially expressed transcripts included prototypical myeloid markers such as, *Cd300lf*, *Cd68* and *Pirb* (*Lilrb3*) (**Table 3.4**). To verify the increase of macrophages within the skin, skin-tissue sections were immunostained for CD68. The number of $CD68^+$ cells increased in oxazolone-challenged skin (122/0.67 mm^2), versus controls (73/0.67 mm^2, $p<0.001$) (**Figure 3.7A-B**). We previously published that the number of $CD68^+$ cells and *Cd68* transcript expression also increases in rejecting renal allografts (46).

Despite the effects of IFNG expression in the inflamed skin and rejecting kidneys, there were molecular and histological features of AMA. Seven of 20 AMA-associated transcripts were found to be differentially expressed in both oxazolone-challenged skin and TCMR of renal allografts. Three of these transcripts included *Chi3l3*, *Adam8* and

Clec7a (Dectin-1) (**Table 3.5**). We then immunostained skin-tissue sections for MRC1 (CD206). And analogous to a previous report in rejecting renal allografts (46), we observed an increase in the number of $MRC1^+$ cells in oxazolone-challenged skin (121/0.67 mm^2), versus controls (64/0.67 mm^2, p<0.001) (**Figure 3.7C-D**).

3.4 TRANSCRIPTS RELATED TO INJURY-REPAIR PROCESSES ARE TISSUE-SELECTIVE, BUT REPRESENT SIMILAR PATHWAYS

3.4.1 Injury-up: the injury- and repair-induced transcripts (IRITs). The IRITs (injury-up) were defined as reversible injury that occurs in mouse isografts (13). However, these PBTs could not differentiate the oxazolone-challenged from the sham-treated skin as most probesets did not meet the statistical cutoff (FDR<0.05); nor was the transcript set score significantly higher in oxazolone-challenged skin (data not shown). This could have resulted from the comparatively small number of epithelial nuclei in skin versus kidney and/or the biological differences of these two tissues.

As such, we derived a PBT that had members related to injury in skin isografts; hence, this transcript set would represent the tissue-selective injury and repair response in skin injury. Transcripts were defined by taking probesets that had an increased expression (fold>1; FDR<0.01) in skin isografts at day 6 post-transplant versus normal (native and untreated) B6 skin. We then further reduced the total transcript count to a final 691 unique transcripts by: one, imposing a fold increase of ≥2 on the isografts versus normal skin; and two, as was carried out with the kidney-selective injury and repair induced transcripts (13), we excluded 291 probesets which belonged to the inflammatory PBTs (cytotoxic T cell, IFNG-induced, macrophage, and AMA-associated transcripts) (**Figure 3.8, Table 3.6**).

We then found that the skin-selective IRITs and kidney-selective IRITs shared very few members; however, their annotated biology was similar. Only 9% (n=64) of the

691 skin-selective IRITs overlapped with the kidney-selective IRITs. On the other hand, in gene ontology (GO) annotations there were many commonly overrepresented categories that were found in both the skin-selective and kidney-selective IRITs (**Table 3.7)**; including: angiogenesis, defense response, response to wounding, wound healing, extracellular matrix parts, and cell-cell adhesion. Additionally, kidney-selective IRITs are enriched in transcripts who's expression is associated with embryonic developing kidneys and kidney-development (13). Therefore, we looked for GO annotations within the skin-selective IRITs, and subsequently found; epithelial development, epidermis development, and ectoderm development. However, only epithelial development met the statistical cutoff of the hypergeometric test (p<0.05, **Table 3.7**). Nonetheless, all three annotations were enriched with small proline-rich region (*Sprr*) transcripts from the skin-selective IRITs (**Table 3.6**). *Sprr* expression is highly expressed in developing ectoderm (75). Therefore, the expression of individual IRITs may vary in different tissues, however, they all represent similar functional annotations and pathways.

3.4.2 Injury-down: the kidney- and skin-associated transcripts (KTs/STs). We previously defined the KTs, a PBT who's members had high expression in normal kidneys, but decreased in kidney allografts manifesting the loss of function (6). These transcripts represent the injury-down component of the injury-repair response. However, the KTs performed similar to the kidney-selective IRITs in the skin; expression of the injury-down KTs in the oxazolone-challenged skin were largely unchanged, based on the transcript set score (data not shown). Thus, they did not exemplify a change or loss of function in the oxazolone-challenged skin.

To interrogate the transcripts involved in skin parenchymal function we took all probesets with a high expression (raw signal ≥500) in normal B6 skin and that changed expression, increased or decreased (to prevent bias) (FDR<0.01), in day 6 skin isografts versus normal B6 skin. We then removed any transcripts which had overlapping membership with the above skin-selective injury and repair induced transcripts and the

inflammatory PBTs, and were left with 465 unique STs. These represented a skin-selective injury-down injury-repair response (**Figure 3.9, Table 3.8**). Moreover, the majority or 80% (n=373) of the 465 transcripts had decreased expression in the day 6 skin isografts; suggesting a loss of parenchymal function in the skin, as occurs in injured kidneys (6).

Similar to the skin and kidney injury and repair induced transcripts, less than 10% (n=39) of the 465 STs had overlapping membership with the KTs. When we examined the GO annotations for the ST and KT sets, we found: one, the KTs were overrepresented with more nephron-specific biological processes such as ion transport (including sodium) and the cellular component, brush border membrane (**Table 3.9**); and two, the STs were overrepresented with annotations relevant to epidermal function such as regulation of actin and keratin components, extracellular matrix and cell-junction components (**Table 3.9**). Nonetheless, there were still overlapping GO annotations between these two transcript sets; many of which were involved in cell metabolism. For example, various carboxylic and amino acid catabolic processes, as well as fatty acid oxidation (**Table 3.10**). To see if the 39 unique transcripts which were shared between the ST and KT sets, were accounting for the overlapping GO annotations, we analyzed the GO annotations of these 39 transcripts. In total, they accounted for five, or 20%, of the overlapping categories (**Table 3.10**). Thus, 80% of the overlapping GO annotations were from non-overlapping probesets of the ST and KT sets. As such, despite the differential functions of skin and kidney that is represented by these two tissue-associated transcript sets, the skin and kidney (and conceivably other tissues), share some basic functions, especially metabolic processes.

3.5 SUMMARIZING THE TRANSCRIPT CHANGES AS TRANSCRIPT SET SCORES REVEAL PARALLEL MOLECULAR CHANGES IN CHS AND TCMR

We expressed the inflammatory and injury-repair response PBTs as individual transcript set scores, which are the geometric means of the normalized signals across all members of a PBT. Overall, the oxazolone-challenged skin showed a similar molecular phenotype to TCMR of renal allografts (**Figure 3.10**). Both, oxazolone-challenged skin and renal allografts with TCMR had increases in the inflammatory response, as shown by the increased cytotoxic T cell score ($p<0.05$); macrophage burden score ($p<0.05$); Ifng-effects ($p<0.05$); and alternative macrophage activation ($p=0.2$) (**Figure 3.10A-D**). Concurrent with the inflammatory burden, the summarized transcript set score of the kidney- and skin-selective injury and repair induced transcripts both increased in their respective tissues compared to controls (injury-up) ($p<0.05$), indicating similar active injury-repair processes in both tissues (**Figure 3.10E**). In a similar fashion, the summarized transcript set score of both STs and KTs were decreased in kidneys with TCMR and oxazolone-challenged skin (injury-down) ($p<0.05$), indicating an essentially identical loss of parenchymal and stromal function in both tissues (**Figure 3.10F**). Thus, the cutaneous application of the hapten oxazolone induced the molecular changes which also occurred in TCMR of mouse renal allografts and could be quantified using respective PBTs.

3.6 TABLES

Table 3.1: Histological data of mouse renal allografts. Assessment of the rejection lesions interstitial inflammation (i-score) and tubulitis (t-score) according to the Banff criteria for diagnosing TCMR in human renal allografts (71).

Experiment	Individual Mouse	Histological Assessment	
		Banff i-score	Banff t-score
Normal CBA Kidney (control)	1	0	0
	2	0	0
Day 7 CBA in B6 Renal Allografts	1	2	1
	2	3	1
	3	3	1
	4	3	1
	5	3	1
	6	3	1

Table 3.2: Unique cytotoxic T cell-associated transcripts found in both oxazolone-challenged skin versus sham-treated skin, and CBA into B6 renal allografts at day 7 versus normal CBA kidneys. Raw signal is calculated from the average probeset signal on the NimbleGen arrays and was normalized using the robust multi-array average.

Transcript	Fold Change (oxa-skin)	Raw Signal (sham-skin)	Fold Change (renal allograft)	Raw Signal (normal kidney)
Gzmb	17.1	113	89.2	132
Gzma	8.5	36	15.3	122
Cst7	2.8	299	12.7	231
Tcra	2.5	176	11.3	1006
Tcra (*V-15* predicted)	2.4	129	48.3	402
Cd8a	2.3	91	164.7	47
Klrk1	2.2	363	2.8	714
Cxcr6	2.2	50	6.9	109
Nell2	0.4	19	0.5	68

Table 3.3: Unique IFNG-induced transcripts (IFNG-effects) found in both oxazolone-challenged skin versus sham-treated skin, and CBA into B6 renal allografts at day 7 versus normal CBA kidneys. Raw signal is calculated from the average probeset signal on the NimbleGen arrays and was normalized using the robust multi-array average.

Transcript	Fold Change (oxa-skin)	Raw Signal (sham-skin)	Fold Change (renal allograft)	Raw Signal (normal kidney)
Cxcl9	15.5	390	74.3	275
Tgtp	10.0	156	25.3	541
Gbp4	9.8	99	28.2	144
Iigp1	9.5	944	12.8	1094
Gbp3	9.1	118	14.3	335
Igtp	8.4	182	23.7	417
Cxcl10	5.8	201	43.7	307
Irgm1	5.0	591	9.6	1724
Ifit1	4.9	264	7.1	315
Psmb8	4.7	1623	18.7	1339
Psmb9	4.6	646	13.2	1899
Mpeg1	3.6	1051	16.8	688
Oasl2	3.6	699	13.7	440
Irgm2	3.4	2453	14.9	2123
Ripk3	3.3	246	7.5	131
Bst2	3.3	865	19.9	305
Xdh	2.9	173	5.4	127
Erap1	2.8	9	3.6	16
Irf7	2.7	1039	14.9	596
Lgals3bp	2.6	2690	8.9	1927
Herc5	2.4	738	5.6	943
Pla2g16	2.3	37	4.3	176
H2-T23	2.2	3428	5.2	3615
Tapbp	2.0	11437	3.4	10952
H2-T10	2.0	2669	4.2	2628
Il18bp	1.3	1299	7.4	686

Table 3.4: Unique macrophage-associated transcripts found in both oxazolone-challenged skin versus sham-treated skin, and CBA into B6 renal allografts at day 7 versus normal CBA kidneys. Raw signal is calculated from the average probeset signal on the NimbleGen arrays and was normalized using the robust multi-array average.

Transcript	Fold Change (oxa-skin)	Raw Signal (sham-skin)	Fold Change (renal allograft)	Raw Signal (normal kidney)
Cd300lf	26.8	28	7.5	193
Pilra	23.9	45	40.6	71
Pira3	10.9	145	20.1	79
Slamf8	8.2	136	31.5	253
Siglec1	6.3	56	5.2	10
Hk3	6.0	1023	65.3	237
Fpr1	5.5	225	5.6	178
Ifi204	4.4	710	9.7	214
Gp49a	4.2	1082	13.0	207
Fcer1g	3.8	2268	31.0	308
Lilrb4	3.4	3851	11.1	786
C5ar1	2.5	2826	18.9	435
Mnda	2.4	3608	22.9	233
Pla2g7	2.3	897	6.6	621
Dmxl2	2.3	469	0.5	1930
Tlr8	2.1	286	33.4	11
Tlr2	1.9	401	8.1	335
Emilin2	1.9	6038	7.4	483
Cd68	1.8	7512	12.8	979
Ncf2	1.8	657	7.8	279
Lilrb3	1.8	1253	13.8	201

Table 3.5: Unique AMA-associated transcripts found in both oxazolone-challenged skin versus sham-treated skin, and CBA into B6 renal allografts at day 7 versus normal CBA kidneys. Raw signal is calculated from the average probeset signal on the NimbleGen arrays and was normalized using the robust multi-array average.

Transcript	Fold Change (oxa-skin)	Raw Signal (sham-skin)	Fold Change (renal allograft)	Raw Signal (normal kidney)
Chi3l3	45.0	52	111.0	10
Clec7a	7.9	279	4.2	472
Ear11	7.2	35	0.5	112
Adam8	5.1	352	14.6	62
Clec4a2	3.5	437	4.8	121
Clec4n	3.3	470	11.5	123
Thbs1	1.9	2195	4.1	1157

Table 3.6: 691 unique skin-selective injury- and repair-induced transcripts and their annotation. Top 30 annotated transcripts are listed by fold change in oxazolone-challenged skin versus sham-treated controls (FDR<0.05). The remaining 661 are listed in alphabetical order by gene name. (Table continued on next page.)

	GenBank	Gene Name	Fold Change	Raw Signal (sham-controls)	Roche NimbleGen Annotation
1	BC055885	***Saa3***	98.8	267	serum amyloid A 3 (acute phase)
2	BC024606	***Saa2***	76.2	59	serum amyloid A 2 (acute phase)
3	BC127035	***Trem3***	63.6	19	triggering receptor on myeloid cells 3
4	AK036935	***Sirpb1***	52.5	34	Signal-regulatory protein beta-1
5	BC052681	***Sell***	44.3	60	L-selectin
6	BC044865	***Slfn4***	39.8	16	schlafen 4
7	BC024392	***Cxcl5***	39.6	5	chemokine (C-X-C motif) ligand 5
8	BC011437	***Il1b***	38.4	61	interleukin 1 beta
9	AK089891	***Irg1***	38.3	16	immunoresponsive gene 1
10	AB034730	***Prg4***	38.1	145	proteoglycan 4 (lubricin)
11	BC060281	***Lce3f***	32.3	8	late cornified envelope 3F
12	BC116199	***Defb14***	23.7	48	defensin beta 14
13	BC028509	***Slpi***	20.7	738	secretory leukocyte peptidase inhibitor
14	BC140340	***Trem1***	16.4	77	triggering receptor expressed on myeloid cells
15	BC051677	***Il8rb***	16.1	188	interleukin 8 receptor, beta (*Cxcr2*)
16	AK170692	***Clec4d***	15.5	83	NOD-derived CD11c +ve dendritic cells
17	BC115865	***Csf3r***	14.8	80	colony stimulating factor 3 receptor
18	BC078629	***S100a8***	13.7	402	S100 calcium binding protein A8, calgranulin A
19	BC003218	***Clec4e***	13.2	48	C-type lectin domain family 4, member e
20	BC022176	***Ptx3***	13.2	384	pentraxin related gene
21	BC146301	***Mmp1b***	12.9	9	matrix metallopeptidase 1b, collagenase
22	BC008107	***Timp1***	12.8	525	tissue inhibitor of metalloproteinase 1
23	BC145867	***Ccl2***	11.5	178	chemokine (C-C motif) ligand 2
24	BC119291	***Epgn***	11.4	449	epithelial mitogen
25	BC011092	***Ccr1***	11.2	58	chemokine (C-C motif) receptor 1
26	BC012639	***Gsta4***	11.0	452	glutathione S-transferase, alpha 4
27	BC103574	***Ccr5***	10.4	188	chemokine (C-C motif) receptor 5
28	BC119228	***Hgf***	10.2	40	hepatocyte growth factor
29	BC090258	***Ifitm1***	9.6	914	interferon induced transmembrane protein 1
30	AK085667	***Tnc***	9.3	61	tenascin C

…Table 3.6 continued on next page.

Table 3.6 (continued…)

	GenBank ID	Gene Name	Roche NimbleGen Annotation
31	BC051545	***1190003J15Rik***	RIKEN 1190003J15 gene
32	AK004674	***1200009I06Rik***	adult male lung
33	XM_001472371	***1200016E24Rik***	RIKEN 1200016E24 gene
34	BC002254	***1500015O10Rik***	RIKEN 1500015O10 gene
35	AK005678	***1700006J14Rik***	adult male testis
36	BC050753	***1700010I14Rik***	RIKEN 1700010I14 gene
37	AK080676	***1700017B05Rik***	10 days neonate cortex
38	AK006734	***1700048O20Rik***	adult male testis
39	XM_358452	***1810011H11Rik***	RIKEN 1810011H11 gene
40	BC141466	***1810033B17Rik***	RIKEN 1810033B17 gene
41	BC012898	***2010002N04Rik***	RIKEN 2010002N04 gene
42	AK149943	***2310014H01Rik***	bone marrow macrophage
43	BC083056	***2310016C08Rik***	RIKEN 2310016C08 gene
44	BC115655	***2310042E22Rik***	RIKEN 2310042E22 gene
45	AK141402	***2610203C20Rik***	12 days embryo spinal cord
46	AK012157	***2610528A11Rik***	10 days embryo whole body
47	AK169506	***4732465J04Rik***	3 days neonate thymus
48	AK160248	***4930503L19Rik***	adult male testis
49	BC049556	***4930583H14Rik***	RIKEN 4930583H14 gene
50	AK137010	***5330426P16Rik***	12 days embryo embryonic body between diaphragm region and neck
51	BC027126	***6430548M08Rik***	RIKEN 6430548M08 gene
52	AK020205	***8030451A03Rik***	15 days embryo male testis
53	XM_982329	***9530059O14Rik***	RIKEN 9530059O14 gene (9530059O14Rik)
54	BC115873	***9930013L23Rik***	RIKEN 9930013L23 gene
55	BC118611	***9930032O22Rik***	RIKEN 9930032O22 gene
56	BC023483	***A730054J21Rik***	RIKEN A730054J21 gene
57	XM_986184	***Aadacl2***	arylacetamide deacetylase-like 2 (Aadacl2)
58	AK137593	***AB124611***	adult male bone
59	AK172420	***Abcc3***	activated spleen
60	BC024677	***Abpb***	androgen binding protein beta
61	BC023343	***Acp2***	acid phosphatase 2, lysosomal
62	DQ288940	***Actn1***	alpha actinin 1a (Actn1a)
63	AK051780	***Adam12***	12 days embryo spinal ganglion
64	BC093480	***Adam19***	a disintegrin and metalloproteinase domain 19 (meltrin)
65	BC034739	***Adamts16***	a disintegrin-like and metallopeptidase (reprolysin type) with thrombospondin
66	BC027773	***Adamts4***	a disintegrin-like and metallopeptidase (reprolysin type) with thrombospondin
67	AK030315	***Adamts6***	11 days pregnant adult female ovary and uterus
68	AY551090	***Adamts7***	ADAMTS7B (Adamts7)
69	BC027165	***Adap2***	centaurin, alpha 2
70	BC052665	***Adm***	adrenomedullin
71	AK046802	***Adra2a***	10 days neonate medulla oblongata
72	BC006801	***AF251705***	Cd300D antigen
73	AK036733	***AI839979***	adult male bone
74	BC005789	***Akr1b8***	aldo-keto reductase family 1, member B8
75	BC034259	***Akr1c18***	aldo-keto reductase family 1, member C18
76	AF246711	***Aldh1a3***	retinaldehyde dehydrogenase 3
77	BC046597	***Aldh3b1***	aldehyde dehydrogenase 3 family, member B1
78	BC027216	***Angpt2***	angiopoietin 2
79	BC006611	***Angptl4***	angiopoietin-like 4
80	AK013850	***Anxa3***	adult male hippocampus
81	BC020015	***Apln***	apelin
82	BC031786	***Apoa2***	apolipoprotein A-II
83	BC003792	***Apobec1***	apolipoprotein B editing complex 1

…Table 3.6 continued on next page.

Table 3.6 (continued…)

	GenBank ID	Gene Name	Roche NimbleGen Annotation
84	AK046043	***Apol8***	adult male corpora quadrigemina
85	NM_001109914	***Apold1***	apolipoprotein L domain containing 1 (Apold1)
86	BC034832	***Apon***	apolipoprotein N
87	BC005667	***Aprt***	adenine phosphoribosyl transferase
88	BC027400	***Aqp3***	aquaporin 3
89	AK154151	***Aqp9***	NOD-derived CD11c +ve dendritic cells
90	AF469622	***Arap3***	ankyrin repeat and plekstrin homology domains-containing protein 3
91	AK147757	***Arhgap30***	melanocyte
92	BC064093	***Arl11***	ADP-ribosylation factor-like 11
93	BC054839	***Armcx2***	armadillo repeat containing
94	BC003441	***Arpc1b***	actin related protein 2/3 complex, subunit 1B
95	AK154874	***Arrb2***	NOD-derived CD11c +ve dendritic cells
96	AK156507	***Artn***	activated spleen
97	AK009814	***As3mt***	adult male tongue
98	BC005552	***Asns***	asparagine synthetase
99	AK049506	***Asph***	7 days embryo whole body
100	AK155372	***Atp11b***	NOD-derived CD11c +ve dendritic cells
101	BC037206	***Atp1a3***	ATPase, Na+/K+ transporting, alpha 3 polypeptide
102	BC087899	***Atp6v0d2***	ATPase, H+ transporting, lysosomal V0 subunit D2
103	BC117946	***Atp8b1***	ATPase, class I, type 8B
104	BC107250	***AU042651***	expressed sequence AU042651
105	BC026418	***B3gnt3***	UDP-GlcNAc:betaGal beta-1, 3-N-acetylglucosaminyltransferase 3
106	BC146437	***B430306N03Rik***	RIKEN B430306N03 gene
107	BC027582	***BC027582***	sequence BC027582
108	BC106195	***BC055004***	sequence BC055004
109	NM_001001332	***BC117090***	sequence BC1179090 (BC117090)
110	BC052032	***Bcan***	brevican
111	BC028762	***Bcl2a1a***	B-cell leukemia/lymphoma 2 related protein A1a
112	BC100462	***Bcl2a1b***	B-cell leukemia/lymphoma 2 related protein A1b
113	BC120720	***Bcl2a1c***	B-cell leukemia/lymphoma 2 related protein A1c
114	BC027536	***Bcl2a1d***	B-cell leukemia/lymphoma 2 related protein A1d
115	AK037885	***Bcl2l11***	16 days neonate thymus
116	BC117780	***Bcl2l15***	Bcl2-like 15
117	BC021610	***Bcl3***	B-cell leukemia/lymphoma 3
118	BC090998	***Bcl6b***	B-cell CLL/lymphoma 6, member B
119	BC057378	***Bend6***	RIKEN B230209C24 gene
120	BC057580	***Bfsp1***	beaded filament structural protein in lens-CP94
121	BC057185	***Bgn***	biglycan
122	BC010720	***Bhlhe40***	basic helix-loop-helix domain containing, class B2
123	XM_001000082	***Bin2***	bridging integrator 2 (Bin2)
124	BC148547	***Bst1***	bone marrow stromal cell antigen 1
125	NM_001040631	***C1qtnf5***	C1q and tumor necrosis factor related protein 5 (C1qtnf5)
126	BC003728	***C3ar1***	complement component 3a receptor 1
127	AK089981	***C430002N11Rik***	RCB-0559 K-1 . F1
128	AK021262	***C430049B03Rik***	7 days embryo whole body
129	AK083339	***C920009B18Rik***	2 days neonate thymus thymic cells
130	L06233	***Cacna1c***	dihydropyridine sensitive cardiac calcium channel
131	AB086123	***Cacna1d***	calcium channel alpha 1D subunit
132	BC003480	***Capg***	capping protein (actin filament), gelsolin-like
133	BC054726	***Capn2***	calpain 2
134	BC120544	***Car9***	carbonic anhydrase 9
135	Y17138	***Cask***	mCASK-B.
136	BC006737	***Casp8***	caspase 8
137	BC092229	***Casq2***	calsequestrin 2

…Table 3.6 continued on next page.

Table 3.6 (continued…)

	GenBank ID	Gene Name	Roche NimbleGen Annotation
138	BC095987	***Ccdc126***	coiled-coil domain containing 126
139	BC002274	***Ccdc23***	coiled-coil domain containing 23
140	BC028487	***Cck***	cholecystokinin
141	BC111443	***Ccl3***	chemokine (C-C motif) ligand 3
142	BC061126	***Ccl7***	chemokine (C-C motif) ligand 7
143	BC148418	***Ccr7***	chemokine (C-C motif) receptor 7 (Ccr7)
144	BC057889	***Cd14***	CD14 antigen
145	AK155114	***Cd276***	NOD-derived CD11c +ve dendritic cells
146	BC107352	***Cd300lb***	CD300 antigen like family member B
147	X66081	***Cd44***	Pgp-1 CD44 (clone M1).
148	BC006799	***Cd5l***	CD5 antigen-like
149	AK154329	***Cd80***	NOD-derived CD11c +ve dendritic cells
150	BC156050	***Cd93***	CD93 antigen (Cd93)
151	CT010326	***Cd97***	CD97 antigen
152	BC046314	***Cdh11***	cadherin 11
153	BC054790	***Cdh5***	cadherin 5
154	BC046823	***Cdk5r1***	cyclin-dependent kinase 5, regulatory subunit (p35) 1
155	AK152437	***Cdk6***	bone marrow macrophage
156	NM_029441	***Cdyl2***	chromodomain protein, Y chromosome-like 2 (Cdyl2)
157	BC085106	***Cep170***	centrosomal protein 170
158	BC003780	***Chi3l1***	chitinase 3-like 1
159	BC051963	***Chst2***	carbohydrate sulfotransferase 2
160	AF401530	***Cklf***	chemokine-like factor 6 (CKLF6)
161	AK166218	***Clcf1***	mammary gland RCB-0526 Jyg-MC(A)
162	BC036347	***Clcn5***	chloride channel 5
163	BC019452	***Clec14a***	C-type lectin domain family 14, member a
164	BC051091	***Clec2e***	C-type lectin domain family 2, member e
165	BC104364	***Clec5a***	C-type lectin domain family 5
166	BC063058	***Clstn2***	calsyntenin 2
167	BC066106	***Cntn2***	contactin 2
168	AK028536	***Col12a1***	0 day neonate skin
169	AK030038	***Col27a1***	adult male testis
170	AF034136	***Col6a3***	collagen alpha3(VI) (Col6a3)
171	BC011061	***Col8a1***	collagen, type VIII
172	BC011068	***Cotl1***	coactosin-like 1 (Dictyostelium)
173	BC012663	***Csrp2***	cysteine and glycine-rich protein 2
174	AK150917	***Ctla2b***	bone marrow macrophage
175	AK150274	***Ctss***	bone marrow macrophage
176	BC119511	***Cxcl2***	chemokine (C-X-C motif) ligand 2
177	BC117014	***Cxcl3***	chemokine (C-X-C motif) ligand 3
178	BC031665	***Cxcr4***	chemokine (C-X-C motif) receptor 4
179	AK154184	***Cyba***	NOD-derived CD11c +ve dendritic cells
180	BC023241	***Cyp2d26***	cytochrome P450
181	BC013494	***Cyp4f18***	cytochrome P450
182	AK170301	***Cytip***	NOD-derived CD11c +ve dendritic cells
183	AK032662	***Cytsb***	10 days neonate cerebellum
184	BC145673	***D14Ertd668e***	DNA segment
185	BC027314	***D17H6S56E-5***	DNA segment
186	AK048080	***Dchs1***	16 days embryo head
187	AY968048	***Dclk1***	CLICK-I beta
188	BC034505	***Ddah1***	dimethylarginine dimethylaminohydrolase 1
189	AK078287	***Ddx58***	adult male olfactory brain
190	BC003751	***Degs1***	degenerative spermatocyte homolog 1 (Drosophila)
191	BC016427	***Degs2***	degenerative spermatocyte homolog 2 (Drosophila), lipid desaturase
192	AK158187	***Dennd4a***	adult inner ear

…Table 3.6 continued on next page.

Table 3.6 (continued…)

	GenBank ID	Gene Name	Roche NimbleGen Annotation
193	BC029209	***Dhx58***	DEXH (Asp-Glu-X-His) box polypeptide 58
194	BC118526	***Disp2***	dispatched homolog 2 (Drosophila)
195	BC042497	***Dll4***	delta-like 4 (Drosophila)
196	AK122347	***Dock10***	mKIAA0694 protein.
197	AK169871	***Dok1***	NOD-derived CD11c +ve dendritic cells
198	AK171155	***Dpep2***	NOD-derived CD11c +ve dendritic cells
199	BC031382	***Dpy19l1***	dpy-19-like 1 (C. elegans)
200	AK151184	***Dram1***	bone marrow macrophage
201	NM_001099297	***Duox1***	dual oxidase 1 (Duox1)
202	BC010207	***Dusp7***	dual specificity phosphatase 7
203	BC100309	***Dusp9***	dual specificity phosphatase 9
204	BC087877	***E030010A14Rik***	RIKEN E030010A14 gene
205	AK054221	***E230032D23Rik***	2 days pregnant adult female oviduct
206	AK017841	***E2f1***	8 days embryo whole body
207	AK051521	***E2f7***	12 days embryo spinal ganglion
208	AK158295	***E2f8***	adult inner ear
209	BC052196	***E330016A19Rik***	RIKEN E330016A19 gene
210	AK075585	***Efemp2***	adult male kidney
211	BC044926	***Egln3***	EGL nine homolog 3 (C. elegans)
212	AK089917	***Ehbp1l1***	RCB-0559 K-1 . F1
213	BC016422	***Eif2ak2***	eukaryotic translation initiation factor 2-alpha kinase 2
214	BC055735	***Elk3***	ELK3
215	BC017134	***Eltd1***	EGF
216	BC003706	***Emcn***	endomucin
217	BC005481	***Emilin1***	elastin microfibril interfacer 1
218	BC062927	***Enah***	enabled homolog (Drosophila)
219	BC085098	***Eno1***	enolase 1, alpha non-neuron
220	BC009018	***Eno2***	enolase 2, gamma neuronal
221	AK166220	***Entpd7***	mammary gland RCB-0526 Jyg-MC(A)
222	AK173080	***Epb4.1l3***	mKIAA0987 protein.
223	BC043088	***Ephb2***	Eph receptor B2
224	BC011224	***Ercc1***	excision repair cross-complementing rodent repair deficiency
225	AB073079	***Erg***	Erg
226	BC104406	***Erp27***	endoplasmic reticulum protein 27
227	BC046766	***Esd***	esterase D/formylglutathione hydrolase
228	BC020038	***Esm1***	endothelial cell-specific molecule 1
229	BC010588	***Ets1***	E26 avian leukemia oncogene 1, 5' domain
230	BC004741	***Ext1***	exostoses (multiple) 1
231	BC050219	***F10***	coagulation factor X
232	BC061149	***F7***	coagulation factor VII
233	AK076887	***Fam126a***	adult male testis
234	AK163654	***Fam131b***	10 days neonate medulla oblongata
235	BC010826	***Fam162a***	RIKEN 2310056P07 gene
236	AK034722	***Fam38b***	12 days embryo embryonic body between diaphragm region and neck
237	AK075613	***Fam49b***	adult male spleen
238	BC005443	***Fbln2***	fibulin 2
239	AK080935	***Fbn1***	4 days neonate male adipose
240	AK082008	***Fbn2***	16 days embryo head
241	AK080885	***Fcgr2b***	4 days neonate male adipose
242	BC052819	***Fcgr3***	Fc receptor, IgG
243	BC148640	***Fcrlb***	Fc receptor-like B
244	BC129919	***Fes***	feline sarcoma oncogene
245	BC018341	***Fetub***	fetuin beta
246	BC132340	***Fgd3***	FYVE

…Table 3.6 continued on next page.

Table 3.6 (continued…)

	GenBank ID	Gene Name	Roche NimbleGen Annotation
247	BC060654	***Fhod1***	formin homology 2 domain containing 1
248	BC027250	***Fibin***	RIKEN 1110018M03 gene
249	BC029546	***Fkbp10***	FK506 binding protein 10
250	BC049596	***Fkbp1b***	FK506 binding protein 1b
251	AF510860	***Flg***	profilaggrin (Flg)
252	BC029674	***Flt1***	FMS-like tyrosine kinase 1
253	AK020206	***Fmnl1***	15 days embryo male testis
254	BC099411	***Fmr1nb***	fragile X mental retardation 1 neighbor
255	AK147346	***Fndc3b***	14 days pregnant adult female placenta
256	BC052917	***Fosl1***	fos-like antigen 1
257	BC052408	***Fscn1***	fascin homolog 1
258	NM_001111073	***Fxyd5***	FXYD domain-containing ion transport regulator 5 (Fxyd5)
259	AK137907	***Fyb***	16 days neonate thymus
260	BC090962	***Galnt1***	UDP-N-acetyl-alpha-D-galactosamine:polypeptide
261	AK036523	***Galnt7***	adult male bone
262	AF334736	***Gfpt1***	glutamine: fructose-6-phosphate amidotransferase 1
263	AK087160	***Gimap5***	0 day neonate lung
264	BC053054	***Gja5***	gap junction membrane channel protein alpha 5
265	BC050840	***Gjc1***	gap junction membrane channel protein alpha 7
266	BC025083	***Glipr1***	GLI pathogenesis-related 1 (glioma)
267	BC031750	***Glipr2***	GLI pathogenesis-related 2
268	AY220846	***Glis3***	GLIS3 (Glis3)
269	BC012642	***Glrx***	glutaredoxin
270	XM_001478803	***Gm10639***	similar to Gsta2 protein (LOC100042314)
271	XM_001474265	***Gm10784***	similar to immediate early response 3 interacting protein 1 (LOC100040099)
272	AK157218	***Gm14005***	activated spleen
273	XM_001480842	***Gm14010***	protein LOC100043729 (LOC100043729)
274	XM_001472704	***Gm2194***	similar to gag protein (LOC100039378)
275	XM_001472866	***Gm2251***	similar to gag protein
276	XM_001473270	***Gm2326***	similar to gag protein (LOC100039583)
277	XM_001474216	***Gm2627***	similar to gag protein (LOC100040148)
278	XM_001475021	***Gm2718***	similar to ribosomal protein L36a (LOC100040331)
279	XM_001475316	***Gm2904***	similar to sid478p (LOC100040682)
280	XM_001475592	***Gm3073***	protein LOC100040977 (LOC100040977)
281	XM_001476237	***Gm3245***	similar to gag protein (LOC100041274)
282	XM_001478461	***Gm3914***	similar to CG4877-PA (LOC100042581)
283	XM_001480672	***Gm4569***	similar to gag protein (LOC100043650)
284	XM_001481052	***Gm4589***	protein LOC100043687 (LOC100043687)
285	XM_001481020	***Gm4610***	protein LOC100043726 (LOC100043726)
286	XM_001480862	***Gm4618***	similar to meltrin alpha (LOC100043741)
287	XM_001476895	***Gm4887***	similar to Twinfilin
288	BC146444	***Gm5416***	MGC:180367 predicted gene
289	XM_484341	***Gm5456***	EG432817 (EG432817)
290	NR_002868	***Gm5476***	EG432985 (EG432985) on chromosome 15.
291	BC089539	***Gm5506***	EG433182
292	XM_486686	***Gm5637***	EG434782 (EG434782)
293	XM_889601	***Gm6551***	EG625060 (EG625060)
294	XM_001003594	***Gm8570***	EG667314 (EG667314)
295	XM_001477646	***Gm9790***	similar to hypoxia induced gene 1
296	XM_001476885	***Gml***	GPI anchored molecule like protein
297	BC061207	***Gmppb***	GDP-mannose pyrophosphorylase B
298	BC111437	***Gng8***	guanine nucleotide binding protein (G protein)
299	BC061005	***Gngt2***	guanine nucleotide binding protein (G protein)
300	BC011152	***Golm1***	golgi membrane protein 1

…Table 3.6 continued on next page.

Table 3.6 (continued…)

	GenBank ID	Gene Name	Roche NimbleGen Annotation
301	AK155580	***Gp49a***	B6-derived CD11 +ve dendritic cells
302	BC061225	***Gpihbp1***	GPI-anchored HDL-binding protein 1
303	AK173020	***Gpr116***	mKIAA0758 protein.
304	BC003212	***Gpr137b***	G protein-coupled receptor 137B
305	NR_003568	***Gpr137b-ps***	G protein-coupled receptor 137B
306	BC052037	***Gpr176***	G protein-coupled receptor 176
307	NM_001104529	***Gpr35***	G protein-coupled receptor 35 (Gpr35)
308	AK155863	***Gpsm3***	B6-derived CD11 +ve dendritic cells
309	BC079905	***Grem2***	gremlin 2 homolog
310	DQ193535	***Grid2ip***	alt '-'
311	AK029845	***Grip1***	adult male testis
312	BC141514	***Gsdmc***	gasdermin C1
313	BC113155	***Gsdmc2***	gasdermin C2
314	BC061134	***Gsta1***	glutathione S-transferase
315	BC031818	***Gstm6***	glutathione S-transferase
316	BC085165	***Gsto1***	glutathione S-transferase omega 1
317	AK082488	***Gtf2ird2***	0 day neonate cerebellum
318	AK041058	***Gusb***	adult male aorta and vein
319	BC146408	***H2-M9***	histocompatibility 2, M region locus 9
320	BC042677	***H6pd***	hexose-6-phosphate dehydrogenase (glucose 1-dehydrogenase)
321	BC089607	***Hbegf***	heparin-binding EGF-like growth factor
322	BC010478	***Hck***	hemopoietic cell kinase
323	BC007469	***Hcls1***	hematopoietic cell specific Lyn substrate 1
324	BC052833	***Hdc***	histidine decarboxylase
325	BC113773	***Hhipl1***	RIKEN 1600002O04 gene
326	AK017853	***Hif1a***	8 days embryo whole body
327	BC090259	***Higd1a***	HIG1 domain family, member 1A
328	BC085085	***Hmga2***	high mobility group AT-hook 2
329	BC010757	***Hmox1***	heme oxygenase (decycling) 1
330	BC095961	***Homer3***	homer homolog 3 (Drosophila)
331	AK143943	***Hoxa1***	adult male kidney
332	BC096612	***Hoxa3***	homeo box A3
333	AK087283	***Hpse***	0 day neonate lung
334	AK083281	***Hs6st2***	adult male hippocampus
335	DQ266428	***Hspg2***	perlecan
336	BC119129	***Htr1b***	5-hydroxytryptamine (serotonin) receptor 1B
337	BC108972	***Htr2a***	5-hydroxytryptamine (serotonin) receptor 2A
338	BC008626	***Icam1***	intercellular adhesion molecule
339	BC006950	***Ier3***	immediate early response 3
340	BC018233	***Ifi202b***	interferon activated gene 202B
341	BC043935	***Ifnar1***	interferon (alpha and beta) receptor 1
342	BC071225	***Ifnar2***	interferon (alpha and beta) receptor 2
343	AK044984	***Igf2bp2***	9.5 days embryo parthenogenote
344	BC052425	***Il13ra1***	interleukin 13 receptor, alpha 1
345	BC003723	***Il13ra2***	interleukin 13 receptor, alpha 2
346	BC120598	***Il18rap***	interleukin 18 receptor accessory protein
347	BC003727	***Il1a***	interleukin 1 alpha
348	BC132600	***Il1f5***	interleukin 1 family, member 5 (delta)
349	AK081783	***Il1f9***	16 days embryo head
350	BC051445	***Il1rl1***	interleukin 1 receptor-like 1
351	BC019953	***Il23a***	interleukin 23, alpha subunit p19
352	AF235006	***Il24***	melanoma differentiation associated gene-7
353	AK075849	***Il33***	adult male stomach
354	BC112911	***Il4ra***	interleukin 4 receptor, alpha

…Table 3.6 continued on next page.

Table 3.6 (continued…)

	GenBank ID	Gene Name	Roche NimbleGen Annotation
355	BC053416	***Impdh1***	inosine 5'-phosphate dehydrogenase 1
356	BC053527	***Inhba***	inhibin beta-A
357	AK050913	***Iqgap3***	9 days embryo whole body
358	BC085324	***Irak2***	interleukin-1 receptor-associated kinase 2
359	BC031424	***Isg15***	ISG15 ubiquitin-like modifier
360	AF217484	***Isg20***	DnaQL
361	AK137169	***Itga1***	adult male urinary bladder
362	BC050943	***Itga5***	integrin alpha 5 (fibronectin receptor alpha)
363	AK159653	***Itga6***	osteoclast-like cell
364	AK089521	***Itgam***	B6-derived CD11 +ve dendritic cells (CD11B)
365	AK135521	***Itgb1***	12 days embryo female mullerian duct includes surrounding region
366	BC145644	***Itgb2***	integrin beta 2 (LFA-1)
367	BC125518	***Itgb3***	integrin beta 3
368	AF115376	***Itgb6***	integrin beta-6 subunit
369	BC054807	***Jak2***	Janus kinase 2
370	AK088365	***Jak3***	2 days neonate thymus thymic cells
371	BC004629	***Kcne3***	potassium voltage-gated channel
372	BC003729	***Kcnk1***	potassium channel
373	AK158645	***Kcnk13***	visual cortex
374	AK135059	***Kcnq2***	adult male olfactory brain
375	BC028748	***Kctd4***	potassium channel tetramerisation domain containing 4
376	BC020530	***Kdr***	kinase insert domain protein receptor
377	AK077868	***Kif17***	13 days embryo forelimb
378	BC120791	***Kif26b***	RIKEN D230039L06 gene
379	AK150559	***Klf7***	bone marrow macrophage
380	AK009217	***Klk12***	adult male tongue
381	BC152778	***Klk13***	kallikrein related-peptidase 13
382	BC031119	***Klk6***	kallikrein 6
383	BC055895	***Klk8***	kallikrein related-peptidase 8
384	BC109326	***Klk9***	kallikrein related-peptidase 9
385	BC064711	***Klra2***	killer cell lectin-like receptor, subfamily A
386	BC103666	***Krt16***	keratin 16
387	BC119554	***Krt6b***	keratin 6B
388	BC043030	***Krtcap2***	keratinocyte associated protein 2
389	BC025901	***Lair1***	leukocyte-associated Ig-like receptor 1
390	X84013	***Lama3***	laminin-5, alpha3A chain
391	BC115942	***Lama4***	laminin, alpha 4
392	BC140417	***Lamc2***	laminin, gamma 2
393	AF257136	***Lat2***	Wbscr15 protein (Wbscr15)
394	BC146004	***Lce1g***	late cornified envelope 1G
395	XM_001478521	***Lce1k***	LOC631101 (LOC631101)
396	BC100538	***Lce3a***	late cornified envelope 3A
397	BC115817	***Lce3b***	late cornified envelope 3B
398	BC119239	***Lce3c***	late cornified envelope 3C
399	BC132069	***Lcn2***	lipocalin 2
400	BC006948	***Lcp2***	lymphocyte cytosolic protein 2
401	BC053041	***Ldlr***	low density lipoprotein receptor
402	BC003754	***Lgals9***	lectin, galactose binding
403	AK148104	***Lgmn***	B16 F10Y cells
404	AK052969	***Lhfpl2***	15 days embryo head
405	BC005621	***Lims1***	LIM and senescent cell antigen-like domains 1
406	AK164007	***Lipa***	7 days embryo whole body
407	XM_001471956	***LOC100038947***	similar to SIRP beta 1 cell surface protein (LOC100038947)
408	XM_994308	***LOC668101***	similar to SIRP beta 1 (LOC668101)

…Table 3.6 continued on next page.

Table 3.6 (continued…)

	GenBank ID	Gene Name	Roche NimbleGen Annotation
409	BC086801	***Loxl2***	lysyl oxidase-like 2
410	BC011298	***Loxl3***	lysyl oxidase-like 3
411	AK076555	***Lrp8***	adult male testis
412	BC025473	***Lrrc8c***	leucine rich repeat containing 8 family
413	AF000428	***Lst1***	B144
414	BC064063	***Ltb4r1***	leukotriene B4 receptor 1
415	BC119785	***Ltbp2***	latent transforming growth factor beta binding protein 2
416	BC025135	***Ly6d***	lymphocyte antigen 6 complex, locus D
417	NM_001111096	***Lyn***	Yamaguchi sarcoma viral (v-yes-1) oncogene homolog (Lyn)
418	BC058581	***Maged2***	melanoma antigen
419	BC113154	***Mal2***	mal, T-cell differentiation protein 2
420	AK129191	***Map4k4***	mKIAA0687 protein.
421	BC048779	***Mapk6***	mitogen-activated protein kinase 6
422	BC132338	***Marco***	macrophage receptor with collagenous structure
423	AB049755	***Masp1***	masp3 MBL-associated serine protease-3
424	AK046702	***Mast4***	4 days neonate male adipose
425	BC026985	***Mcam***	melanoma cell adhesion molecule
426	BC146373	***Mdfic***	MyoD family inhibitor domain containing
427	BC139762	***Mecom***	ecotropic viral integration site 1
428	BC108993	***Mefv***	Mediterranean fever
429	AF482999	***Mest***	mesoderm-specific transcript isoform 2 (Mest)
430	BC025131	***Mfap5***	microfibrillar associated protein 5
431	BC094604	***Mgat5b***	mannoside acetylglucosaminyltransferase 5
432	BC023755	***Mlkl***	mixed lineage kinase domain-like
433	BC130027	***Mmp10***	matrix metallopeptidase 10
434	BC125320	***Mmp13***	matrix metallopeptidase 13
435	AK136517	***Mmp19***	matrix metallopeptidase 19
436	BC042742	***Mmp8***	matrix metallopeptidase 8
437	BC132153	***Morc4***	microrchidia 4
438	AK150204	***Mov10***	bone marrow macrophage
439	AK165261	***Mpp1***	6 days neonate spleen
440	BC060043	***Mrpl52***	mitochondrial ribosomal protein L52
441	XM_357051	***Ms4a14***	gene model 1276
442	BC027496	***Ms4a4c***	membrane-spanning 4-domains
443	BC018331	***Ms4a6d***	membrane-spanning 4-domains
444	BC047366	***Msn***	moesin
445	BC003814	***Msr1***	macrophage scavenger receptor 1
446	BC053039	***Mtap6***	microtubule-associated protein 6
447	AK151613	***Mtap7d1***	bone marrow macrophage
448	AK075931	***Mthfd1l***	ES cells
449	NM_010846	***Mx1***	myxovirus (influenza virus) resistance 1 (Mx1)
450	BC002140	***Mxra8***	matrix-remodelling associated 8
451	NM_001093764	***Myadm***	myeloid-associated differentiation marker (Myadm)
452	BC096559	***Myct1***	myc target 1
453	BC005591	***Myd88***	myeloid differentiation primary response gene 88
454	AK012133	***Myef2***	10 days embryo whole body
455	AK036840	***Myo1f***	adult female vagina
456	AY821853	***Myo7a***	myosin VIIA
457	AK086107	***Myof***	15 days embryo head
458	AF192382	***N/A***	prion protein-like protein
459	BC116626	***Naip2***	NLR family, apoptosis inhibitory protein 2
460	AK158038	***Nav1***	adult inner ear
461	AK122404	***Nav3***	mKIAA0938 protein.
462	X15052	***Ncam1***	Mouse 3'-end of NCAM-140 and NCAM-180 isoforms.

…Table 3.6 continued on next page.

Table 3.6 (continued…)

	GenBank ID	Gene Name	Roche NimbleGen Annotation
463	AK170854	***Ncf4***	NOD-derived CD11c +ve dendritic cells
464	AK129207	***Nfasc***	mKIAA0756 protein.
465	AK029360	***Nfe2l2***	0 day neonate head
466	AK155969	***Nfkbid***	activated spleen
467	AB047549	***Nfkbiz***	IkappaB-zeta
468	BC156604	***Ngf***	nerve growth factor
469	BC120715	***Niacr1***	G protein-coupled receptor 109A
470	BC131669	***Nid1***	nidogen 1
471	BC054746	***Nid2***	nidogen 2
472	BC116391	***Nkain1***	Na+/K+ transporting ATPase interacting 1
473	BC116175	***Nlrp3***	NLR family, pyrin domain containing 3
474	BC062378	***Nos2***	nitric oxide synthase 2, inducible
475	AK141037	***Nrg1***	0 day neonate cerebellum
476	BC008272	***Nsg1***	neuron specific gene family member 1
477	BC031848	***Nsmce1***	non-SMC element 1 homolog (S. cerevisiae)
478	NM_001085502	***Nt5c1a***	5'-nucleotidase, cytosolic IA (Nt5c1a)
479	BC003223	***Nus1***	nuclear undecaprenyl pyrophosphate synthase 1 homolog (S. cerevisiae)
480	BC025514	***Oaf***	OAF homolog (Drosophila)
481	BC013715	***Oas1a***	2'-5' oligoadenylate synthetase 1A
482	AK049218	***Oas2***	ES cells
483	AK158392	***Oas3***	adult inner ear
484	AF426289	***Oasl1***	oligoadenylate synthetase-like protein-2
485	AK135844	***Odz3***	in vitro fertilized eggs
486	BC026021	***Opn1sw***	opsin 1 (cone pigments), short-wave-sensitive
487	BC099866	***Osm***	oncostatin M
488	BC119043	***P2ry13***	purinergic receptor P2Y, G-protein coupled 13, G-protein coupled 13
489	BC082538	***P4ha3***	procollagen-proline, 2-oxoglutarate 4-dioxygenase (proline 4-hydroxylase)
490	AK005563	***Parp14***	adult female placenta
491	BC156141	***Pcdh12***	protocadherin 12
492	BC042454	***Pcdh21***	protocadherin 21
493	BC013068	***Pcsk5***	proprotein convertase subtilisin/kexin type 5
494	BC031778	***Pctk2***	PCTAIRE-motif protein kinase 2
495	AK039249	***Pde10a***	adult male spinal cord
496	AK004772	***Pde1b***	adult male lung
497	BC071259	***Pde4b***	phosphodiesterase 4B, cAMP specific
498	AK035501	***Pdgfra***	adult male urinary bladder
499	BC009151	***Pdia5***	protein disulfide isomerase associated 5
500	BC026551	***Pdpn***	podoplanin
501	AK169431	***Pecam1***	17 days embryo stomach
502	BC020097	***Pfkl***	phosphofructokinase, liver
503	BC016567	***Pgf***	placental growth factor
504	BC128291	***Pglyrp3***	peptidoglycan recognition protein 3
505	BC120840	***Pglyrp4***	peptidoglycan recognition protein 4
506	BC023843	***Picalm***	phosphatidylinositol binding clathrin assembly protein
507	BC113141	***Pik3ap1***	phosphoinositide-3-kinase adaptor protein 1
508	AK089348	***Pik3r5***	B6-derived CD11 +ve dendritic cells
509	AK083076	***Pkm2***	12 days embryo spinal cord
510	AK004232	***Pla2g2d***	18-day embryo whole body
511	BC113770	***Pla2g4d***	phospholipase A2
512	BC060600	***Pla2g4e***	phospholipase A2
513	BC011256	***Plat***	plasminogen activator, tissue
514	BC120709	***Plau***	plasminogen activator, urokinase

…Table 3.6 continued on next page.

Table 3.6 (continued…)

	GenBank ID	Gene Name	Roche NimbleGen Annotation
515	U87868	***Pld1***	phosphatidylcholine-specific phospholipase D1b (mPLD1)
516	BC047268	***Pld2***	phospholipase D2
517	AK038804	***Plek***	adult male hypothalamus
518	BC024792	***Plekhg4***	pleckstrin homology domain containing, family G (with RhoGef domain)
519	AK158288	***Plekho2***	adult inner ear
520	BC054766	***Plin2***	adipose differentiation related protein
521	BC050821	***Pmaip1***	phorbol-12-myristate-13-acetate-induced protein 1
522	BC031449	***Postn***	periostin, osteoblast specific factor
523	AK042123	***Ppp1r16b***	3 days neonate thymus
524	AK169990	***Pram1***	NOD-derived CD11c +ve dendritic cells
525	BC003349	***Prdx4***	peroxiredoxin 4
526	BC033408	***Prei4***	preimplantation protein 4
527	BC119251	***Prelid2***	PRELI domain containing 2
528	AK043023	***Prnd***	7 days neonate cerebellum
529	BC117009	***Prss27***	protease, serine 27
530	BC075675	***Prss35***	protease, serine
531	BC087878	***Prss46***	RIKEN 1700112C13 gene
532	AK163576	***Prune2***	adult male corpora quadrigemina
533	BC110462	***Psca***	prostate stem cell antigen
534	BC024960	***Ptges***	prostaglandin E synthase
535	AK154272	***Ptgir***	NOD-derived CD11c +ve dendritic cells
536	BC052900	***Ptgs2***	prostaglandin-endoperoxide synthase 2
537	BC020155	***Ptplad2***	protein tyrosine phosphatase-like A domain containing 2
538	BC079621	***Ptprm***	protein tyrosine phosphatase, receptor type
539	BC013673	***Pvr***	poliovirus receptor
540	AK010185	***Pxdn***	adult male tongue
541	BC013063	***Rab31***	RAB31, member RAS oncogene family
542	BC132022	***Raet1b***	retinoic acid early transcript beta
543	NM_009018	***Raet1c***	retinoic acid early transcript gamma (Raet1c)
544	BC132308	***Raet1e***	retinoic acid early transcript 1E
545	BC006907	***Ralb***	v-ral simian leukemia viral oncogene homolog B (ras related)
546	AK161416	***Rbms1***	adult male testis
547	BC125551	***Rbp2***	retinol binding protein 2, cellular
548	AK217036	***Rcbtb2***	clone:Y2G0140G19
549	BC014821	***Renbp***	renin binding protein
550	AK078208	***Rgs20***	adult male olfactory brain
551	BC004627	***Rhoc***	ras homolog gene family, member C
552	BC058162	***Ripk1***	receptor (TNFRSF)-interacting serine-threonine kinase 1
553	BC003873	***Rnasel***	ribonuclease L (2', 5'-oligoisoadenylate synthetase-dependent)
554	BC048531	***Rnd1***	Rho family GTPase 1
555	XM_001477846	***Rnf213***	LOC672511 (LOC672511)
556	BC057868	***Rsad2***	radical S-adenosyl methionine domain containing 2
557	BC024872	***Rtp4***	receptor transporter protein 4
558	AK143826	***S100a9***	6 days neonate spleen
559	BC064007	***S1pr3***	endothelial differentiation, sphingolipid G-protein-coupled receptor
560	BC119383	***Samd12***	sterile alpha motif domain containing 12
561	AK152815	***Samhd1***	bone marrow macrophage
562	BC054795	***Sdc3***	syndecan 3
563	NM_001098227	***Sdcbp***	syndecan binding protein (Sdcbp)
564	AK031307	***Sema6d***	13 days embryo male testis
565	BC037673	***Sept4***	septin 4
566	BC062134	***Serpinb12***	serine (or cysteine) peptidase inhibitor, clade B

…Table 3.6 continued on next page.

Table 3.6 (continued…)

	GenBank ID	Gene Name	Roche NimbleGen Annotation
567	BC054091	***Serpine1***	serine (or cysteine) peptidase inhibitor, clade E
568	BC044853	***Sestd1***	SEC14 and spectrin domains 1
569	AF325264	***Sfxn5***	sideroflexin 5 (Sfxn5) precursor RNA
570	NM_001099631	***Sh2d5***	SH2 domain containing 5 (Sh2d5)
571	AK156912	***Sh3bp2***	activated spleen
572	AK159617	***Sirpa***	osteoclast-like cell
573	AK076000	***Skap2***	10 days embryo whole body
574	BC030031	***Slamf6***	SLAM family member 6
575	BC109137	***Slc11a1***	solute carrier family 11 (proton-coupled divalent metal ion transporters)
576	BC080678	***Slc16a2***	solute carrier family 16 (monocarboxylic acid transporters)
577	BC046525	***Slc16a3***	solute carrier family 16 (monocarboxylic acid transporters)
578	AK079757	***Slc16a5***	0 day neonate thymus
579	AK089184	***Slc20a1***	NOD-derived CD11c +ve dendritic cells
580	BC010472	***Slc28a3***	solute carrier family 28 (sodium-coupled nucleoside transporter)
581	BC055340	***Slc2a1***	solute carrier family 2 (facilitated glucose transporter)
582	BC058811	***Slc2a3***	solute carrier family 2 (facilitated glucose transporter)
583	BC063326	***Slc37a2***	solute carrier family 37 (glycerol-3-phosphate transporter)
584	BC003845	***Slc5a1***	solute carrier family 5 (sodium/glucose cotransporter)
585	AK077593	***Slc7a3***	8 days embryo whole body
586	BC079673	***Slc8a1***	solute carrier family 8 (sodium/calcium exchanger)
587	BC052869	***Slfn1***	schlafen 1
588	BC141535	***Slfn10***	schlafen 10 (Slfn10)
589	BC132627	***Slfn3***	schlafen 3
590	AK050355	***Slfn9***	adult male liver tumor
591	BC029097	***Smurf1***	SMAD specific E3 ubiquitin protein ligase 1
592	AK138230	***Snph***	adult male hypothalamus
593	AK150878	***Snx10***	bone marrow macrophage
594	BC052031	***Socs3***	suppressor of cytokine signaling 3
595	BC119067	***Sox15***	SRY-box containing gene 15
596	AK146054	***Sp100***	14 days pregnant adult female placenta
597	AK006861	***Spata6***	adult male testis
598	BC014764	***Spats2l***	RIKEN 2810022L02 gene
599	BC020531	***Spon1***	spondin 1, (f-spondin) extracellular matrix protein
600	BC062119	***Spred3***	sprouty-related, EVH1 domain containing 3
601	BC119288	***Sprr1b***	small proline-rich protein 1B
602	BC010818	***Sprr2a***	small proline-rich protein 2A
603	BC099393	***Sprr2a3***	small proline-rich protein 2A
604	BC132518	***Sprr2b***	small proline-rich protein 2B
605	BC130233	***Sprr2g***	small proline-rich protein 2G
606	BC037076	***Srgn***	serglycin
607	BC028307	***Srpx2***	sushi-repeat-containing protein, X-linked 2
608	BC049247	***Stab1***	stabilin 1
609	AB010122	***Stambpl1***	AMSH-LP
610	AK157263	***Stat1***	activated spleen
611	BC119354	***Stfa2l1***	stefin A2 like 1
612	BC107224	***Stfa3***	stefin A3
613	BC003789	***Stom***	stomatin
614	XM_001472888	***Stx11***	syntaxin 11 (Stx11)
615	BC034547	***Sulf1***	sulfatase 1
616	AK045217	***Svep1***	9.5 days embryo parthenogenote
617	AK049207	***Syk***	ES cells
618	NM_177340	***Synpo***	synaptopodin (Synpo), transcript variant A

…Table 3.6 continued on next page.

Table 3.6 (continued…)

	GenBank ID	Gene Name	Roche NimbleGen Annotation
619	BC145691	***Tbx18***	T-box18
620	BC029014	***Tbxas1***	thromboxane A synthase 1, platelet
621	BC119346	***Tcf23***	transcription factor 23
622	BC098494	***Tcfec***	transcription factor EC
623	AF218254	***Tcirg1***	vacuolar proton-translocating ATPase 100 kDa subunit isoform a3
624	BC010465	***Tes***	testis derived transcript
625	AF016313	***Tfpi***	TFPIbeta (TFPIbeta)
626	BC021639	***Tfpi2***	tissue factor pathway inhibitor 2
627	BC013738	***Tgfb1***	transforming growth factor, beta 1
628	DQ143894	***Tgfb1i1***	transforming growth factor beta 1 isoform alpha-C (Tgfb1i1)
629	BC019154	***Thbd***	thrombomodulin
630	BC053702	***Thbs2***	thrombospondin 2
631	BC046452	***Tie1***	tyrosine kinase receptor 1
632	BC005738	***Tinagl1***	tubulointerstitial nephritis antigen-like
633	BC068173	***Tiparp***	TCDD-inducible poly(ADP-ribose) polymerase
634	AK052301	***Tln2***	13 days embryo heart
635	AK143721	***Tlr1***	6 days neonate spleen
636	BC117913	***Tlr13***	toll-like receptor 13
637	AK154253	***Tlr6***	NOD-derived CD11c +ve dendritic cells
638	BC120596	***Tlr7***	toll-like receptor 7
639	XM_205829	***Tm4sf19***	transmembrane 4 L six family member 19 (Tm4sf19)
640	BC025600	***Tmem119***	transmembrane protein 119
641	AK158458	***Tmem173***	adult inner ear
642	BC132482	***Tmem202***	RIKEN 4930425N13 gene
643	AK045675	***Tmem44***	adult male corpora quadrigemina
644	BC018222	***Tmem45b***	transmembrane protein 45b
645	BC004013	***Tmem49***	transmembrane protein 49
646	BC003277	***Tmem51***	transmembrane protein 51
647	NM_001085521	***Tmem90b***	predicted gene
648	BC115419	***Tmprss11b***	transmembrane protease, serine 11b
649	BC117057	***Tnf***	tumor necrosis factor
650	AK170719	***Tnfaip2***	NOD-derived CD11c +ve dendritic cells
651	BC021155	***Tnfaip6***	tumor necrosis factor alpha induced protein 6
652	AK170464	***Tnfrsf1b***	NOD-derived CD11c +ve dendritic cells
653	AY165627	***Tnfrsf22***	decoy TRAIL receptor 2 long form (Dctrailr2)
654	BC106828	***Tnfrsf23***	tumor necrosis factor receptor superfamily, member 23
655	BC152358	***Tnfrsf26***	tumor necrosis factor receptor superfamily, member 26
656	BC014809	***Tpm2***	tropomyosin 2, beta
657	AF317223	***Tpm3***	tropomyosin 3
658	BC058239	***Tpp2***	tripeptidyl peptidase II
659	BC012401	***Tram1***	translocating chain-associating membrane protein 1
660	BC018212	***Tram2***	translocating chain-associating membrane protein 2
661	BC033485	***Trem2***	triggering receptor expressed on myeloid cells 2
662	AY465532	***Treml4***	alt '5031403H21Rik#BB137214#IDCP1#TLT4#Treml3'
663	BC006908	***Trim25***	tripartite motif protein 25
664	AK142316	***Trp53i11***	13 days embryo heart
665	AK134735	***Trpm2***	adult male medulla oblongata
666	AK053973	***Tsku***	2 days pregnant adult female oviduct
667	BC130230	***Tslp***	thymic stromal lymphopoietin
668	BC002055	***Tspo***	translocator protein
669	BC056616	***Ttc12***	tetratricopeptide repeat domain 12
670	BC156421	***Ttc37***	tetratricopeptide repeat domain 37
671	AK007856	***Ttc39b***	10 day old male pancreas
672	BC015081	***Twf1***	twinfilin, actin-binding protein

…Table 3.6 continued on next page.

Table 3.6 (continued…)

	GenBank ID	Gene Name	Roche NimbleGen Annotation
673	BC053436	***Ubash3b***	RIKEN 2810457I06 gene
674	BC050828	***Ugcg***	UDP-glucose ceramide glucosyltransferase
675	BC006749	***Ugdh***	UDP-glucose dehydrogenase
676	NM_029975	***Ulbp1***	UL16 binding protein 1 (Ulbp1)
677	AY771616	***Umodl1***	alt 'D17Ertd488e'
678	AK039526	***Unc93b1***	adult male spinal cord
679	BC086688	***Vash1***	vasohibin 1
680	AK157021	***Vasp***	activated spleen
681	AK169478	***Vav1***	3 days neonate thymus
682	AK016465	***Vcam1***	adult male testis
683	AK014525	***Vcan***	0 day neonate skin
684	BC008520	***Vcl***	vinculin
685	AY263146	***Vegfa***	FVB/N vascular endothelial growth factor A splice variant VEGF 102
686	BC052677	***Wisp1***	WNT1 inducible signaling pathway protein 1
687	BC020033	***Zbp1***	Z-DNA binding protein 1
688	AK143568	***Zc3hav1***	6 days neonate spleen
689	BC052028	***Zfp57***	zinc finger protein 57
690	BC050889	***Zic1***	zinc finger protein of the cerebellum 1
691	AK163477	***Zic4***	adult male corpora quadrigemina

END Table 3.6.

Table 3.7: Overlapping skin-selective IRITs and the kidney-selective IRITs gene ontology (GO) annotations within biological process, molecular function and cellular compartment categories. *P*-value is representative of a hypergeometric test from selecting the skin or kidney IRITs found within each GO category by chance alone. (Table continued on next page.)

			Skin-selective IRITs			Kidney-selective IRITs		
Term (Biological Process Category)		**Genes in Category**	**Genes in IRITs in Category**	**% of Genes in IRITs in Category**	***p*-value**	**Genes in IRITs in Category**	**% of Genes in IRITs in Category**	***p*-value**
GO:0009611	response to wounding	347	52	7.5	0.000	36	7.0	0.000
GO:0006952	defense response	448	57	8.3	0.000	30	5.8	0.000
GO:0006954	inflammatory response	225	40	5.8	0.000	23	4.5	0.000
GO:0006928	cell motion	367	42	6.1	0.000	21	4.1	0.005
GO:0016477	cell migration	240	32	4.6	0.000	17	3.3	0.002
GO:0048870	cell motility	284	33	4.8	0.000	17	3.3	0.009
GO:0051674	localization of cell	284	33	4.8	0.000	17	3.3	0.009
GO:0001817	regulation of cytokine production	139	22	3.2	0.000	12	2.3	0.002
GO:0006935	chemotaxis	109	19	2.8	0.000	8	1.6	0.039
GO:0042330	taxis	109	19	2.8	0.000	8	1.6	0.039
GO:0001944	vasculature development	250	29	4.2	0.000	23	4.5	0.000
GO:0001568	blood vessel development	244	28	4.1	0.000	22	4.3	0.000
GO:0050900	leukocyte migration	43	12	1.7	0.000	7	1.4	0.001
GO:0001525	angiogenesis	133	20	2.9	0.000	13	2.5	0.000
GO:0030595	leukocyte chemotaxis	27	10	1.4	0.000	5	1.0	0.007
GO:0060326	cell chemotaxis	27	10	1.4	0.000	5	1.0	0.007
GO:0048514	blood vessel morphogenesis	198	24	3.5	0.000	17	3.3	0.000
GO:0001775	cell activation	246	27	3.9	0.000	14	2.7	0.027
GO:0001819	positive regulation of cytokine production	62	13	1.9	0.000	7	1.4	0.009
GO:0045321	leukocyte activation	219	23	3.3	0.000	14	2.7	0.012
GO:0042060	wound healing	112	15	2.2	0.000	13	2.5	0.000
GO:0030334	regulation of cell migration	92	13	1.9	0.000	10	1.9	0.001
GO:0040012	regulation of locomotion	110	14	2.0	0.000	11	2.1	0.001
GO:0050764	regulation of phagocytosis	25	7	1.0	0.000	5	1.0	0.005

…Table 3.7 continued on next page.

Table 3.7: (continued…)

			Skin-selective IRITs			Kidney-selective IRITs		
		Genes in Category	Genes in IRITs in Category	% of Genes in IRITs in Category	*p*-value	Genes in IRITs in Category	% of Genes in IRITs in Category	*p*-value
GO:0051240	positive regulation of multicellular organismal process	163	17	2.5	0.000	14	2.7	0.001
GO:0044236	multicellular organismal metabolic process	26	7	1.0	0.000	5	1.0	0.006
GO:0016337	cell-cell adhesion	236	21	3.0	0.000	13	2.5	0.043
GO:0051130	positive regulation of cellular component organization	122	14	2.0	0.000	10	1.9	0.009
GO:0051270	regulation of cell motion	107	13	1.9	0.000	10	1.9	0.004
GO:0030155	regulation of cell adhesion	94	12	1.7	0.000	13	2.5	0.000
GO:0060429	epithelium development	271	22	3.2	0.001	16	3.1	0.013
GO:0060627	regulation of vesicle-mediated transport	83	11	1.6	0.001	7	1.4	0.033
GO:0032963	collagen metabolic process	23	6	0.9	0.001	5	1.0	0.004
GO:0009967	positive regulation of signal transduction	172	16	2.3	0.001	14	2.7	0.002
GO:0044259	multicellular organismal macromolecule metabolic process	24	6	0.9	0.001	5	1.0	0.005
GO:0006909	phagocytosis	49	8	1.2	0.002	6	1.2	0.013
GO:0030100	regulation of endocytosis	52	8	1.2	0.002	6	1.2	0.017
GO:0030574	collagen catabolic process	17	5	0.7	0.002	4	0.8	0.012
GO:0043122	regulation of I-kappaB kinase/NF-kappaB cascade	40	7	1.0	0.003	5	1.0	0.028
GO:0035295	tube development	264	20	2.9	0.003	18	3.5	0.002
GO:0010647	positive regulation of cell communication	189	16	2.3	0.003	15	2.9	0.001
GO:0035239	tube morphogenesis	171	15	2.2	0.003	13	2.5	0.004
GO:0044243	multicellular organismal catabolic process	18	5	0.7	0.003	4	0.8	0.014
GO:0002697	regulation of immune effector process	88	10	1.4	0.004	7	1.4	0.042
GO:0044057	regulation of system process	201	16	2.3	0.005	12	2.3	0.033

…Table 3.7 continued on next page.

Table 3.7: (continued…)

			Skin-selective IRITs			Kidney-selective IRITs		
		Genes in Category	Genes in IRITs in Category	% of Genes in IRITs in Category	*p*-value	Genes in IRITs in Category	% of Genes in IRITs in Category	*p*-value
GO:0048584	positive regulation of response to stimulus	186	15	2.2	0.006	15	2.9	0.001
GO:0010627	regulation of protein kinase cascade	155	13	1.9	0.009	10	1.9	0.037
GO:0008219	cell death	507	29	4.2	0.012	25	4.9	0.013
GO:0032680	regulation of tumor necrosis factor production	27	5	0.7	0.014	5	1.0	0.007
GO:0016265	death	519	29	4.2	0.017	26	5.1	0.009
GO:0045785	positive regulation of cell adhesion	43	6	0.9	0.017	10	1.9	0.000
GO:0050778	positive regulation of immune response	136	11	1.6	0.022	10	1.9	0.018
GO:0043123	positive regulation of I-kappaB kinase/NF-kappaB cascade	33	5	0.7	0.028	5	1.0	0.015
GO:0002684	positive regulation of immune system process	206	14	2.0	0.030	12	2.3	0.038
GO:0001763	morphogenesis of a branching structure	125	10	1.4	0.032	10	1.9	0.011
GO:0042981	regulation of apoptosis	553	29	4.2	0.034	27	5.3	0.011
GO:0060322	head development	21	4	0.6	0.036	4	0.8	0.022
GO:0007596	blood coagulation	70	7	1.0	0.036	7	1.4	0.016
GO:0050817	coagulation	70	7	1.0	0.036	7	1.4	0.016
GO:0051781	positive regulation of cell division	36	5	0.7	0.037	5	1.0	0.020
GO:0007599	hemostasis	71	7	1.0	0.038	7	1.4	0.017
GO:0043067	regulation of programmed cell death	560	29	4.2	0.039	27	5.3	0.012
GO:0010941	regulation of cell death	563	29	4.2	0.042	27	5.3	0.014
GO:0048754	branching morphogenesis of a tube	93	8	1.2	0.045	8	1.6	0.018

…Table 3.7 continued on next page.

Table 3.7: (continued…)

Term (Molecular Function Category)		Genes in Category	Skin-selective IRITs: Genes in IRITs in Category	Skin-selective IRITs: % of Genes in IRITs in Category	Skin-selective IRITs: *p*-value	Kidney-selective IRITs: Genes in IRITs in Category	Kidney-selective IRITs: % of Genes in IRITs in Category	Kidney-selective IRITs: *p*-value
GO:0001871	pattern binding	128	20	2.9	0.000	20	3.9	0.000
GO:0003779	actin binding	288	21	3.0	0.003	24	4.7	0.000
GO:0004857	enzyme inhibitor activity	243	18	2.6	0.006	16	3.1	0.005
GO:0004866	endopeptidase inhibitor activity	161	15	2.2	0.002	12	2.3	0.008
GO:0005201	extracellular matrix structural constituent	30	5	0.7	0.020	9	1.8	0.000
GO:0005509	calcium ion binding	840	61	8.8	0.000	52	10.1	0.000
GO:0005539	glycosaminoglycan binding	114	16	2.3	0.000	19	3.7	0.000
GO:0008092	cytoskeletal protein binding	414	26	3.8	0.007	26	5.1	0.000
GO:0008201	heparin binding	83	8	1.2	0.027	13	2.5	0.000
GO:0030246	carbohydrate binding	317	34	4.9	0.000	30	5.8	0.000
GO:0030247	polysaccharide binding	128	20	2.9	0.000	20	3.9	0.000
GO:0030414	peptidase inhibitor activity	176	16	2.3	0.001	12	2.3	0.014

Term (Cellular Component Category)		Genes in Category	Skin-selective IRITs: Genes in IRITs in Category	Skin-selective IRITs: % of Genes in IRITs in Category	Skin-selective IRITs: *p*-value	Kidney-selective IRITs: Genes in IRITs in Category	Kidney-selective IRITs: % of Genes in IRITs in Category	Kidney-selective IRITs: *p*-value
GO:0005578	proteinaceous extracellular matrix	297	36	5.2	0.000	45	8.8	0.000
GO:0031012	extracellular matrix	309	37	5.4	0.000	46	9.0	0.000
GO:0044420	extracellular matrix part	92	14	2.0	0.000	22	4.3	0.000
GO:0044421	extracellular region part	774	80	11.6	0.000	73	14.2	0.000

END Table 3.7.

Table 3.8: 465 unique skin-associated transcripts and their annotation, listed in alphabetical order by Gene Name. (Table continued on next page.)

	GenBank ID	Gene Name	Roche NimbleGen Annotation
1	AK028217	***0610010O12Rik***	embryo whole body
2	XM_001474332	***1110025L11Rik***	RIKEN 1110025L11 gene (1110025L11Rik)
3	BC107298	***1700021C14Rik***	RIKEN 1700021C14 gene
4	BC025637	***1700029G01Rik***	RIKEN 1700029G01 gene
5	AK039052	***2010300C02Rik***	adult male hypothalamus
6	BC065789	***2310007H09Rik***	RIKEN 2310007H09 gene
7	BC043033	***2310057J16Rik***	RIKEN 2310057J16 gene
8	BC133700	***2310061N02Rik***	RIKEN 2310061N02 gene
9	AK019114	***2400009B08Rik***	ES cells
10	BC052467	***2410066E13Rik***	RIKEN 2410066E13 gene
11	BC099613	***2610019F03Rik***	RIKEN 2610019F03 gene
12	AK162965	***2610507I01Rik***	adult male spinal cord
13	BC013800	***2810432L12Rik***	RIKEN 2810432L12 gene
14	AK015576	***4930474M22Rik***	adult male testis
15	BC085508	***4930481A15Rik***	RIKEN 4930481A15 gene
16	BC049703	***4933411K16Rik***	RIKEN 4933411K16 gene
17	XM_001478748	***4933423P22Rik***	RIKEN 4933423P22 gene (4933423P22Rik)
18	BC060136	***4933431E20Rik***	RIKEN 4933431E20 gene
19	AK017319	***5430419D17Rik***	6 days neonate head
20	AK133718	***5430421N21Rik***	6 days neonate head
21	AK036974	***5930430L01Rik***	adult female vagina
22	NM_001101461	***9130204L05Rik***	RIKEN 9130204L05 gene (9130204L05Rik)
23	AK034141	***9330159F19Rik***	adult male diencephalon
24	XM_001471948	***A230103O09Rik***	RIKEN A230103O09 gene (A230103O09Rik)
25	BC075684	***A430105I19Rik***	RIKEN A430105I19 gene
26	BC096642	***A530016L24Rik***	RIKEN A530016L24 gene
27	AK040806	***A530026G17***	adult male aorta and vein
28	BC079617	***Abca3***	ATP-binding cassette, sub-family A (ABC1)
29	BC026770	***Abhd3***	abhydrolase domain containing 3
30	AK154494	***Ablim2***	NOD-derived CD11c +ve dendritic cells
31	BC019882	***Acaa1b***	acetyl-Coenzyme A acyltransferase 1B
32	AK008207	***Acbd4***	adult male small intestine
33	BC108959	***Acot10***	acyl-CoA thioesterase 10
34	BC030930	***Acss1***	acyl-CoA synthetase short-chain family member 1
35	BC080806	***Actr3***	ARP3 actin-related protein 3 homolog (yeast)
36	AK035798	***Actr3b***	16 days neonate cerebellum
37	AK142441	***Adam17***	13 days embryo stomach
38	BC013477	***Adh1***	alcohol dehydrogenase 1 (class I)
39	BC047267	***Adh7***	alcohol dehydrogenase 7 (class IV)
40	BC026584	***Adhfe1***	alcohol dehydrogenase, iron containing
41	BC028770	***Adipoq***	adiponectin, C1Q and collagen domain containing

…Table 3.8 continued on next page.

Table 3.8: (continued…)

	GenBank ID	Gene Name	Roche NimbleGen Annotation
42	BC052061	***Aff3***	AF4/FMR2 family
43	AF057287	***Agfg1***	RAB/Rip protein
44	BC063086	***Agps***	alkylglycerone phosphate synthase
45	AK134826	***Agrn***	adult male medulla oblongata
46	AK144241	***Aldh3a1***	colon RCB-0549 Cle-H3
47	BC031148	***Aldh6a1***	aldehyde dehydrogenase family 6
48	BC013751	***Alox12e***	arachidonate lipoxygenase, epidermal
49	BC011110	***Amd1***	S-adenosylmethionine decarboxylase 1
50	NM_001110505	***Amy1***	amylase 1, salivary (Amy1)
51	M11896	***Amy2b***	Mouse pancreatic amylase B-1
52	BC140357	***Ang2***	angiogenin
53	BC023373	***Angptl7***	angiopoietin-like 7
54	AK144563	***Apol6***	adult male vesicular gland
55	AK037070	***Ar***	adult female vagina
56	AK039617	***Arhgap24***	adult male spinal cord
57	AK167978	***Arpc1b***	CRL-1722 L5178Y-R
58	BC060143	***Arpc5***	actin related protein 2/3 complex
59	BC052393	***Arvcf***	armadillo repeat gene deleted in velo-cardio-facial syndrome
60	BC013479	***AU018778***	expressed sequence AU018778
61	BC119613	***AY026312***	sequence AY026312
62	BC019406	***Bbox1***	butyrobetaine (gamma), 2-oxoglutarate dioxygenase 1
63	BC038904	***BC006965***	sequence BC006965
64	AK031825	***Bcas1***	adult male medulla oblongata
65	M99492	***Bche***	Mouse butyrylcholinesterase
66	BC003787	***Bckdha***	branched chain ketoacid dehydrogenase E1
67	BC036998	***Bdh2***	3-hydroxybutyrate dehydrogenase
68	AK147534	***Bmp1***	RIKEN full-length enriched library
69	BC013459	***Bmp4***	bone morphogenetic protein 4
70	BC011251	***C6***	complement component 6
71	BC058676	***Cachd1***	cache domain containing 1
72	BC056389	***Cacna2d2***	calcium channel, voltage-dependent
73	BC079837	***Cadm3***	immunoglobulin superfamily
74	BC054783	***Calcoco1***	calcium binding and coiled coil domain 1
75	BC016232	***Capza1***	capping protein (actin filament) muscle Z-line
76	AK051470	***Cbara1***	12 days embryo spinal ganglion
77	AK045714	***Cbx7***	adult male corpora quadrigemina
78	BC006583	***Ccdc136***	coiled-coil domain containing 136
79	BC096547	***Ccdc67***	coiled-coil domain containing 67
80	BC107226	***Ccl27a***	chemokine (C-C motif) ligand 27
81	AK011412	***Ccnd2***	10 days embryo whole body
82	NM_001097644	***Ccnyl1***	cyclin Y-like 1 (Ccnyl1)

…Table 3.8 continued on next page.

Table 3.8: (continued…)

	GenBank ID	Gene Name	Roche NimbleGen Annotation
83	AK007973	***Ccpg1***	10 day old male pancreas
84	AY072796	***Ccrl1***	chemokine receptor CCX CKR
85	BC054759	***Cd200***	Cd200 antigen
86	BC146457	***Cd207***	CD 207 antigen, Langerin (Langerhans cells)
87	BC141546	***Cd209b***	CD209b antigen, DC-SIGN
88	AK007638	***Cd209f***	10 day old male pancreas
89	AK137770	***Cd27***	16 days neonate thymus
90	AK135381	***Cd82***	12 days embryo female mullerian duct includes surrounding region
91	AK044291	***Cdc37l1***	adult retina
92	BC013638	***Cdo1***	cysteine dioxygenase 1
93	BC019198	***Ces3***	carboxylesterase 3
94	AK018143	***Cgn***	adult male medulla oblongata
95	BC099676	***Cidec***	cell death-inducing DFFA-like effector c
96	BC019860	***Cisd1***	CDGSH iron sulfur domain 1
97	BC010260	***Clca1***	chloride channel calcium activated 1
98	AK040195	***Clic5***	0 day neonate thymus
99	AB059646	***Clmn***	calmin isoform e calmin delta
100	BC053843	***Clstn1***	calsyntenin 1
101	BC079897	***Cltc***	clathrin, heavy polypeptide (Hc)
102	AK049730	***Cobl***	12 days embryo spinal cord
103	BC057648	***Col4a6***	collagen, type IV
104	BC085498	***Coro1c***	coronin, actin binding protein 1C
105	BC018397	***Crabp2***	cellular retinoic acid binding protein II
106	BC006668	***Crat***	carnitine acetyltransferase
107	BC116360	***Crip3***	cysteine-rich protein 3
108	BC094033	***Cryab***	crystallin, alpha B
109	BC045159	***Crym***	crystallin, mu
110	AK140960	***Ctnnd2***	16 days embryo head
111	AK081137	***Cttnbp2***	10 days neonate cerebellum
112	BC055353	***CU104690.1***	clone IMAGE:5054356
113	BC056974	***Cyfip2***	cytoplasmic FMR1 interacting protein 2
114	AK029227	***Cyp2b19***	0 day neonate head
115	BC013451	***Cyp2e1***	cytochrome P450
116	BC011089	***Cyp2f2***	cytochrome P450
117	NM_001100182	***Cyp2j12***	cytochrome P450
118	BC119556	***Cyp2j9***	cytochrome P450
119	BC051993	***Dab1***	disabled homolog 1 (Drosophila)
120	BC024378	***Dad1***	defender against cell death 1
121	BC116916	***Dapl1***	death associated protein-like 1
122	BC005583	***Darc***	Duffy blood group, chemokine receptor
123	BC022712	***Dci***	dodecenoyl-Coenzyme A delta isomerase (3,2 trans-enoyl-Coenyme A isomerase)

…Table 3.8 continued on next page.

Table 3.8: (continued…)

	GenBank ID	Gene Name	Roche NimbleGen Annotation
124	BC024380	***Defb1***	defensin beta 1
125	BC119422	***Defb6***	defensin beta 6
126	BC075715	***Dmpk***	dystrophia myotonica-protein kinase
127	AK122431	***Dock9***	mKIAA1058 protein.
128	AK168478	***Dynlt1***	13 days embryo liver
129	AJ537610	***Dyrk1b***	dual-specificity tyrosine-(Y)-phosphorylation regulated kinase 1b
130	BC044854	***E330016A19Rik***	RIKEN E330016A19 gene
131	BC140220	***Ear10***	eosinophil-associated, member 10
132	BC148661	***Ear3***	eosinophil-associated, member 3
133	BC117776	***Ear5***	eosinophil-associated, member 5
134	NM_001110195	***Echdc1***	enoyl Coenzyme A hydratase domain containing 1 (Echdc1)
135	BC065151	***Ecm2***	extracellular matrix protein 2
136	BC117702	***Egfl6***	EGF-like-domain
137	BC049160	***Elmod1***	ELMO domain containing 1
138	BC022911	***Elovl5***	ELOVL family member 5, elongation of long chain fatty acids (yeast)
139	BC041670	***Emp2***	epithelial membrane protein 2
140	AK177529	***Enpp2***	clone:Y0G0103A19
141	AJ245853	***Epb4.1l2***	partial 4.1G protein (Epb4.1l2 gene).
142	AK165783	***Epb4.1l4b***	adult male intestinal mucosa
143	BC057857	***Ephx1***	epoxide hydrolase 1
144	BC019558	***Erp44***	thioredoxin domain containing 4 (endoplasmic reticulum)
145	BC120890	***Extl1***	exostoses (multiple)-like 1
146	U61110	***Eya1***	Eya1 homolog
147	BC050213	***Fads6***	fatty acid desaturase domain family
148	BC010767	***Fah***	fumarylacetoacetate hydrolase
149	BC030182	***Fahd2a***	fumarylacetoacetate hydrolase domain containing 2A
150	BC038020	***Fam111a***	RIKEN 4632417K18 gene
151	BC093505	***Fam57b***	RIKEN 1500016O10 gene
152	BC005745	***Fam96a***	RIKEN 5730536A07 gene
153	BC027211	***Fbxo32***	F-box protein 32
154	AK077773	***Fcgbp***	adult male thymus
155	BC033436	***Fermt2***	pleckstrin homology domain containing, family C (with FERM domain)
156	BC048229	***Fgf10***	fibroblast growth factor 10
157	BC152852	***Fgf18***	fibroblast growth factor 18
158	BC119135	***Fgf22***	fibroblast growth factor 22
159	BC065069	***Fgfr2***	fibroblast growth factor receptor 2
160	L23636	***Flt3l***	Mouse flt3 ligand
161	AK135758	***Fmn1***	in vitro fertilized eggs
162	AK133675	***Fmo5***	adult male pituitary gland
163	AK081259	***Fyco1***	adult male corpus striatum

…Table 3.8 continued on next page.

Table 3.8: (continued…)

	GenBank ID	Gene Name	Roche NimbleGen Annotation
164	BC056990	***Gabbr1***	gamma-aminobutyric acid (GABA-B) receptor
165	AK082864	***Gas2l1***	ES cells
166	AK156634	***Gata3***	activated spleen
167	BC006663	***Gba***	glucosidase, beta
168	BC011148	***Gjb5***	gap junction protein, beta 5
169	AK143057	***Glb1l2***	0 day neonate eyeball
170	BC082561	***Glt8d2***	glycosyltransferase 8 domain containing 2
171	XM_001474426	***Gm10061***	similar to MGC58416 protein (LOC100040281)
172	XM_001474297	***Gm10228***	similar to keratin associated protein 6-1 (LOC100040214)
173	XM_001474256	***Gm10229***	similar to glycine tyrosine-rich hair keratin protein (LOC100040201)
174	XM_001474347	***Gm11563***	similar to Keratin associated protein 4-7 (LOC100040248)
175	XM_001474444	***Gm11564***	similar to 2300006N05Rik protein (LOC670496)
176	NM_001101613	***Gm11567***	similar to ultra-high sulphur keratin (LOC670533)
177	XM_001474404	***Gm11595***	similar to 2300006N05Rik protein (LOC100040276)
178	NM_001099311	***Gm11596***	novel member of the keratin associated protein 4 (Krtap4) family (LOC670464)
179	XM_001477787	***Gm11937***	similar to Krtap2-4 protein (LOC100041488)
180	BC118042	***Gm12568***	RIKEN 2810416G20 gene
181	NM_001085536	***Gm13178***	similar to arylacetamide deacetylase (LOC546849)
182	AK005520	***Gm13306***	adult female placenta
183	XM_001474208	***Gm13667***	protein LOC100040172 (LOC100040172)
184	XM_001481030	***Gm14066***	protein LOC100043792 (LOC100043792)
185	XM_891736	***Gm1614***	gene model 1614
186	XM_001472234	***Gm2069***	protein LOC100039151 (LOC100039151)
187	XM_001473717	***Gm2472***	protein LOC100039880 (LOC100039880)
188	XM_001474192	***Gm2640***	similar to Ubtf protein (LOC100040164)
189	XM_001474181	***Gm2692***	similar to MGC58416 protein (LOC100040288)
190	XM_001474233	***Gm2724***	similar to keratin associated protein 20-2 (LOC100040346)
191	XM_001474267	***Gm2740***	similar to MGC58416 protein (LOC100040374)
192	XM_001474343	***Gm2758***	similar to MGC58416 protein (LOC100040415)
193	XM_001474371	***Gm2764***	similar to MGC58416 protein (LOC100040425)
194	XM_001474418	***Gm2782***	similar to keratin associated protein 21-1 (LOC100040456)
195	XM_001475284	***Gm2957***	similar to Ubtf protein (LOC100040768)
196	XM_001480779	***Gm4552***	similar to keratin associated protein 5-5 (LOC100043616)
197	XM_001480790	***Gm4559***	protein LOC100043627 (LOC100043627)
198	XM_001480974	***Gm4653***	protein LOC100043795 (LOC100043795)
199	XM_001475540	***Gm5509***	similar to zinc finger
200	XM_990264	***Gm577***	LOC667386 (LOC667386)
201	XM_001472135	***Gm6127***	similar to dentin sialophosphoprotein precursor (LOC620104)
202	XM_896406	***Gm6217***	EG621362 (EG621362)

…Table 3.8 continued on next page.

Table 3.8: (continued…)

	GenBank ID	Gene Name	Roche NimbleGen Annotation
203	XM_897326	***Gm6358***	EG622794 (EG622794)
204	XM_897455	***Gm6381***	EG622998 (EG622998)
205	XM_897466	***Gm6383***	EG623011 (EG623011)
206	XM_897479	***Gm6385***	EG623026 (EG623026)
207	XM_897498	***Gm6388***	EG623049 (EG623049)
208	XM_890670	***Gm6525***	EG624713 (EG624713)
209	XM_001474703	***Gm7262***	EG639116 (EG639116)
210	XM_924640	***Gm7288***	EG640223 (EG640223)
211	XM_978919	***Gm7303***	EG640636 (EG640636)
212	XM_001474284	***Gm7304***	similar to MGC58416 protein (LOC640652)
213	XM_001474324	***Gm7305***	similar to MGC58416 protein (LOC640654)
214	XM_974788	***Gm7510***	EG665134 (EG665134)
215	XM_975463	***Gm7544***	similar to keratin associated protein 5-2 (LOC665225)
216	XM_975542	***Gm7548***	EG665236 (EG665236)
217	XM_978513	***Gm7735***	EG665661 (EG665661)
218	AK142214	***Gm8113***	13 days embryo heart
219	XM_001474147	***Gm9789***	ENSMUSG00000044227 (ENSMUSG00000044227)
220	XM_001477636	***Gm9790***	similar to hypoxia induced gene 1
221	XM_001474241	***Gm9829***	similar to sequence AY026312 (LOC100040191)
222	BC059712	***Gng13***	guanine nucleotide binding protein 13, gamma
223	AK168707	***Gsn***	16 days embryo kidney
224	BC003822	***Gstm1***	glutathione S-transferase, mu1
225	BC008206	***Gstm5***	glutathione S-transferase, mu 5
226	BC012254	***Gstt1***	glutathione S-transferase, theta 1
227	BC062201	***Gstt3***	glutathione S-transferase, theta 3
228	AB041613	***Gstz1***	brain
229	BC086927	***H2-Ke6***	H2-K region expressed gene 6
230	AK083190	***Hhip***	adult male hippocampus
231	BC132371	***Higd1a***	HIG1 domain family
232	BC057693	***Hlf***	hepatic leukemia factor
233	BC118008	***Hrnr***	hornerin
234	BC094508	***Hspa13***	stress 70 protein chaperone, microsome-associated
235	BC011219	***Hspb8***	heat shock protein 8
236	M83997	***Hspg2***	.
237	BC017372	***Htatip2***	HIV-1 tat interactive protein 2, homolog (human)
238	BC006921	***Id2***	inhibitor of DNA binding 2
239	NM_001110498	***Ifnar2***	interferon (alpha and beta) receptor 2 (Ifnar2)
240	BC053409	***Igh-6***	immunoglobulin heavy chain 6 (heavy chain of IgM)
241	BC145791	***Il10rb***	interleukin 10 receptor, beta
242	BC013518	***Inmt***	indolethylamine N-methyltransferase

…Table 3.8 continued on next page.

Table 3.8: (continued…)

	GenBank ID	Gene Name	Roche NimbleGen Annotation
243	AY162380	***Irak2***	interleukin-1 receptor-associated kinase 2c (Irak2)
244	BC156076	***Irs1***	insulin receptor substrate 1
245	AK077398	***Ism1***	6 days neonate head
246	BC058095	***Itga6***	integrin alpha 6
247	BC050906	***Itgb1***	integrin beta 1 (fibronectin receptor beta)
248	BC043314	***Itih5***	inter-alpha (globulin) inhibitor H5
249	AK049015	***Itpr1***	0 day neonate cerebellum
250	BC018325	***Ivd***	isovaleryl coenzyme A dehydrogenase
251	AK147945	***Kank1***	melanocyte
252	AK155095	***Kazald1***	NOD-derived CD11c +ve dendritic cells
253	BC033442	***Kcnj16***	potassium inwardly-rectifying channel, subfamily J
254	NM_001109040	***Kif21a***	kinesin family member 21A (Kif21a)
255	BC013486	***Klf15***	Kruppel-like factor 15
256	BC052438	***Kpnb1***	karyopherin (importin) beta 1
257	BC057934	***Krt15***	keratin 15
258	BC003472	***Krt23***	keratin 23
259	BC129847	***Krt24***	keratin 24
260	BC029257	***Krt33a***	keratin 33A
261	BC125420	***Krt34***	keratin 34
262	BC156168	***Krt72***	keratin 72
263	AF312018	***Krt81***	type II hair keratin
264	BC132658	***Krtap16-10***	keratin associated protein 16-10
265	BC156156	***Krtap16-8***	keratin associated protein 16-8
266	NM_001099774	***Krtap17-1***	keratin associated protein 17-1 (Krtap17-1)
267	XM_896462	***Krtap19-7***	EG621595
268	XM_897414	***Krtap20-2***	EG622935 (EG622935)
269	XM_897249	***Krtap22-2***	RIKEN 1110032D16 gene (1110032D16Rik)
270	XM_001477761	***Krtap2-4***	keratin associated protein 2-4 (Krtap2-4)
271	XM_896478	***Krtap28-10***	similar to keratin associated protein 5-2 (LOC621495)
272	D86424	***Krtap3-1***	high-sulfur keratin protein
273	BC117058	***Krtap3-2***	keratin associated protein 3-3
274	BC120760	***Krtap3-3***	keratin associated protein 3-3
275	BC016249	***Krtap4-16***	predicted gene
276	BC156698	***Krtap4-2***	keratin associated protein 4-2
277	NM_026834	***Krtap4-6***	RIKEN 1110054P19 gene (1110054P19Rik)
278	BC115508	***Krtap4-7***	keratin associated protein 4-7
279	NM_001085547	***Krtap4-8***	novel member of the keratin associated protein 4 (Krtap4) family (LOC665992)
280	NM_001085548	***Krtap4-9***	novel member of the keratin associated protein 4 (Krtap4) family (LOC665998)
281	BC156385	***Krtap5-1***	keratin associated protein 5-1
282	BC107313	***Krtap6-1***	keratin associated protein 6-1

…Table 3.8 continued on next page.

Table 3.8: (continued…)

	GenBank ID	Gene Name	Roche NimbleGen Annotation
283	XM_001474473	***Krtap7-1***	RIKEN 5430433J05 gene (5430433J05Rik)
284	AK133727	***Krtap8-1***	10 days neonate head
285	BC116210	***Krtap9-1***	keratin associated protein 9-1
286	BC030890	***Lgals12***	lectin, galactose binding
287	AK029526	***Lgals8***	adult male testis
288	BC055741	***Lhx2***	LIM homeobox protein 2
289	AK170166	***Limk1***	NOD-derived CD11c +ve dendritic cells
290	DQ003608	***Lims1***	LIM and senescent cell antigen-like domains 1
291	BC021642	***Lipe***	lipase
292	AK013259	***LOC100189605***	embryo whole body
293	AK051967	***Lrp4***	12 days embryo eyeball
294	AK008713	***Lrrc28***	adult male stomach
295	BC006877	***Lrrc59***	leucine rich repeat containing 59
296	AK157031	***Ltbp4***	activated spleen
297	BC115521	***Lxn***	latexin
298	AJ315547	***Ly6g6c***	truncated Ly6g6c protein (Ly6g6c gene), splice variant 2.
299	BC031461	***Maged1***	melanoma antigen, family D
300	AK036505	***Manba***	adult male bone
301	BC054754	***Map2k1***	mitogen activated protein kinase kinase 1
302	BC040381	***Map4k5***	mitogen-activated protein kinase kinase kinase kinase 5
303	AK075781	***Mcfd2***	10 day old male pancreas
304	BC111520	***Mgl2***	macrophage galactose N-acetyl-galactosamine specific lectin 2
305	BC057965	***Mgll***	monoglyceride lipase
306	BC027526	***Mlf1***	myeloid leukemia factor 1
307	AK160235	***Mmaa***	embryo whole body
308	BC013444	***Mpp1***	membrane protein, palmitoylated
309	AK161666	***Mpped2***	8 days embryo whole body
310	BC012221	***Mup1***	major urinary protein 1
311	AJ309921	***Mup10***	major urinary protein (group 1 major urinary protein gene).
312	AK013972	***Mup11***	13 days embryo head
313	XM_001472149	***Mup12***	similar to major urinary protein 1 (LOC100039054)
314	XM_001472190	***Mup13***	similar to major urinary protein 1 (LOC100039089)
315	XM_001472299	***Mup16***	similar to major urinary protein 1 (LOC100039177)
316	XM_001472354	***Mup17***	similar to major urinary protein 1 (LOC100039206)
317	XM_001472374	***Mup18***	similar to major urinary protein 1 (LOC100039228)
318	BC012259	***Mup2***	major urinary protein 2
319	BC132310	***Mup5***	major urinary protein 5
320	XM_001471958	***Mup9***	similar to major urinary protein 1 (LOC100038948)
321	BC048518	***N/A***	protein LOC622866
322	BC003307	***Nans***	N-acetylneuraminic acid synthase (sialic acid synthase)

…Table 3.8 continued on next page.

Table 3.8: (continued…)

	GenBank ID	Gene Name	Roche NimbleGen Annotation
323	AK049772	***Nfib***	12 days embryo spinal cord
324	AB196497	***Nfkbiz***	IkappaB-zeta IkappaB-zeta(D)
325	AK087325	***Nipal2***	0 day neonate lung
326	AK165116	***Nkd2***	2 days pregnant adult female ovary
327	BC002019	***Nmi***	N-myc (and STAT) interactor
328	AB004048	***Nnat***	neuronatin
329	AK079196	***Npr3***	adult male urinary bladder
330	BC060532	***Nrcam***	neuron-glia-CAM-related cell adhesion molecule
331	AK076951	***Ntrk3***	adult male testis
332	BC076581	***Opcml***	opioid binding protein/cell adhesion molecule-like
333	BC012725	***Orm1***	orosomucoid 1
334	AY038074	***Osr2***	odd-skipped related 2
335	XM_001474519	***Gm11559***	OTTMUSG00000002191 (OTTMUSG00000002191)
336	XM_991213	***Otud1***	OTU domain containing 1 (Otud1)
337	BC015297	***Palm***	paralemmin
338	BC156243	***Pappa***	pregnancy-associated plasma protein A
339	AK161542	***Paqr7***	10 days neonate intestine
340	AK008055	***Pard3b***	adult male small intestine
341	BC051174	***Pcolce2***	procollagen C-endopeptidase enhancer 2
342	AK172320	***Pcx***	activated spleen
343	BC004809	***Pdlim1***	PDZ and LIM domain 1 (elfin)
344	BC115886	***Pdzd2***	PDZ domain containing 2
345	AK036345	***Per3***	16 days neonate cerebellum
346	AK076776	***Pex11a***	adult male testis
347	EU034675	***Pfkfb3***	6-phosphofructo-2-kinase/fructose-2,6-biphosphatase 3
348	BC024363	***Pfn2***	profilin 2
349	AK008665	***Pgam1***	adult male stomach
350	BC108372	***Pgk1***	phosphoglycerate kinase 1
351	AK207773	***Pgs1***	clone:Y2G0109B09
352	NM_001102613	***Phldb3***	pleckstrin homology-like domain, family B
353	BC011470	***Picalm***	phosphatidylinositol binding clathrin assembly protein
354	BC085501	***Pik3r2***	phosphatidylinositol 3-kinase, regulatory subunit
355	AK034517	***Pisd-ps3***	adult male diencephalon
356	BC070452	***Pitpnm2***	phosphatidylinositol transfer protein
357	BC030899	***Pla2g5***	phospholipase A2, group V
358	BC025841	***Plekha6***	pleckstrin homology domain containing
359	BC058945	***Pnkd***	paroxysmal nonkinesiogenic dyskinesia
360	BC019188	***Pnpla2***	patatin-like phospholipase domain containing 2
361	BC028792	***Pnpla3***	patatin-like phospholipase domain containing 3
362	AK014771	***Pnpla5***	0 day neonate head

…Table 3.8 continued on next page.

Table 3.8: (continued…)

	GenBank ID	Gene Name	Roche NimbleGen Annotation
363	AK149460	***Ppara***	adult male liver tumor
364	BC066868	***Ppargc1a***	peroxisome proliferative activated receptor, gamma
365	BC052769	***Ppp1r3c***	protein phosphatase 1, regulatory (inhibitor) subunit 3C
366	BC059811	***Ppp2r2c***	protein phosphatase 2 (formerly 2A), regulatory subunit B (PR 52)
367	AK087749	***Prlr***	2 days pregnant adult female ovary
368	BC125327	***Prodh***	proline dehydrogenase
369	XM_001480001	***Prr24***	RIKEN 2610014I16 gene
370	AK021185	***Prss36***	ES cells
371	AK153093	***Psat1***	bone marrow macrophage
372	BC056196	***Psmd10***	proteasome (prosome, macropain) 26S subunit
373	BC002064	***Ptn***	pleiotrophin
374	AK086515	***Ptpn14***	15 days embryo head
375	D83072	***Ptpn21***	PTP-RL10b
376	AK045359	***Rapgefl1***	adult male corpora quadrigemina
377	AK077393	***Rarres1***	6 days neonate head
378	AK133054	***Rbms1***	adult male testis
379	BC026811	***Rdm1***	RAD52 motif 1
380	BC029741	***Reep6***	receptor accessory protein 6
381	AK167648	***Renbp***	15 days pregnant adult female placenta
382	BC051196	***Retn***	resistin
383	AK161129	***Rgs12***	10 days neonate skin
384	BC033271	***Riok3***	RIO kinase 3 (yeast)
385	BC146014	***Rnase12***	ribonuclease, RNase A family
386	AK141351	***Rnh1***	7 days embryo whole body
387	AF163668	***Rorc***	RORgamma t
388	BC100690	***S100a3***	S100 calcium binding protein A3
389	BC016096	***Scara5***	scavenger receptor class A
390	BC118033	***Scd3***	stearoyl-coenzyme A desaturase 3
391	BC112380	***Scel***	sciellin
392	BC063328	***Scin***	scinderin
393	BC019400	***Sdcbp***	syndecan binding protein
394	BC064820	***Sdr9c7***	orphan short chain dehydrogenase/reductase
395	BC026948	***Sec14l4***	SEC14-like 4 (S. cerevisiae)
396	BC034610	***Sec23a***	SEC23A (S. cerevisiae)
397	AK134412	***Sema3d***	13 days embryo male testis
398	BC057956	***Sema3e***	sema domain, immunoglobulin domain (Ig)
399	AK141915	***Sept3***	12 days embryo spinal ganglion
400	BC125418	***Serpina3b***	serine (or cysteine) peptidase inhibitor, clade A, member 3B
401	BC116724	***Serpina3c***	serine (or cysteine) peptidase inhibitor, clade A, member 3C
402	BC132647	***Serpina3h***	serine (or cysteine) peptidase inhibitor, clade A, member 3H

…Table 3.8 continued on next page.

Table 3.8: (continued…)

	GenBank ID	Gene Name	Roche NimbleGen Annotation
403	BC156605	***Sh3kbp1***	SH3-domain kinase binding protein 1
404	BC036172	***Shc1***	src homology 2 domain-containing transforming protein C1
405	BC049934	***Skil***	SKI-like
406	AK040044	***Skint10***	0 day neonate thymus
407	EU099306	***Skint7***	selection and upkeep of intraepithelial T cells 7
408	EU099308	***Skint8***	selection and upkeep of intraepithelial T cells 8
409	AJ493663	***Slc11a2***	divalent metal transporter
410	BC058711	***Slc1a3***	solute carrier family 1 (glial high affinity glutamate transporter)
411	BC017615	***Slc24a3***	solute carrier family 24 (sodium/potassium/calcium exchanger)
412	AK018566	***Slc26a3***	adult male colon
413	BC116314	***Slc2a12***	solute carrier family 2 (facilitated glucose transporter)
414	AK002607	***Slc38a3***	adult male kidney
415	BC005474	***Slc39a1***	solute carrier family 39 (zinc transporter)
416	BC027516	***Slc7a10***	solute carrier family 7 (cationic amino acid transporter, y+ system)
417	AK132394	***Slco2b1***	1 day pregnant adult female mammary gland
418	AK031280	***Slco3a1***	13 days embryo male testis
419	AK040931	***Smoc1***	adult male aorta and vein
420	AK172312	***Smoc2***	activated spleen
421	AK147087	***Snap91***	RIKEN full-length enriched library
422	BC003748	***Sntb1***	syntrophin, basic 1
423	BC085245	***Socs6***	suppressor of cytokine signaling 6
424	AK217459	***Sorbs1***	clone:Y2G0141N17
425	AK004941	***Spr***	adult male liver
426	BC003227	***Sptlc2***	serine palmitoyltransferase, long chain base subunit 2
427	BC056392	***Srrm4***	serine/arginine repetitive matrix 4
428	BC019168	***Stat3***	signal transducer and activator of transcription 3
429	BC005413	***Sult1a1***	sulfotransferase family 1A
430	BC012677	***Sult5a1***	sulfotransferase family 5A
431	BC003280	***Surf4***	surfeit gene 4
432	AK082445	***Syn3***	0 day neonate cerebellum
433	AK004560	***Tanc1***	adult male lung
434	BC128306	***Tcf7l1***	transcription factor 3
435	AK035827	***Tcfap2b***	16 days neonate cerebellum
436	XM_001000857	***Tchh***	trichohyalin (Tchh)
437	AK027965	***Tef***	18-day embryo whole body
438	AK010463	***Tesc***	ES cells
439	AK015337	***Tgfbr1***	adult male testis
440	BC014713	***Timp3***	tissue inhibitor of metalloproteinase 3
441	BC039182	***Tlcd1***	TLC domain containing 1
442	BC004641	***Tmem111***	transmembrane protein 111

…Table 3.8 continued on next page.

Table 3.8: (continued…)

	GenBank ID	Gene Name	Roche NimbleGen Annotation
443	BC006689	***Tmem159***	transmembrane protein 159
444	NM_001085508	***Tmem8b***	transmembrane protein 8B
445	BC082588	***Tob1***	transducer of ErbB-2.1
446	BC069857	***Tpcn2***	two pore segment channel 2
447	AK168843	***Tpm3***	17 days pregnant adult female amnion
448	BC023701	***Tpm4***	tropomyosin 4
449	BC054803	***Tppp***	tubulin polymerization promoting protein
450	BC106114	***Trappc6a***	trafficking protein particle complex 6A
451	BC034276	***Trim25***	tripartite motif protein 25
452	NM_001110202	***Trim9***	tripartite motif protein 9 (Trim9)
453	BC018317	***Tspan13***	tetraspanin 13
454	BC043072	***Tspan3***	tetraspanin 3
455	BC030922	***Tspyl4***	TSPY-like 4
456	BC005644	***Tst***	thiosulfate sulfurtransferase, mitochondrial
457	AK016396	***Ttll10***	adult male testis
458	BC066058	***Tyro3***	TYRO3 protein tyrosine kinase 3
459	XM_885266	***Vmn2r72***	EG244114 (EG244114)
460	NM_001110015	***Wdr36***	WD repeat domain 36 (Wdr36)
461	BC060187	***Wnk2***	WNK lysine deficient protein kinase 2
462	AK164356	***Ywhag***	12 days embryo spinal ganglion
463	BC080272	***Zfp365***	zinc finger protein 365
464	BC108353	***Zfp772***	sequence BC023179
465	AK047931	***Zfp826***	16 days embryo head

END Table 3.8.

Table 3.9: Kidney-associated transcripts (KTs) top gene ontology (GO) annotations within biological process, molecular function, and cellular compartment categories. *P*-value is representative of a hypergeometric test from selecting the KTs found within each GO category by chance alone. Sorted by increasing *p*-value. (Table continued on next page.)

	Top 20 Annotations in Biological Process Category (total n=113, $p<0.05$)	Genes in Category	Genes in KTs in Category	% of Genes in KTs in Category	*p*-value
GO:0055085	transmembrane transport	460	48	7.8	0.000
GO:0046395	carboxylic acid catabolic process	81	19	3.1	0.000
GO:0016054	organic acid catabolic process	81	19	3.1	0.000
GO:0006814	sodium ion transport	125	21	3.4	0.000
GO:0006006	glucose metabolic process	140	21	3.4	0.000
GO:0009063	cellular amino acid catabolic process	54	13	2.1	0.000
GO:0005996	monosaccharide metabolic process	191	24	3.9	0.000
GO:0009310	amine catabolic process	65	14	2.3	0.000
GO:0019318	hexose metabolic process	169	22	3.6	0.000
GO:0001655	urogenital system development	146	20	3.3	0.000
GO:0001822	kidney development	107	17	2.8	0.000
GO:0006811	ion transport	712	52	8.5	0.000
GO:0015672	monovalent inorganic cation transport	303	29	4.7	0.000
GO:0006570	tyrosine metabolic process	10	6	1.0	0.000
GO:0008202	steroid metabolic process	161	19	3.1	0.000
GO:0006090	pyruvate metabolic process	25	8	1.3	0.000
GO:0006812	cation transport	515	39	6.4	0.000
GO:0006559	L-phenylalanine catabolic process	6	5	0.8	0.000
GO:0006094	gluconeogenesis	20	7	1.1	0.000
GO:0009069	serine family amino acid metabolic process	22	7	1.1	0.000

…Table 3.9 continued on next page.

Table 3.9: (continued…)

	Top 20 Annotations in Molecular Function Category (total n=51, p<0.05)	Genes in Category	Genes in KTs in Category	% of Genes in KTs in Category	p-value
GO:0031402	sodium ion binding	103	21	3.4	0.000
GO:0031420	alkali metal ion binding	206	28	4.6	0.000
GO:0015293	symporter activity	132	22	3.6	0.000
GO:0048037	cofactor binding	226	28	4.6	0.000
GO:0019842	vitamin binding	121	19	3.1	0.000
GO:0046906	tetrapyrrole binding	151	20	3.3	0.000
GO:0016712	oxidoreductase activity	44	11	1.8	0.000
GO:0050662	coenzyme binding	160	20	3.3	0.000
GO:0009055	electron carrier activity	202	22	3.6	0.000
GO:0020037	heme binding	144	18	2.9	0.000
GO:0016229	steroid dehydrogenase activity	29	8	1.3	0.000
GO:0008509	anion transmembrane transporter activity	130	16	2.6	0.000
GO:0016836	hydro-lyase activity	42	9	1.5	0.000
GO:0033764	steroid dehydrogenase activity, acting on the CH-OH group of donors, NAD or NADP as acceptor	23	7	1.1	0.000
GO:0015103	inorganic anion transmembrane transporter activity	24	7	1.1	0.000
GO:0015103	inorganic anion transmembrane transporter activity	24	7	1.1	0.000
GO:0004089	carbonate dehydratase activity	18	6	1.0	0.000
GO:0015101	organic cation transmembrane transporter activity	11	5	0.8	0.001
GO:0005506	iron ion binding	343	27	4.4	0.001
GO:0016620	oxidoreductase activity, acting on the aldehyde or oxo group of donors, NAD or NADP as acceptor	29	7	1.1	0.001

…Table 3.9 continued on next page.

Table 3.9: (continued…)

	Top Annotations in Cellular Component Category (total n=19, $p<0.05$)	Genes in Category	Genes in KTs in Category	% of Genes in KTs in Category	p-value
GO:0000267	cell fraction	596	56	9.1	0.000
GO:0005792	microsome	176	26	4.2	0.000
GO:0042598	vesicular fraction	182	26	4.2	0.000
GO:0005626	insoluble fraction	528	46	7.5	0.000
GO:0005624	membrane fraction	510	44	7.2	0.000
GO:0044421	extracellular region part	774	51	8.3	0.000
GO:0005759	mitochondrial matrix	163	18	2.9	0.000
GO:0031980	mitochondrial lumen	163	18	2.9	0.000
GO:0005615	extracellular space	511	37	6.0	0.000
GO:0044429	mitochondrial part	524	36	5.9	0.000
GO:0005576	extracellular region	1680	87	14.2	0.001
GO:0005743	mitochondrial inner membrane	296	23	3.8	0.001
GO:0005783	endoplasmic reticulum	838	48	7.8	0.002
GO:0019866	organelle inner membrane	312	23	3.8	0.003
GO:0031966	mitochondrial membrane	368	25	4.1	0.005
GO:0005740	mitochondrial envelope	391	25	4.1	0.010
GO:0031526	brush border membrane	14	4	0.7	0.013
GO:0005604	basement membrane	73	8	1.3	0.017
GO:0005905	coated pit	32	5	0.8	0.029

END Table 3.9.

Table 3.10: Skin-associated transcripts (STs) top gene ontology (GO) annotations within biological process, molecular function, and cellular compartment categories. *P*-value is representative of a hypergeometric test from selecting the STs found within each GO category by chance alone. Sorted by increasing *p*-value. (Table continued on next page.)

	Top 20 Annotations in Biological Process Category (total n=117, $p<0.05$)	Genes in Category	Genes in STs in Category	% of Genes in STs in Category	*p*-value
GO:0032271	regulation of protein polymerization	57	11	2.5	0.000
GO:0044087	regulation of cellular component biogenesis	89	13	3.0	0.000
GO:0043254	regulation of protein complex assembly	65	11	2.5	0.000
GO:0030833	regulation of actin filament polymerization	45	9	2.1	0.000
GO:0008064	regulation of actin polymerization or depolymerization	50	9	2.1	0.000
GO:0030832	regulation of actin filament length	51	9	2.1	0.000
GO:0009719	response to endogenous stimulus	184	15	3.4	0.000
GO:0009725	response to hormone stimulus	165	14	3.2	0.000
GO:0032956	regulation of actin cytoskeleton organization	60	9	2.1	0.000
GO:0032970	regulation of actin filament-based process	61	9	2.1	0.000
GO:0051493	regulation of cytoskeleton organization	99	10	2.3	0.000
GO:0007167	enzyme linked receptor protein signaling pathway	273	16	3.6	0.000
GO:0043062	extracellular structure organization	149	11	2.5	0.000
GO:0016054	organic acid catabolic process	81	8	1.8	0.001
GO:0046395	carboxylic acid catabolic process	81	8	1.8	0.001
GO:0032535	regulation of cellular component size	161	11	2.5	0.001
GO:0048545	response to steroid hormone stimulus	60	7	1.6	0.001
GO:0010033	response to organic substance	505	21	4.8	0.001
GO:0001655	urogenital system development	146	10	2.3	0.001
GO:0045893	positive regulation of transcription, DNA-dependent	416	18	4.1	0.001

…Table 3.10 continued on next page.

Table 3.10: (continued…)

	Top Annotations in Molecular Function Category (total n=15, p<0.05)	Genes in Category	Genes in STs in Category	% of Genes in STs in Category	p-value
GO:0003779	actin binding	288	18	4.1	0.000
GO:0008092	cytoskeletal protein binding	414	22	5.0	0.000
GO:0005509	calcium ion binding	840	33	7.5	0.001
GO:0004522	pancreatic ribonuclease activity	20	5	1.1	0.001
GO:0016892	endoribonuclease activity, producing 3'-phosphomonoesters	23	5	1.1	0.001
GO:0001871	pattern binding	128	10	2.3	0.001
GO:0030247	polysaccharide binding	128	10	2.3	0.001
GO:0008201	heparin binding	83	8	1.8	0.002
GO:0016894	endonuclease activity, active with either ribo- or deoxyribonucleic acids and producing 3'-phosphomonoesters	26	5	1.1	0.002
GO:0030246	carbohydrate binding	317	15	3.4	0.006
GO:0005539	glycosaminoglycan binding	114	8	1.8	0.009
GO:0004521	endoribonuclease activity	52	5	1.1	0.022
GO:0019900	kinase binding	85	6	1.4	0.031
GO:0004806	triacylglycerol lipase activity	14	3	0.7	0.033
GO:0046983	protein dimerization activity	340	13	3.0	0.050

…Table 3.10 continued on next page.

Table 3.10: (continued…)

	Top Annotations in Cellular Component Category (total n=23, p<0.05)	Genes in Category	Genes in STs in Category	% of Genes in STs in Category	p-value
GO:0005882	intermediate filament	137	32	7.3	0.000
GO:0045111	intermediate filament cytoskeleton	140	32	7.3	0.000
GO:0005856	cytoskeleton	1122	70	15.9	0.000
GO:0045095	keratin filament	64	18	4.1	0.000
GO:0044430	cytoskeletal part	774	48	10.9	0.000
GO:0043228	non-membrane-bounded organelle	1919	78	17.8	0.000
GO:0043232	intracellular non-membrane-bounded organelle	1919	78	17.8	0.000
GO:0005912	adherens junction	106	10	2.3	0.001
GO:0015629	actin cytoskeleton	205	14	3.2	0.001
GO:0016323	basolateral plasma membrane	141	11	2.5	0.001
GO:0070161	anchoring junction	123	10	2.3	0.002
GO:0030054	cell junction	470	22	5.0	0.002
GO:0005924	cell-substrate adherens junction	61	7	1.6	0.002
GO:0030055	cell-substrate junction	66	7	1.6	0.003
GO:0044420	extracellular matrix part	92	8	1.8	0.004
GO:0005604	basement membrane	73	7	1.6	0.006
GO:0005578	proteinaceous extracellular matrix	297	15	3.4	0.007
GO:0005925	focal adhesion	57	6	1.4	0.009
GO:0031012	extracellular matrix	309	15	3.4	0.009
GO:0000267	cell fraction	596	23	5.2	0.014

END Table 3.10.

Table 3.11: Overlapping skin-associated (STs) and kidney-associated transcripts (KTs) gene ontology (GO) annotations within biological process, molecular function and cellular compartment categories. *P*-value is representative of a hypergeometric test from selecting the skin or kidney IRITs found within each GO category by chance alone. (Table continued on next page.)

			Skin-associated (ST)			Kidney-associated (KTs)		
	Overlapping GO Biological Process Categories	**Genes in Category**	**Genes in STs in Category**	**% of Genes in STs in Category**	***p*-value**	**Genes in KTs in Category**	**% of Genes in KTs in Category**	***p*-value**
*GO:0009725	response to hormone stimulus	165	14	3.2	0.000	12	2.0	0.037
*GO:0016054	organic acid catabolic process	81	8	1.8	0.001	19	3.1	0.000
GO:0046395	carboxylic acid catabolic process	81	8	1.8	0.001	19	3.1	0.000
GO:0001655	urogenital system development	146	10	2.3	0.001	20	3.3	0.000
GO:0001822	kidney development	107	8	1.8	0.003	17	2.8	0.000
GO:0044242	cellular lipid catabolic process	56	6	1.4	0.003	9	1.5	0.001
GO:0006820	anion transport	130	8	1.8	0.009	15	2.4	0.000
GO:0060688	regulation of morphogenesis of a branching structure	25	4	0.9	0.010	6	1.0	0.002
GO:0009309	amine biosynthetic process	73	6	1.4	0.010	10	1.6	0.001
GO:0016053	organic acid biosynthetic process	141	8	1.8	0.014	15	2.4	0.001
*GO:0046394	carboxylic acid biosynthetic process	141	8	1.8	0.014	15	2.4	0.001
*GO:0009063	cellular amino acid catabolic process	54	5	1.1	0.016	13	2.1	0.000
GO:0007155	cell adhesion	561	18	4.1	0.026	31	5.1	0.021
GO:0022610	biological adhesion	562	18	4.1	0.026	31	5.1	0.021
GO:0010817	regulation of hormone levels	128	7	1.6	0.028	10	1.6	0.042
*GO:0009310	amine catabolic process	65	5	1.1	0.030	14	2.3	0.000
GO:0006635	fatty acid beta-oxidation	16	3	0.7	0.033	4	0.7	0.018
GO:0019318	hexose metabolic process	169	8	1.8	0.034	22	3.6	0.000
GO:0051384	response to glucocorticoid stimulus	19	3	0.7	0.045	4	0.7	0.029

*indicates the five GO categories annotated from the 39 overlapping transcripts found in both, skin-associated and kidney-associated transcript sets.

…Table 3.11 continued on next page.

Table 3.11: (continued…)

Overlapping GO Molecular Function Categories	Genes in Category	Skin-selective IRITs: Genes in STs in Category	Skin-selective IRITs: % of Genes in STs in Category	Skin-selective IRITs: *p*-value	Kidney-selective IRITs: Genes in KTs in Category	Kidney-selective IRITs: % of Genes in KTs in Category	Kidney-selective IRITs: *p*-value

There were no overlapping molecular function categories within the STs' and KTs' GO annotations.

Overlapping GO Cellular Component Categories		Genes in Category	Skin-selective IRITs: Genes in STs in Category	Skin-selective IRITs: % of Genes in STs in Category	Skin-selective IRITs: *p*-value	Kidney-selective IRITs: Genes in KTs in Category	Kidney-selective IRITs: % of Genes in KTs in Category	Kidney-selective IRITs: *p*-value
GO:0005604	basement membrane	73	7	1.6	0.006	8	1.3	0.017
GO:0000267	cell fraction	596	23	5.2	0.014	56	9.1	0.000
GO:0005792	microsome	176	9	2.1	0.043	26	4.2	0.000
GO:0005626	insoluble fraction	528	19	4.3	0.048	46	7.5	0.000

END Table 3.11.

3.7 FIGURES

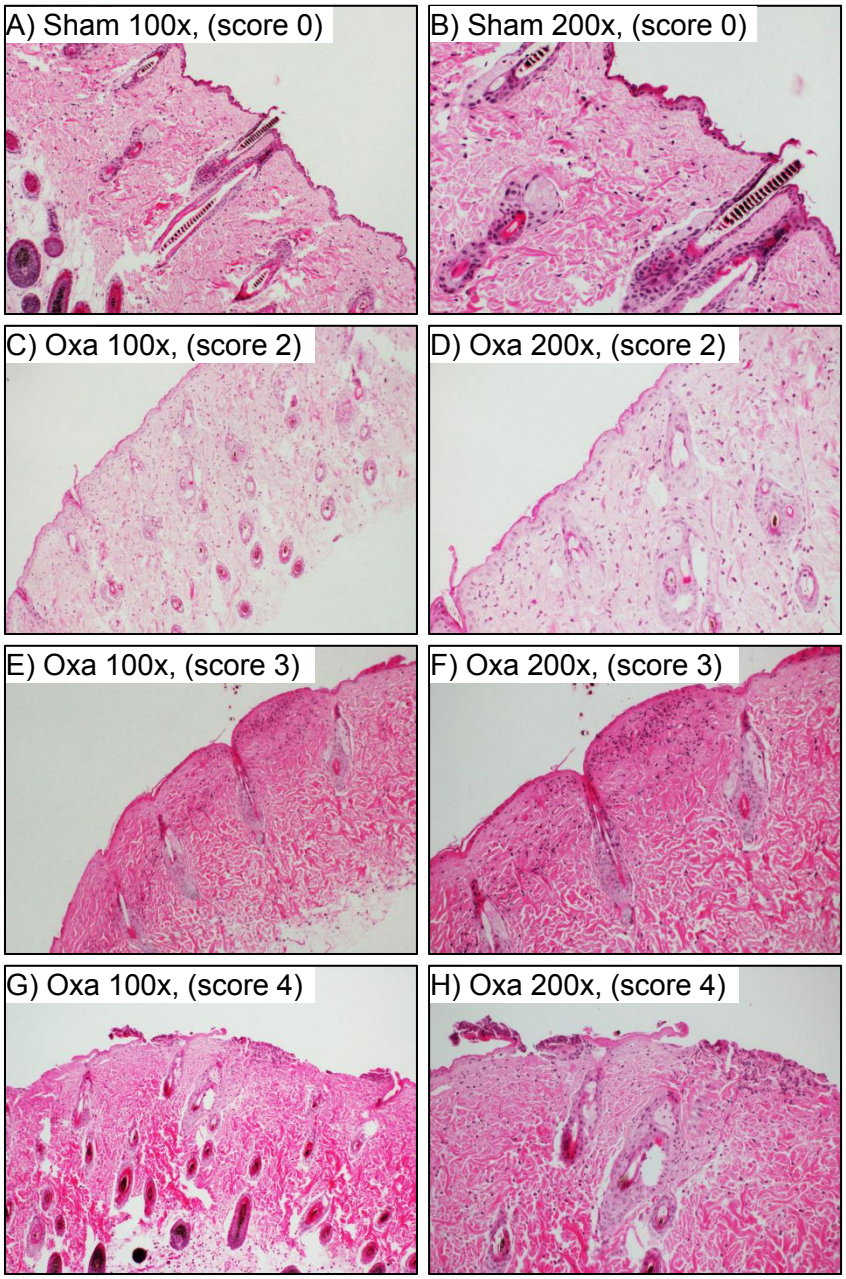

Figure 3.1: Histopathology of sham-treated B6 skin and oxazolone-challenged B6 skin. Sham-treated skin day 6 with a histological score of 0, show no inflammatory cell infiltrate, 100x **(A)** and 200x magnifications **(B)**. Oxazolone-challenged skin day 6 **(C-H)**; example of histological score of: 2, showing moderate dermal inflammatory infiltrate but intact epithelium, 100x **(C)** and 200x magnifications **(D)**; histological score of 3, showing dermal inflammatory infiltrate with focal epithelial ulcerations, 100x **(E)** and 200x magnifications **(F)**; histological score of 4, showing dermal inflammatory infiltrate with multiple erosive epithelial ulcerations, 100x **(G)** and 200x magnifications **(H)**. No samples received a histological score of 1. (H&E stain.)

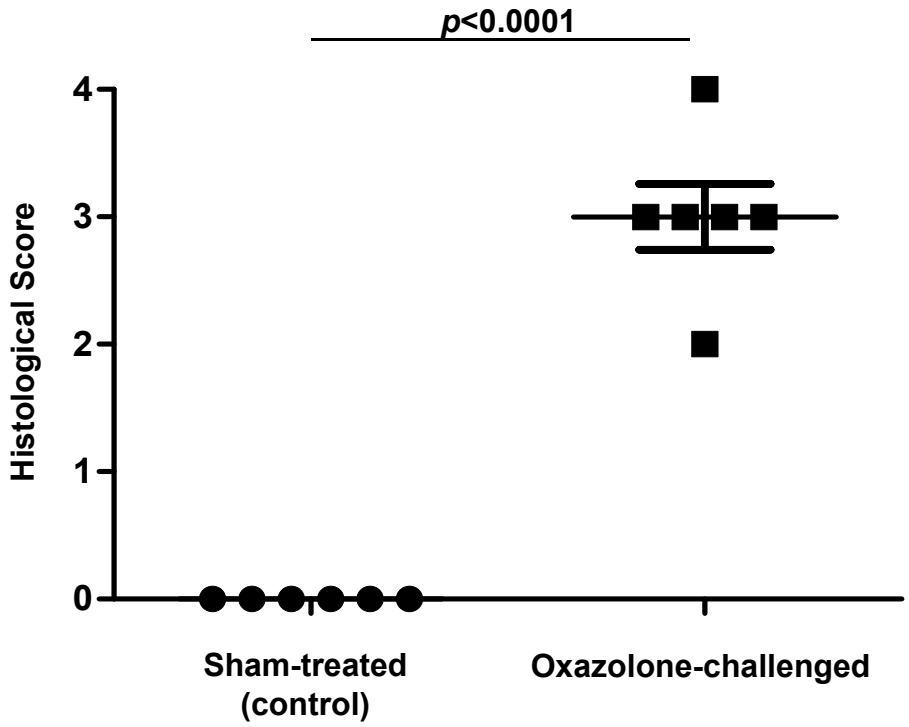

Figure 3.2: Oxazolone-challenged skin experiences greater inflammation than sham-treated controls. Skin tissue sections were stained with H&E, and lesions were scored semi-quantitatively on a scale of 0 through 4. Skin from sham-treated mice (N=6) was absent of inflammation, while inflammation in the skin of oxazolone-challenged mice (N=6) resulted in a mean histological score of 3.0 (p<0.0001, one-sample t-test using a hypothetical value).

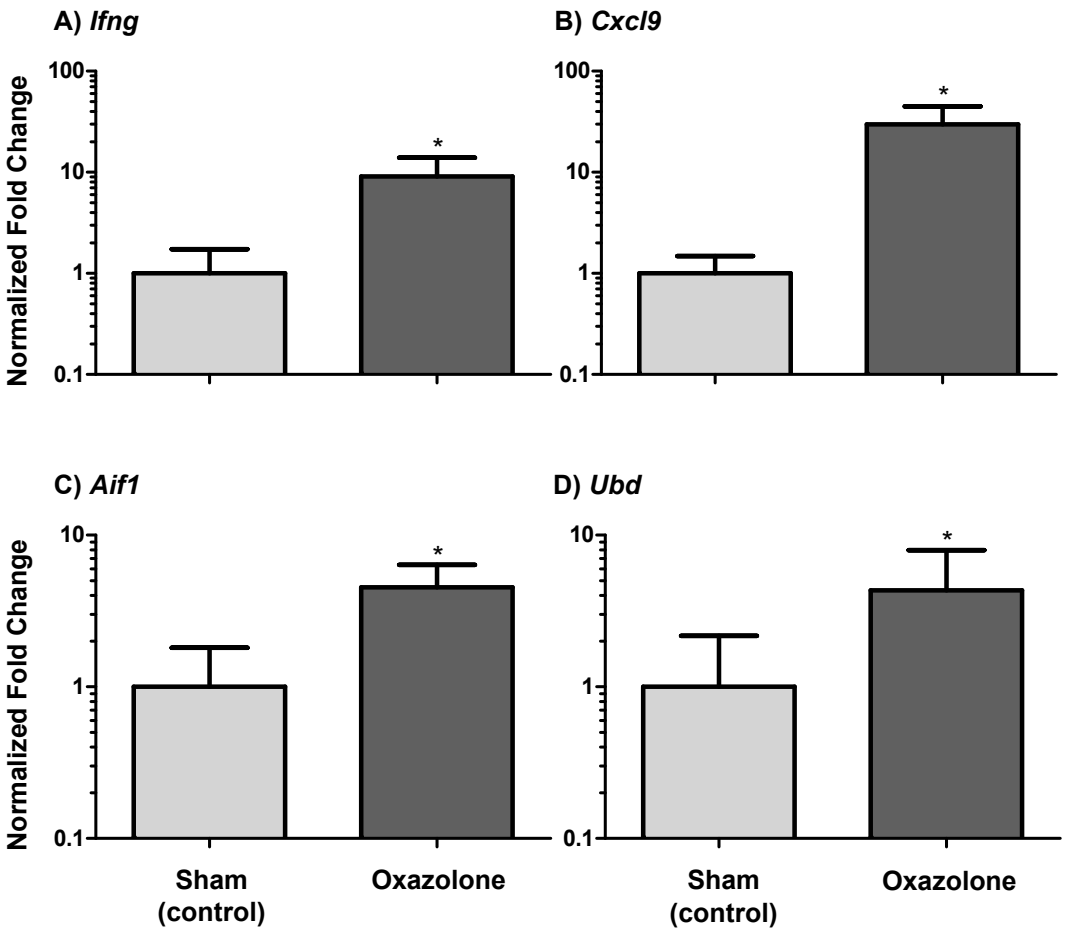

Figure 3.3. *Ifng* transcript expression and expression of IFNG-induced transcripts (*Cxcl9*, *Aif1* and *Ubd*) within sham-treated and oxazolone-challenged B6 mouse skin assessed by real time RT-PCR. Transcript expression was expressed as fold change in the oxazolone-challenged mice (N=6) and normalized to the relative levels in sham-treated mice (N=6) using the ddCt formula. Within the oxazolone-challenged skin, transcript expression of: *Ifng* increased 9.1x ±4.8 **(A)**; *Cxcl9* increased 29.8x ±14.9 **(B)**; *Aif1* increased 4.5x ±1.9 **(C)**; and, *Ubd* increased 4.3x ±3.6 **(D)**. Data is ± standard deviation and includes three PCR replicates for each mouse. Transcript expression is significantly different, as determined by a one-way ANOVA and adjusted with Bonferroni correction, $p<0.05$ between oxazolone and sham conditions is indicated by *.

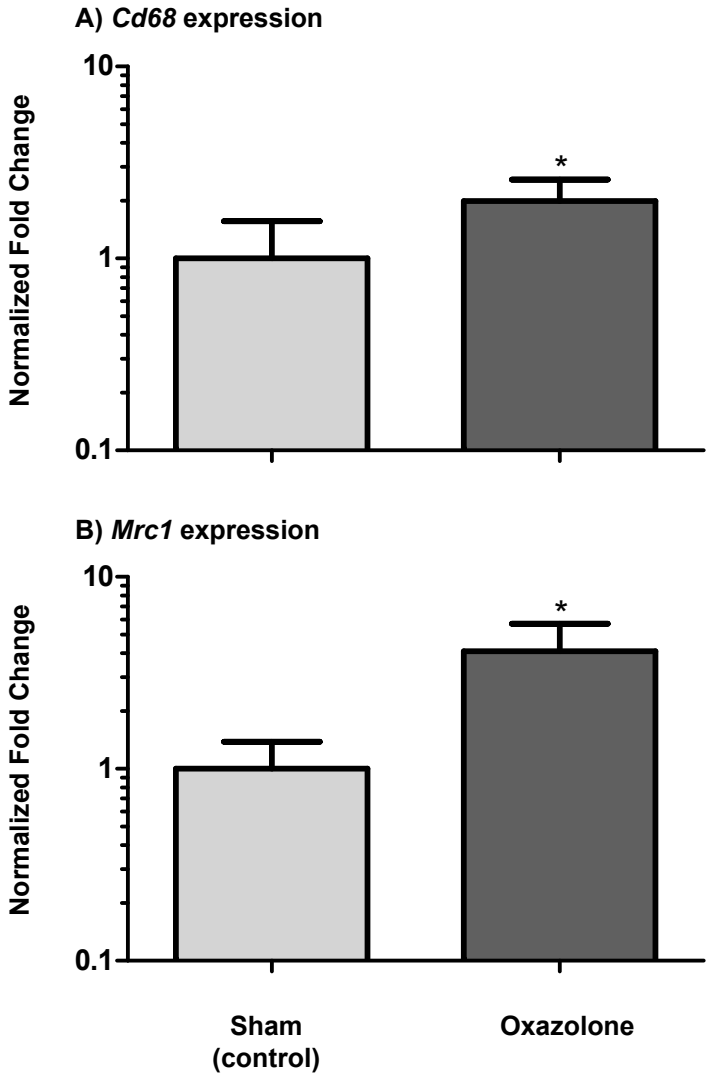

Figure 3.4: Transcript expression of the macrophage surface markers *Cd68* and *Mrc1* within sham-treated and oxazolone-challenged B6 mouse skin assessed by real time RT-PCR. Transcript expression was expressed as fold change in the oxazolone-challenged mice (N=6) and normalized to the relative levels in sham-treated mice (N=6) using the ddCt formula. Within the oxazolone-challenged skin, transcript expression of: *Cd68* increased 2.0x ±0.6 **(A)**; and, *Mrc1* increased 4.1x ±1.6 **(B)**. Data is ± standard deviation and includes three PCR replicates for each mouse. Transcript expression is significantly different, as determined by a one-way ANOVA and adjusted with Bonferroni correction, $p<0.05$ between oxazolone and sham conditions is indicated by *.

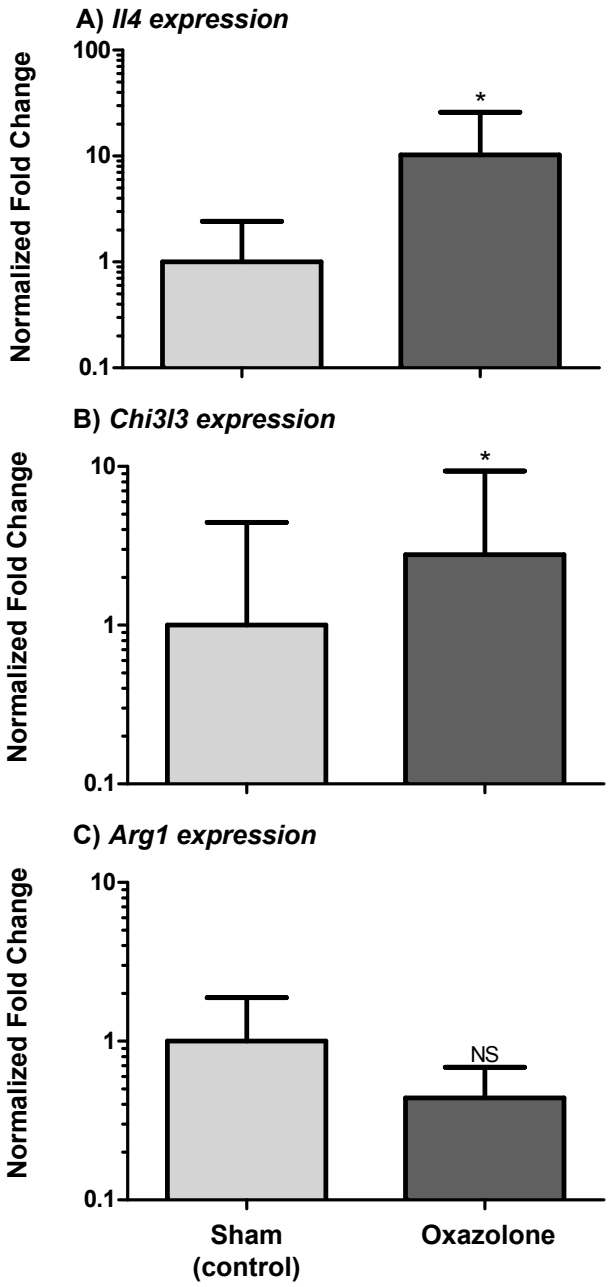

Figure 3.5: Transcript expression of *Il4*, *Chi3l3* and *Arg1*, AMA-associated transcripts, within sham-treated and oxazolone-challenged B6 mouse skin assessed by real time RT-PCR. Transcript expression was expressed as fold change in the oxazolone-challenged mice (N=6) and normalized to the relative levels in sham-treated mice (N=6) using the ddCt formula. Within the oxazolone-challenged skin, transcript expression of: *Il4* increased 10.3x ±15.7 **(A)**; *Chi3l3* increased 2.8x ±6.6 **(B)**; and, *Arg1* did not change 0.5x ±0.2 **(C)**. Data is ± standard deviation and includes three PCR replicates for each mouse. Transcript expression is significantly different, as determined by a one-way ANOVA and adjusted with Bonferroni correction, $p<0.05$ between oxazolone and sham conditions is indicated by *. (NS, not significant by $p>0.05$.)

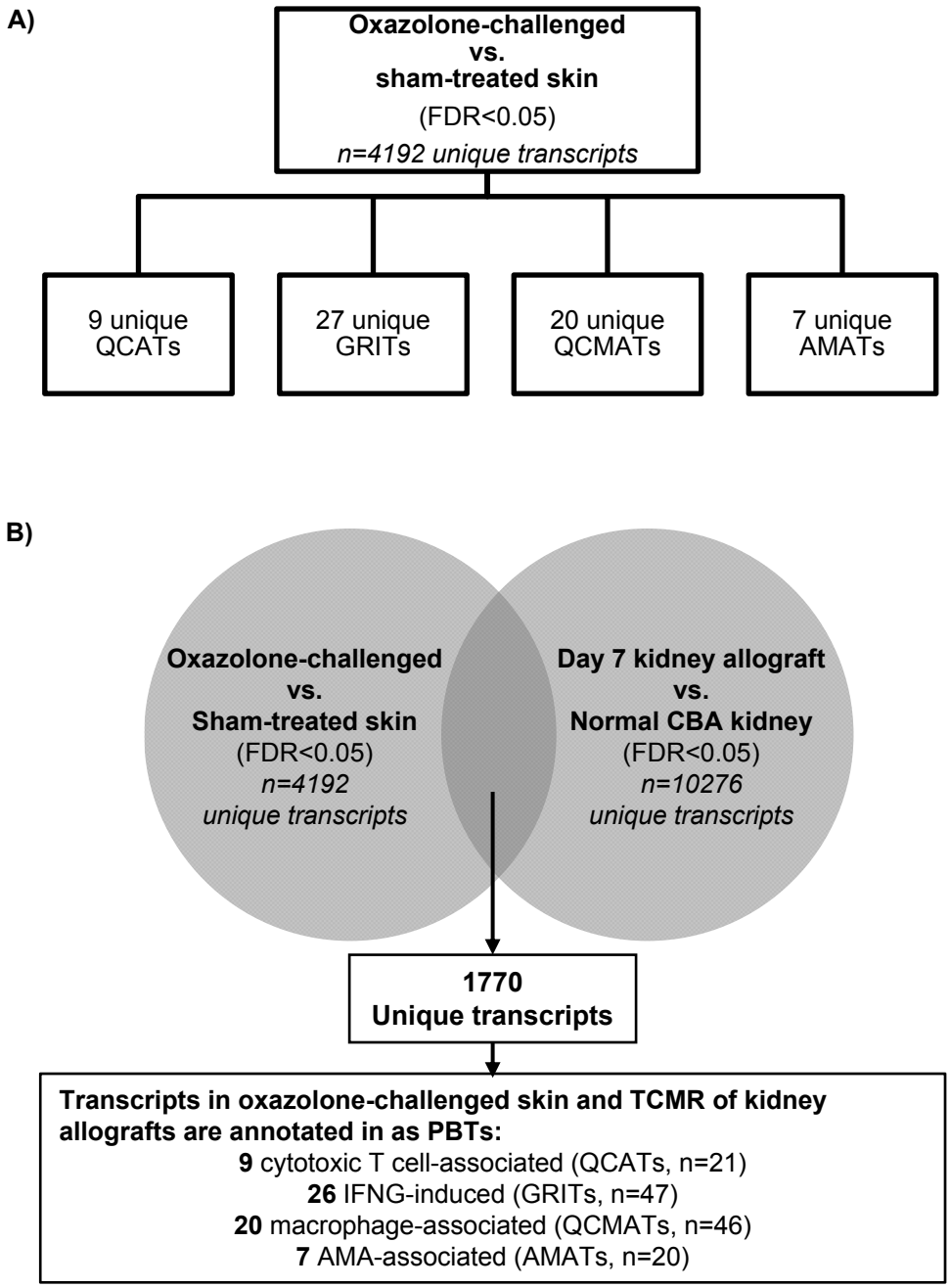

Figure 3.6: PBT annotated transcripts in oxazolone-challenged skin are also found in TCMR of kidney allografts. (A) 4192 unique transcripts are differentially expressed in oxazolone-challenged skin versus sham-treated controls, and many of these transcripts are annotated as members of PBTs. **(B)** Of these 4192 unique transcripts, 1770 unique transcripts are also differentially expressed in rejecting kidney allografts. Many of these transcripts found in both the inflamed skin and kidney tissues are also PBT annotated.

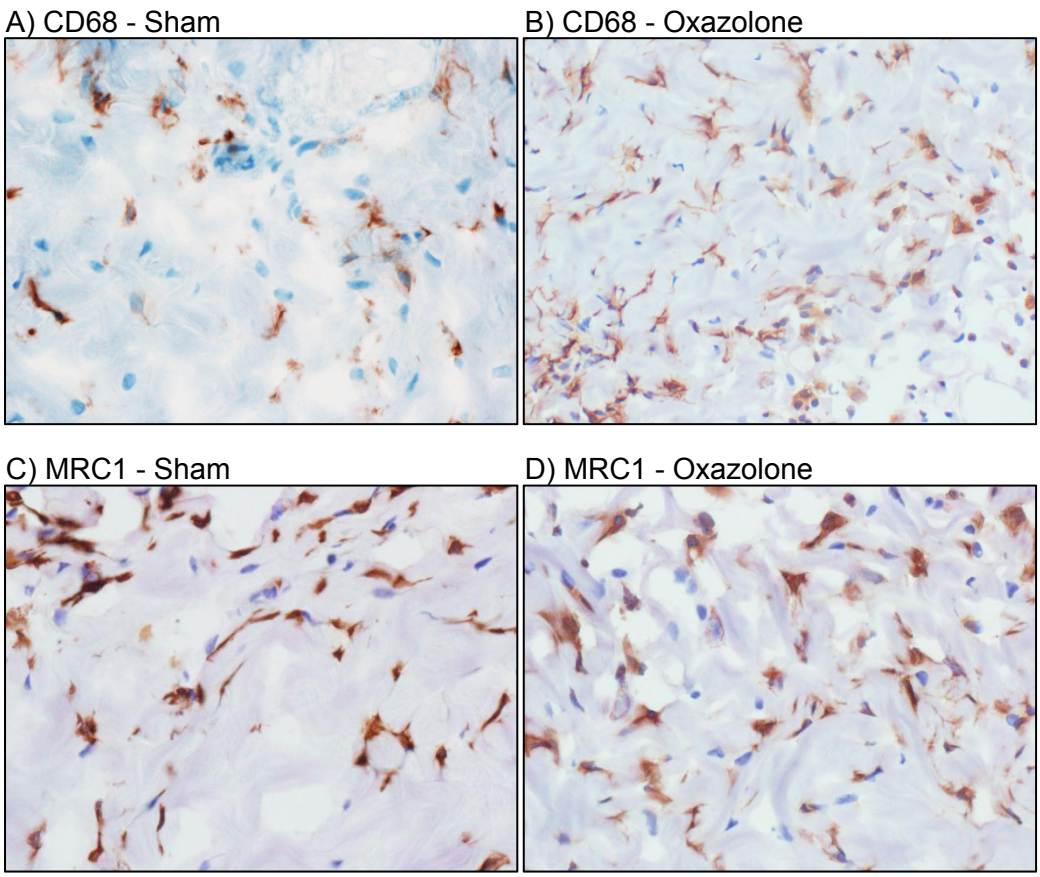

Figure 3.7: Expression of the general macrophage marker CD68, and the AMA marker MRC1, by immunohistochemistry in mouse skin sham-treated or oxazolone-challenged. Higher number of CD68 positive cells (A, B) and a higher number of MRC1 positive cells (C,D), are seen in the oxazolone-challenged skin than the sham-treated skin. (Immunoperoxidase, original magnification, x600.)

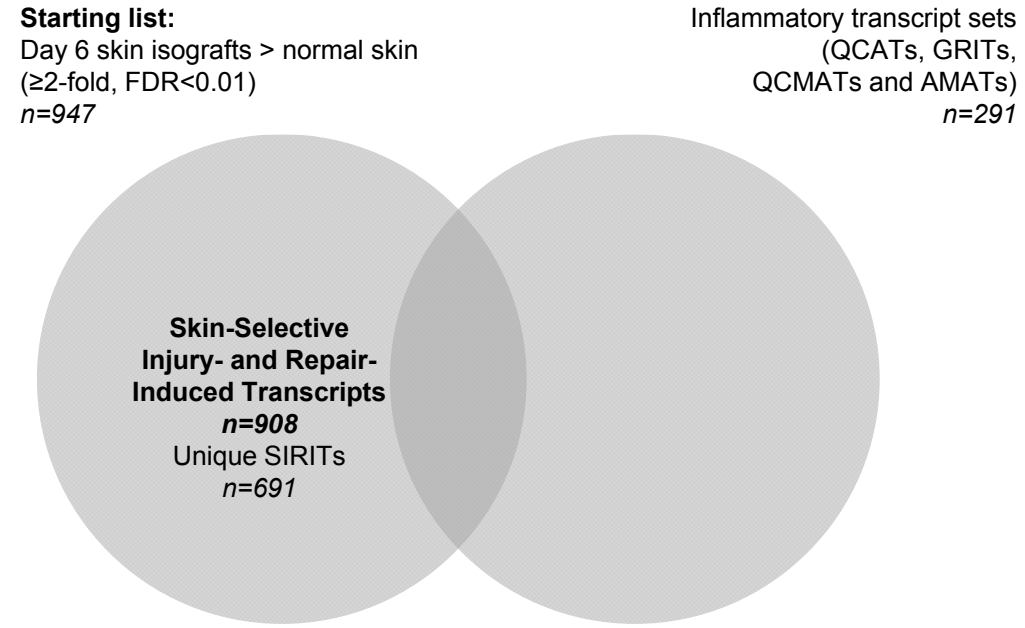

Figure 3.8: Algorithm for selection of the skin-selective injury- and repair-induced transcripts (SIRITs). SIRITs were defined by probesets that had a fold change of ≥2 in day 6 B6 skin isografts over normal B6 skin (FDR<0.05). All members belonging to the inflammatory PBTs were removed from this list to give a final list of 908 transcripts (691 unique transcripts).

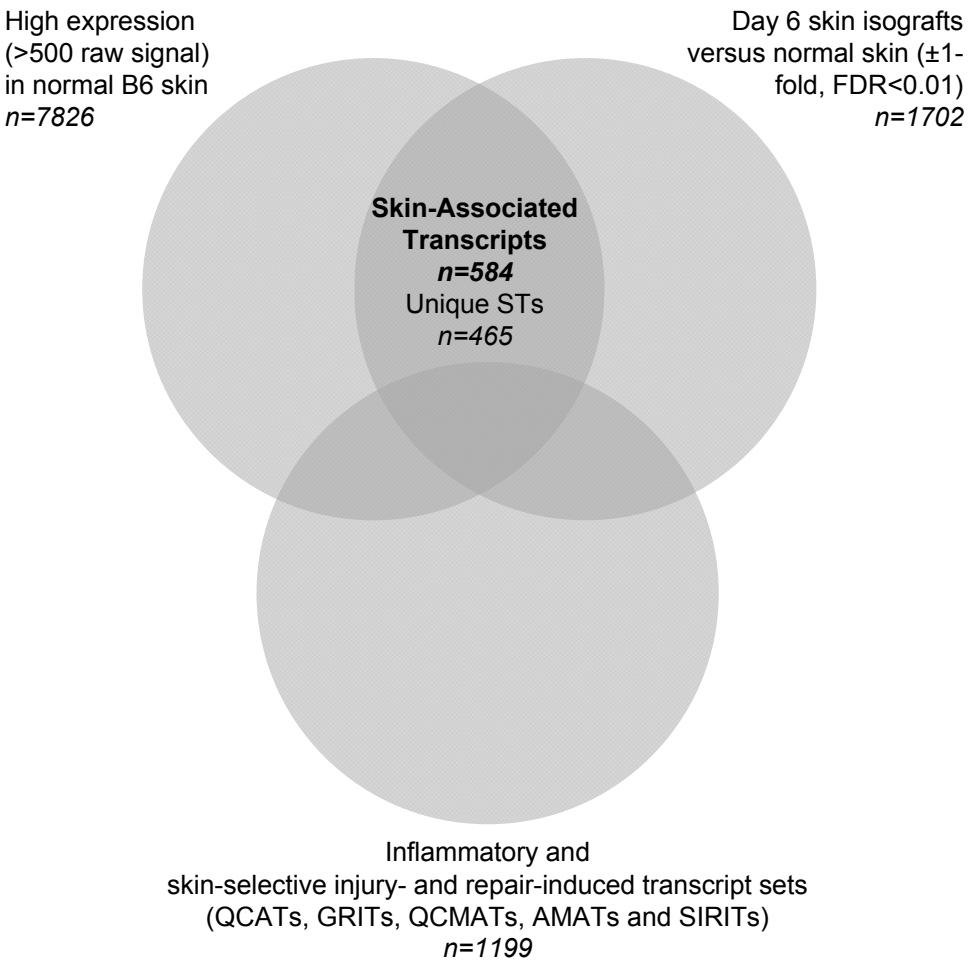

Figure 3.9: Algorithm for selection of the skin-associated transcripts (STs). 465 unique STs were defined by probesets that had a high expression (>500 raw signal) in normal B6 skin, and also were differentially expressed (up or down) in day 6 B6 skin isografts over normal B6 skin (FDR<0.05); but, were not a member of the inflammatory or skin-selective injury- and repair-induced transcript sets.

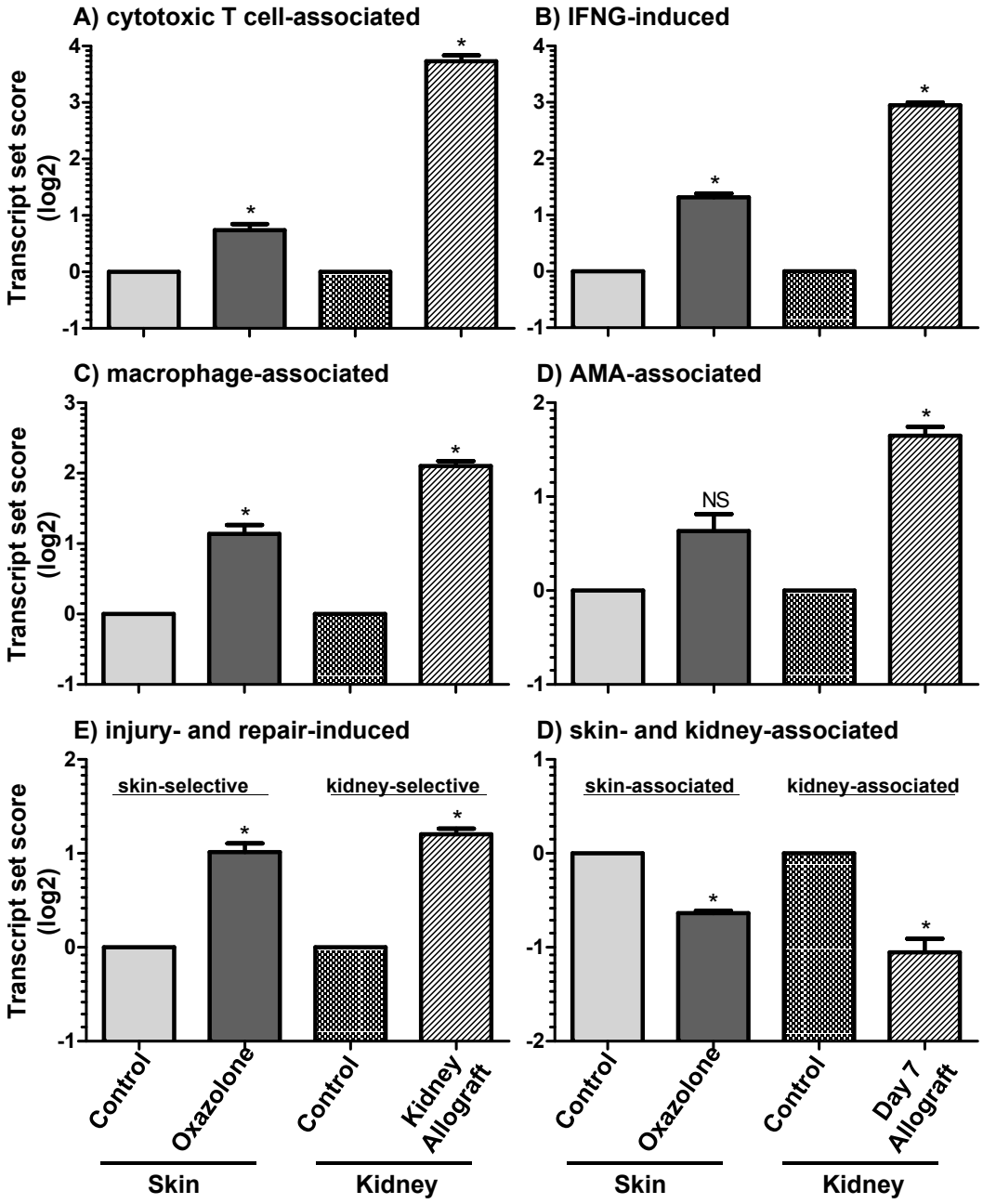

Figure 3.10: Transcript set scores of the inflammatory and injury-repair response PBTs in oxazolone-challenged skin and kidney allografts. Inflammatory PBTs have increased expression (increased score) within the inflamed skin or kidney tissue **(A-D)**: cytotoxic T cell associated **(A)**; IFNG-induced **(B)**; macrophage associated **(C)**; and, AMA-associated **(D)**. The skin- and kidney-selective injury- and repair-induced PBTs increase expression in the inflamed tissues **(E)**, and the skin- and kidney-associated PBTs decrease expression in the inflamed tissues **(F)**. Values are mean ± SEM. Significance of difference is determined by a student's T-test, $p<0.05$, sham-treated skin and oxazolone-challenged skin, or normal kidneys and day 7 kidney allografts.

CHAPTER 4

INTERFERON-GAMMA-DEPENDENT MOLECULAR CHANGES IN OXAZOLONE-INDUCED CONTACT HYPERSENSITIVITY

4.1 OVERVIEW

Mouse renal allografts unable to receive IFNG (deficient in IFNG-signaling), either because the donor graft lacks the IFNG-receptor-1 (*Ifngr1 deficient*, GRKO) or because the host is unable to produce IFNG (*Ifng* deficient, GKO) experience severe necrosis and microvascular congestion (41). This is unlike the typical TCMR lesions, interstitial infiltrate and tubulitis seen in rejecting mouse (wild type) renal allografts. The renal allografts which are unable to respond to IFNG experience an increased burden of kidney-selective IRITs and AMA-associated transcripts. These IRITs and AMA-associated transcripts were originally defined as IFNG-suppressed transcripts (48). The purpose of this study was to describe the histological and molecular changes of CHS in GRKO skin. Our aim was to assess the burden of IFNG-suppressed transcripts and their relationship with injury and AMA within CHS on a GRKO background. As we did the previous chapter, we used histology and real time RT-PCR to assess the initial inflammatory burden and phenotype. We then used microarrays to study the genome wide gene expression changes in oxazolone-challenged GRKO skin compared to oxazolone-challenged B6 (wild-type) skin. We annotated changes in transcript expression to the following PBTs: IFNG-induced transcripts, IFNG-suppressed transcripts, injury-repair response (both injury-up and injury-down) and AMA-associated transcripts.

4.2 IFNG-DEPENDENT CHANGES IN A CUTANEOUS OXAZOLONE-CHALLENGE IN MICE

4.2.1 Histology of oxazolone-challenged GRKO skin does not differ to that of oxazolone-challenged wild type mouse skin. We described the gross and histological appearance of B6 sham-treated and oxazolone-challenged skin previously (**Section 3.2.1**). Similar to the sham-treated B6 skin, sham-treated GRKO skin appeared normal with no gross or histological abnormalities. Oxazolone-challenged GRKO skin displayed marked gross-superficial and histological changes which included edematous dermatosis with ulceration and epidermal sloughing, as was described in the oxazolone-challenged B6 skin (**Section 3.2.1**). As a result the GRKO oxazolone-challenged skin had a significantly higher histological score than the GRKO sham-treated skin ($p<0.0001$, **Figure 4.1-4.2**). However, the degrees of inflammation observed in oxazolone-challenged B6 and GRKO skin did not differ as assessed by histology ($p=0.34$).

4.2.2 Real time RT-PCR analysis of IFNG-effects and AMA in oxazolone-challenged GRKO native skin. IFNG-effects and AMA are two active biological processes that our laboratory has previously described which are active during mouse renal allograft rejection (6,47). Interestingly, these two processes undergo marked transcript expression changes during the rejection of GRKO renal allografts in wild type hosts (41). As such, we wanted to observe which changes in cutaneously oxazolone-challenged skin are IFNG-dependent. To begin, we used real time RT-PCR to assess transcript expression changes relating to IFNG-effects and AMA in oxazolone-challenged GRKO skin, and compared these changes to the relative transcript expression changes in GRKO sham-treated skin and B6 oxazolone-challenged skin. The transcripts we chose to measure included: *Cxcl9*, *Aif1* and *Ubd*, that represent IFNG-effects; *Il4* and *Inhba*, inducers of AMA; *Mrc1*, *Chi3l3* and *Arg1*, which represent AMA. We also measured the transcript

expression of *Ifng* and the general macrophage marker *Cd68*, as was done in the wild type B6 oxazolone-challenged and sham-treated mice (**Section 3.2.2**).

The induction of *Ifng* in oxazolone-challenged GRKO mice was nearly as robust as that observed in WT mice. *Ifng* transcript expression was significantly increased in GRKO oxazolone-challenged skin compared to sham-treated (GRKO) controls ($p<0.05$, **Figure 4.3**) However, *Ifng* expression within the oxazolone-challenged GRKO skin was not as strongly induced as that observed in oxazolone-challenged B6 skin ($p<0.05$, **Figure 4.3**). Although, the reduced induction is very small, thus, more experimentation is necessary to determine a true biological significance.

The Ifng-induced transcripts, *Cxcl9*, *Aif1* and *Ubd* all failed to increase in the GRKO oxazolone-challenged skin compared to the sham-treated controls ($p>0.05$, **Figures 4.4A-C**). Thus, IFNG was unable to act on the cells within the oxazolone-challenged skin compartment.

Transcript expression of the macrophage marker, *Cd68*, increased in oxazolone-challenged GRKO skin compared to sham-treated GRKO controls ($p<0.05$, **Figure 4.5A**), indicating infiltration of macrophages into the skin. Albeit, the normalized fold change from sham-treated to oxazolone-challenged skin, was essentially equal in both GRKO and B6 skin ($p>0.05$, **Figure 4.5B**).

AMA mannose receptor, *Mrc1*, also increased in oxazolone-challenged GRKO skin compared to sham-treated GRKO controls ($p<0.05$, **Figure 4.6A**). The normalized fold change of *Mrc1* transcript expression, was greater in GRKO oxazolone-challenged skin than the increase in B6 oxazolone-challenged skin when compared with respective sham-treated controls ($p<0.05$, **Figure 4.6B**).

Arg1 transcript expression also increased in GRKO oxazolone-challenged skin compared to GRKO sham-treated skin ($p<0.05$, **Figure 4.7A**). Similarly, the normalized fold change in *Arg1* expression was greater in GRKO oxazolone-challenged skin than it was in the B6 oxazolone-challenged skin, when compared to the respective sham-treated controls ($p<0.05$, **Figure 4.7B**).

Chi3l3 transcript expression increased in GRKO oxazolone-challenged skin compared to GRKO sham-treated controls (p<0.05, **Figure 4.8A**). the normalized fold change was significantly greater in GRKO oxazolone-challenged skin than it was in B6 oxazolone-challenged skin when compared to respective sham controls (p<0.05, **Figure 4.8B**).

Last, we assessed transcript expression levels of inducers of AMA, *Il4* and *Inhba*. *Il4* transcript expression increased in GRKO oxazolone-challenged skin versus oxazolone-challenged B6 skin (p<0.05, **Figure 4.9A**). The normalized fold change was also larger in the GRKO oxazolone-challenged skin than it was in the B6 oxazolone-challenged skin when compared to respective sham-treated controls (p<0.05, **Figure 4.9B**). Nonetheless, it is difficult to conclude any biological effects *Il4* expression may have had in the oxazolone-challenged skin, as the changes in transcript expression observed were so minimal and the actual Ct values for both transcripts were relatively high (>30, data not shown); in other words *Il4* cDNA levels were not detectable until the last few PCR amplification cycles. *Inhba* transcript expression did increase in GRKO oxazolone-challenged skin (p<0.05, **Figure 4.10A**); although it is interesting that the normalized fold change was less in the oxazolone-challenged GRKO skin than it was in the B6 skin compared to sham-treated controls (p<0.05, **Figure 4.10B**).

4.2.3 Genome wide gene expression analysis of oxazolone-challenged GRKO native skin. Using the Roche NimbleGen MM9_EXP_HX12 12x135K Arrays, we compared genome wide gene expression changes in the oxazolone-challenged GRKO native skin to oxazolone-challenged B6 native skin in order to study IFNG-dependent changes in global transcript expression. Analysis revealed 1279 differentially expressed unique transcripts (IQR>0.5, FDR<0.05), that originated from a total list of 17472 unique transcripts before the IQR and statistical filters were applied.

To identify the biological processes which were affected by the deficient *Ifngr1*, we identified transcripts from the list of 1279 differentially expressed unique transcripts

that were annotated as members belonging to our inflammatory PBTs; cytotoxic T cell-associated, IFN-gamma induced, macrophage-associated and AMA-associated. We also identified transcripts with memberships in the PBTs depicting the active injury-repair response, by selecting transcripts that were annotated as injury- and repair-induced, or skin-associated. Last, we also identified transcripts that were annotated as IFNG-suppressed transcripts (48). In addition, we summarized the burden of the biological processes represented by the PBTs, by comparing the transcript set scores in the GRKO oxazolone-challenged skin to the scores in the B6 oxazolone-challenged skin.

4.2.4 T cells and macrophages. Of the 1279 differentially expressed unique transcripts there were no transcripts that were annotated as cytotoxic T cell-associated, macrophage-associated, or AMA-associated. In accordance with this observation, the summarized expression of each of these transcript sets as the transcript set score was not significantly different between the oxazolone-challenged GRKO and B6 skin (**Figure 4.11A, C-D**)

4.2.5 IFNG-effects. Unlike the T cell-, macrophage-, and AMA-associated transcript sets, there were significant expression changes in transcripts annotated as IFNG-induced transcripts. Of the 1279 differentially expressed unique transcripts were annotated as IFN-gamma-induced transcripts (total n=47), and furthermore; all 30 unique transcripts decreased expression in the oxazolone-challenged GRKO skin compared to the oxazolone-challenged B6 skin (FDR<0.05, **Table 4.1**). Some of these transcripts included (with fold change): the chemotactins, *Cxcl9* (-16.9x) and *Cxcl10* (-5.3x); and those involved in antigen processing and presentation, such as *Psmb8* (-3.6x), *Psmb9* (-5.1x), *Tapbd* (tapasin, -2.4x) and *Cd74* (class II invariant chain, -1.8x).

In the real time RT-PCR analysis (**Section 4.2.2**), we described detectable and significant changes in *Aif1* and *Ubd* transcript expression; however, these transcripts were not found within these 30 IFNG-induced transcripts. *Aif1*, although IFNG-inducible,

is not a member of this PBT due to the initial defining restrictions for members (47). Though, according to the microarray data, its expression did decrease (-1.9x) in the oxazolone-challenged GRKO skin compared to the oxazolone-challenged B6 skin (FDR=0.04). *Ubd* however, is a member of the IFNG-induced transcript set, and although *Ubd* transcript expression did not meet the FDR<0.05 cut-off, *Ubd* did experience a fold decrease (-2.0, FDR=0.34) in the oxazolone-challenged GRKO skin compared to the oxazolone-challenged B6 skin. Concomitant with the individual changes in expression of the IFNG-induced transcripts, transcript set score was significantly less in the GRKO oxazolone-challenged skin than it was in the B6 oxazolone-challenged skin (p<0.05, **Figure 4.11B**).

4.2.7 Injury-repair response. Of the 1279 differentially expressed transcripts in the oxazolone-challenged GRKO skin over the oxazolone-challenged B6 skin, we assessed the active injury-repair response by identifying the presence of the skin-selective injury and repair induced transcripts (IRITs, injury up) and the skin-associated transcripts (STs, injury down).

Of the 691 unique skin-selective IRITs, there were 124 unique transcripts that were differentially expressed (FDR<0.05) in the oxazolone-challenged GRKO skin compared to the oxazolone-challenged B6 skin. Of these, 103 (83%) unique transcripts increased expression in the oxazolone-challenged GRKO skin compared to the oxazolone-challenged B6 skin. Furthermore, some of the most overrepresented GO annotations from the 103 increased IRITs included: defense and inflammatory response; as well as chemotaxis and angiogenesis (**Table 4.2**). In accordance with these observations, the IRIT set score was significantly higher in the oxazolone-challenged GRKO skin versus the oxazolone-challenged B6 skin (p<0.05, **Figure 4.11E**).

Of the 465 unique STs, there were 104 unique transcripts that were differentially expressed (FDR<0.05) between oxazolone-challenged GRKO skin compared to the oxazolone-challenged B6 skin. Compared to the injury and repair induced transcripts

where the majority of these increased expression in the GRKO oxazolone-challenged skin, 100 (96%) unique STs decreased expression in the oxazolone-challenged GRKO skin compared to the oxazolone-challenged B6 skin. GO analysis of the 100 decreased transcripts revealed many overrepresented annotations, including: keratin and intermediate filament components; response to endogenous (hormone) stimulus; various epithelial development processes (such as epithelial, and mammary gland development); and various metabolic gene expression regulatory processes (such as regulation of gene expression, and transcription, and metabolic processes) (**Table 4.3**). The ST set score significantly decreased in the GRKO oxazolone-challenged skin, compared to the B6 oxazolone-challenged skin ($p<0.05$, **Figure 4.11F**). Thus, oxazolone-induced inflammation within GKRO mouse skin appears to induce a greater active injury-repair response than what is observed in the wild type B6 oxazolone-challenged skin.

4.2.8 IFNG-suppressed effects. Our laboratory previously defined a transcript set who's members increased expression within mouse renal GRKO allografts into wild type hosts and wild type allografts into GKO hosts (48). Of the 185 unique IFNG-suppressed transcripts, 33 unique transcripts were differentially expressed (FDR<0.05) between the oxazolone-challenged GRKO skin and the oxazolone-challenged B6 skin. Of these 33 transcripts, 26 (79%) increased expression in the oxazolone-challenged GRKO skin over oxazolone-challenged B6 skin. Accordingly, the IFNG-suppressed transcript set score also significantly increased in the GRKO oxazolone-challenged skin over the B6 oxazolone-challenged skin ($p<0.05$, **Figure 4.12**). Therefore, IFNG suppresses similar transcripts in oxazolone-induced cutaneous inflammation, as it does in rejecting mouse renal allografts (48). Furthermore, our laboratory previously showed that in rejecting GRKO renal allografts, or rejecting wild type renal allografts in GKO hosts, IFNG-suppressed transcripts have overlapping memberships with the kidney-selective IRITs and the AMA-associated transcripts (48). Here, in the oxazolone-challenged GRKO skin we also observed a similar phenomenon; 13 (39%) of the 33 differentially expressed

transcripts were also members of the skin-selective IRITs. However, there were no overlapping differentially expressed IFNG-suppressed and AMA-associated transcripts in the oxazolone-challenged GRKO skin; but this was expected given that the AMA burden did not show any gross increase in the GRKO oxazolone-challenged skin over the B6 oxazolone-challenged skin.

4.3 TABLES

Table 4.1: 30 unique IFNG-induced transcripts (IFNG-effects) differentially expressed in oxazolone-challenged GRKO skin over oxazolone-challenged B6 skin. Ordered by fold change.

GenBank	Gene Name	Fold Change	Roche NibleGen Annotation
BC034256	Tgtp	-48.2	T-cell specific GTPase
BC003343	Cxcl9	-16.9	chemokine (C-X-C motif) ligand 9
BC019195	Gbp3	-14.8	guanylate nucleotide binding protein 3
AJ007971	Iigp1	-14.2	IIGP protein
AK165065	Igtp	-13.3	interferon gamma induced GTPase
EF494423	Gbp4	-11.1	guanylate binding protein 4
BC050835	Ifit2	-5.6	interferon-induced protein with tetratricopeptide repeats 2
BC030067	Cxcl10	-5.3	chemokine (C-X-C motif) ligand 10
BC116364	Psmb9	-5.1	proteasome (prosome, macropain) subunit, beta type 9
NM_019440	Irgm2	-4.0	interferon inducible GTPase 2
BC013785	Psmb8	-3.6	proteasome (prosome, macropain) subunit, beta type 8
BC087949	Bst2	-3.6	bone marrow stromal cell antigen 2
BC003768	Ifit1	-3.6	interferon-induced protein with tetratricopeptide repeats 1
M35246	H2-T10	-3.4	Mouse MHC class I H2-TL-T10-b mRNA (b haplotype)
AK002830	Irf7	-3.4	interferon regulatory factor 7
BC145957	Irgm1	-2.7	immunity-related GTPase family, M
BC034361	Oasl2	-2.6	2'-5' oligoadenylate synthetase-like 2
BC005648	H2-T23	-2.5	histocompatibility 2, T region locus 23
BC090658	Lgals3bp	-2.4	lectin, galactoside-binding, soluble, 3 binding protein
BC011086	C2	-2.4	complement component 2 (within H-2S)
BC015074	Tapbp	-2.4	TAP binding protein
AK147960	Herc5	-2.3	hect domain and RLD 6
BC001996	H2-DMa	-2.1	histocompatibility 2, class II, locus Dma
BC129843	Mpeg1	-2.0	macrophage expressed gene 1
BC019721	H2-Aa	-1.9	histocompatibility 2, class II antigen A, alpha
BC088981	Psme1	-1.8	proteasome (prosome, macropain) 28 subunit, alpha
BC046610	Erap1	-1.8	endoplasmic reticulum aminopeptidase 1
BC010322	H2-Ab1	-1.8	histocompatibility 2, class II antigen A, beta 1
BC003476	Cd74	-1.8	CD74 antigen (invariant polypeptide)
AK003370	Il18bp	-1.6	interleukin-18 binding protein

Table 4.2: GRKO enriched skin-selective IRITs top gene ontology (GO) annotations within biological process, molecular function, and cellular compartment categories. *P*-value is representative of a hypergeometric test from selecting the IRITs found within each GO category by chance alone. Sorted by increasing *p*-value. (Table continued on next page.)

	Top 20 Annotations in Biological Process Category (total n=67, $p<0.05$)	Genes in Category	Genes in IRITs in Category	% of Genes in IRITs in Category	*p*-value
GO:0006952	defense response	448	21	17.1	0.000
GO:0009611	response to wounding	347	18	14.6	0.000
GO:0016477	cell migration	240	15	12.2	0.000
GO:0048870	cell motility	284	15	12.2	0.000
GO:0051674	localization of cell	284	15	12.2	0.000
GO:0006928	cell motion	367	16	13.0	0.000
GO:0006954	inflammatory response	225	13	10.6	0.000
GO:0006935	chemotaxis	109	9	7.3	0.000
GO:0042330	taxis	109	9	7.3	0.000
GO:0007626	locomotory behavior	239	11	8.9	0.000
GO:0007610	behavior	405	13	10.6	0.000
GO:0030595	leukocyte chemotaxis	27	5	4.1	0.000
GO:0060326	cell chemotaxis	27	5	4.1	0.000
GO:0001817	regulation of cytokine production	139	8	6.5	0.000
GO:0042060	wound healing	112	7	5.7	0.000
GO:0050900	leukocyte migration	43	5	4.1	0.000
GO:0050865	regulation of cell activation	156	7	5.7	0.001
GO:0001819	positive regulation of cytokine production	62	5	4.1	0.001
GO:0001568	blood vessel development	244	8	6.5	0.002
GO:0001944	vasculature development	250	8	6.5	0.002

…Table 4.2 continued on next page.

Table 4.2: (continued…)

	Annotations in Molecular Function (total n=7, $p<0.05$)	Genes in Category	Genes in IRITs in Category	% of Genes in IRITs in Category	p-value
GO:0008009	chemokine activity	38	4	3.3	0.002
GO:0042379	chemokine receptor binding	39	4	3.3	0.002
GO:0005125	cytokine activity	180	6	4.9	0.008
GO:0004713	protein tyrosine kinase activity	164	5	4.1	0.027
GO:0032553	ribonucleotide binding	1796	20	16.3	0.037
GO:0032555	purine ribonucleotide binding	1796	20	16.3	0.037
GO:0032559	adenyl ribonucleotide binding	1460	17	13.8	0.042

	Annotations in Molecular Function and Cellular Component Category (total n=2, $p<0.05$)	Genes in Category	Genes in IRITs in Category	% of Genes in IRITs in Category	p-value
GO:0005886	plasma membrane	2906	36	29.3	0.000
GO:0005615	extracellular space	511	9	7.3	0.020

END Table 4.2.

Table 4.3: GRKO enriched skin-associated transcripts top gene ontology (GO) annotations within biological process, molecular function, and cellular compartment categories. *P*-value is representative of a hypergeometric test from selecting the STs found within each GO category by chance alone. Sorted by increasing *p*-value. (Table continued on next page.)

	Top 20 Annotations in Biological Process Category (total n=34, $p<0.05$)	Genes in Category	Genes in STs in Category	% of Genes in STs in Category	*p*-value
GO:0005882	intermediate filament	137	20	21.1	0.000
GO:0045111	intermediate filament cytoskeleton	140	20	21.1	0.000
GO:0045095	keratin filament	64	13	13.7	0.000
GO:0005856	cytoskeleton	1122	29	30.5	0.000
GO:0044430	cytoskeletal part	774	22	23.2	0.000
GO:0043228	non-membrane-bounded organelle	1919	30	31.6	0.000
GO:0043232	intracellular non-membrane-bounded organelle	1919	30	31.6	0.000
GO:0009725	response to hormone stimulus	165	6	6.3	0.000
GO:0009719	response to endogenous stimulus	184	6	6.3	0.000
GO:0045893	positive regulation of transcription, DNA-dependent	416	7	7.4	0.003
GO:0051254	positive regulation of RNA metabolic process	419	7	7.4	0.003
GO:0030879	mammary gland development	86	4	4.2	0.003
GO:0043434	response to peptide hormone stimulus	95	4	4.2	0.005
GO:0045941	positive regulation of transcription	475	7	7.4	0.006
GO:0010604	positive regulation of macromolecule metabolic process	633	8	8.4	0.006
GO:0010628	positive regulation of gene expression	488	7	7.4	0.007
GO:0008285	negative regulation of cell proliferation	224	5	5.3	0.008
GO:0045944	positive regulation of transcription from RNA polymerase II promoter	358	6	6.3	0.008
GO:0045935	positive regulation of nucleic acid metabolic process	510	7	7.4	0.009
GO:0060429	epithelium development	271	5	5.3	0.010

…Table 4.3 continued on next page.

Table 4.3: (continued…)

	Annotations in Molecular Function (total n=2, p<0.05)	Genes in Category	Genes in IRITs in Category	% of Genes in STs in Category	p-value
GO:0019900	kinase binding	85	3	3.2	0.044
GO:0005509	calcium ion binding	840	8	8.4	0.044

	Annotations in Cellular Component Category (total n=7, p<0.05)	Genes in Category	Genes in STs in Category	% of Genes in STs in Category	p-value
GO:0005882	intermediate filament	137	20	21.1	0.000
GO:0045111	intermediate filament cytoskeleton	140	20	21.1	0.000
GO:0045095	keratin filament	64	13	13.7	0.000
GO:0005856	cytoskeleton	1122	29	30.5	0.000
GO:0044430	cytoskeletal part	774	22	23.2	0.000
GO:0043228	non-membrane-bounded organelle	1919	30	31.6	0.000
GO:0043232	intracellular non-membrane-bounded organelle	1919	30	31.6	0.000

END Table 4.3.

4.4 FIGURES

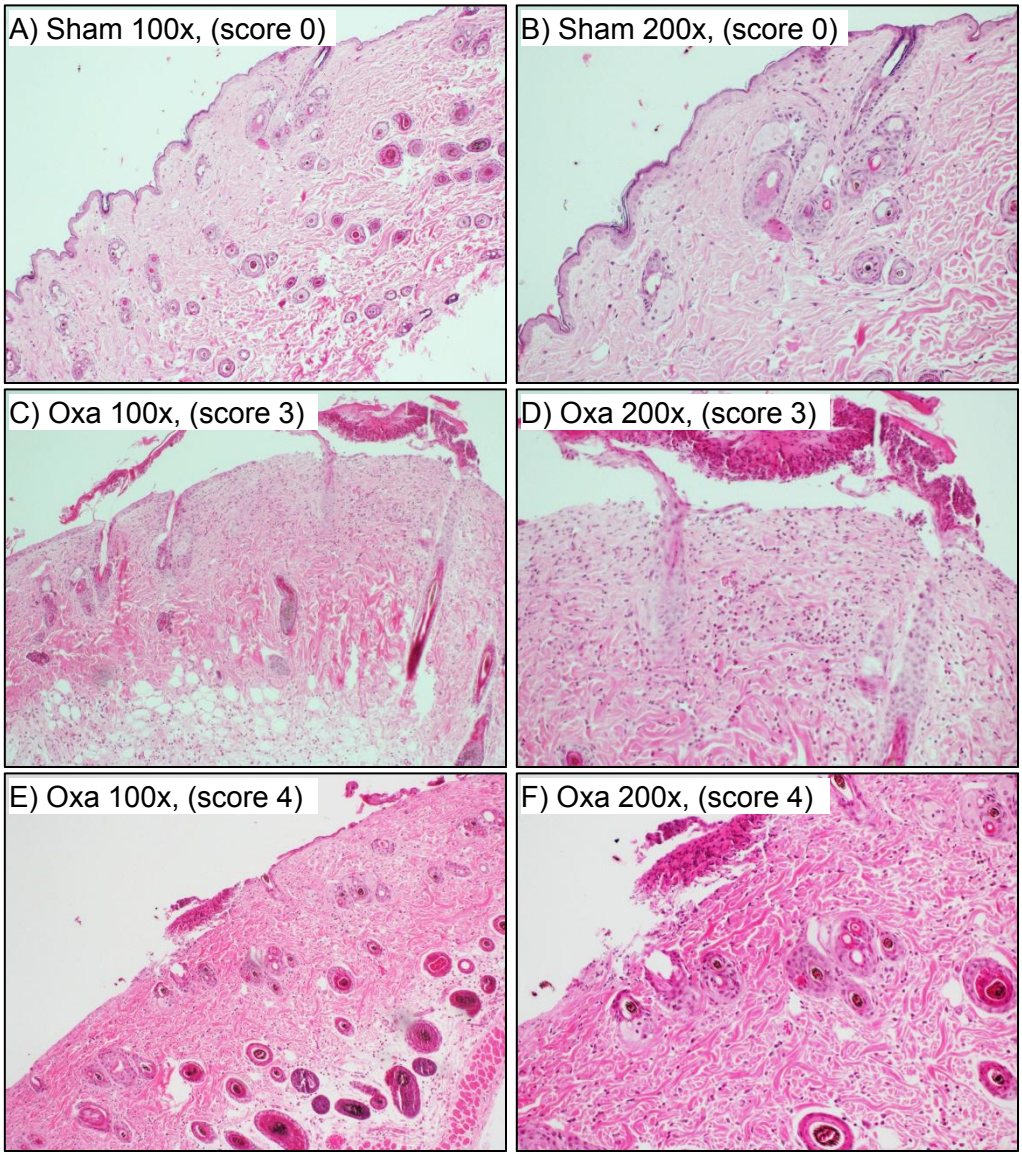

Figure 4.1: Histopathology of sham-treated GRKO skin and oxazolone-challenged GRKO skin. Sham-treated GRKO skin day 6 with a histological score of 0, show no inflammatory cell infiltrate, 100x **(A)** and 200x magnifications **(B)**. Oxazolone-challenged GRKO skin day 6 **(C-H)**; showing dermal inflammatory infiltrate with focal epithelial ulcerations, 100x **(C)** and 200x magnifications **(D)**; histological score of 4, showing dermal inflammatory infiltrate with multiple erosive epithelial ulcerations, 100x **(E)** and 200x magnifications **(F)**. No samples received a histological score of 1 or 2. (H&E stain.)

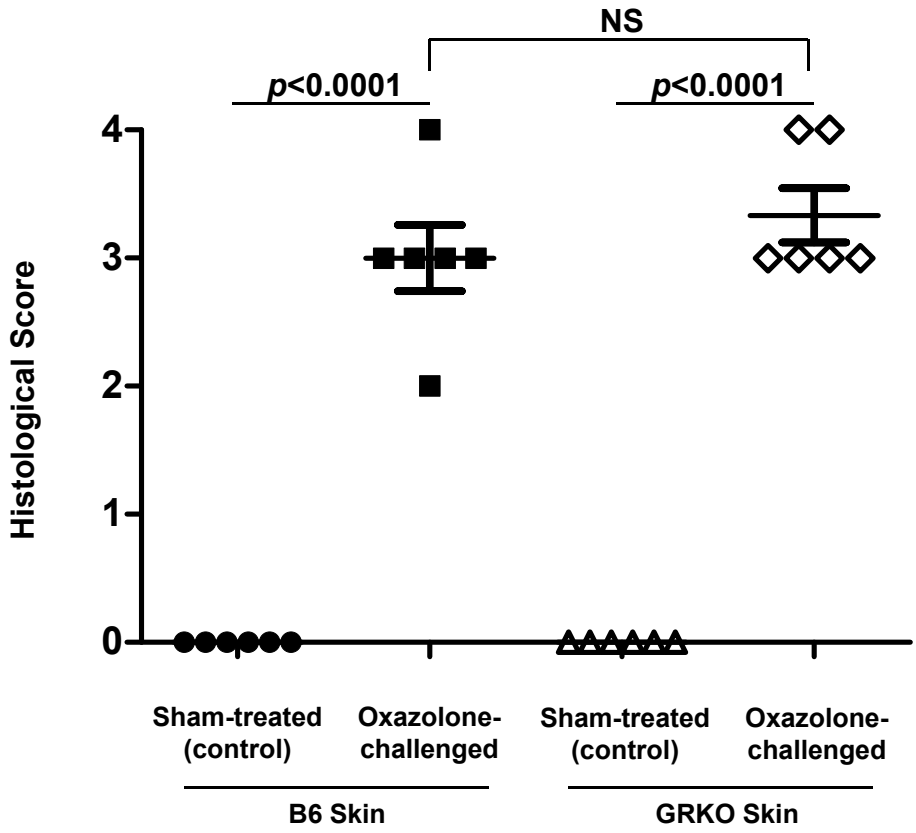

Figure 4.2: Oxazolone-challenged B6 and B6.GRKO skin appear histological similar to each other, despite being significantly more inflamed than sham-treated controls. Skin tissue sections were stained with H&E, and lesions were scored semi-quantitatively on a scale of 0 through 4. Skin from sham-treated B6 and B6.GRKO mice (N=6 each) was absent of inflammation, while inflammation in the skin of oxazolone-challenged B6 and B6.GRKO mice (N=6 each) resulted in a mean histological score of 3.0 and 3.3, respectively. Significance of difference in histology scores were determined by a two-way ANOVA; NS, not significant (p>0.05).

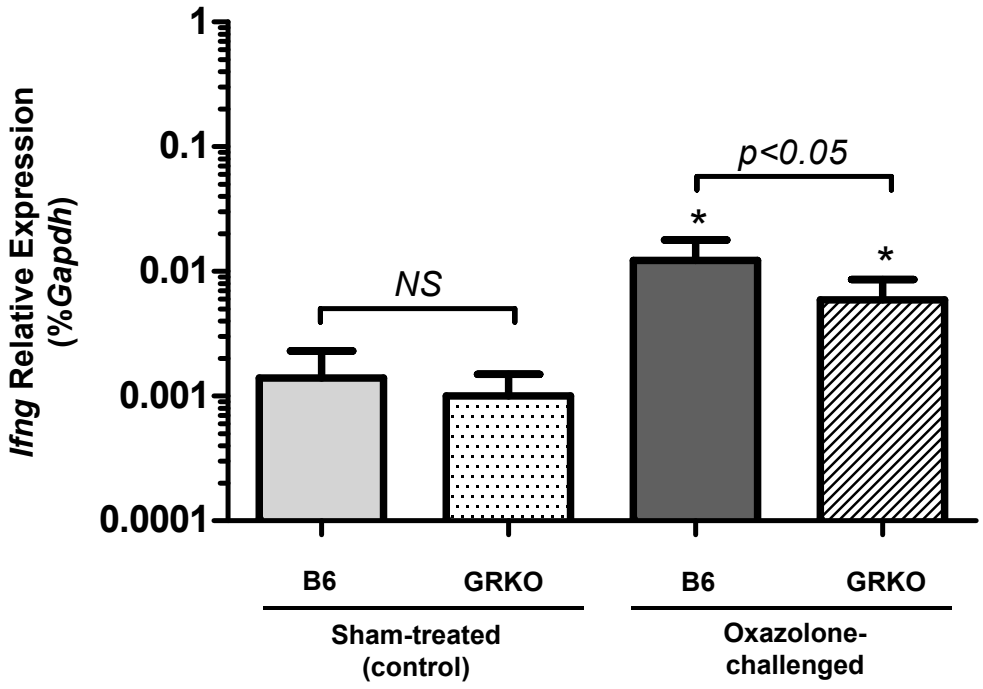

Figure 4.3: *Ifng* transcript expression within sham-treated and oxazolone-challenged B6 and GRKO mouse skin assessed by real time RT-PCR. Transcript expression is expressed as %*Gapdh* transcript expression using the dCt formula. Transcript expression is significantly different, as determined by a two-way ANOVA and adjusted with Bonferroni correction: $p<0.05$ between oxazolone and respective (strain controlled) sham condition is indicated by *; horizontal bars indicate level of significance between B6 and GRKO mouse strains of the same treatment, oxazolone or sham (NS, not significant $p>0.05$).

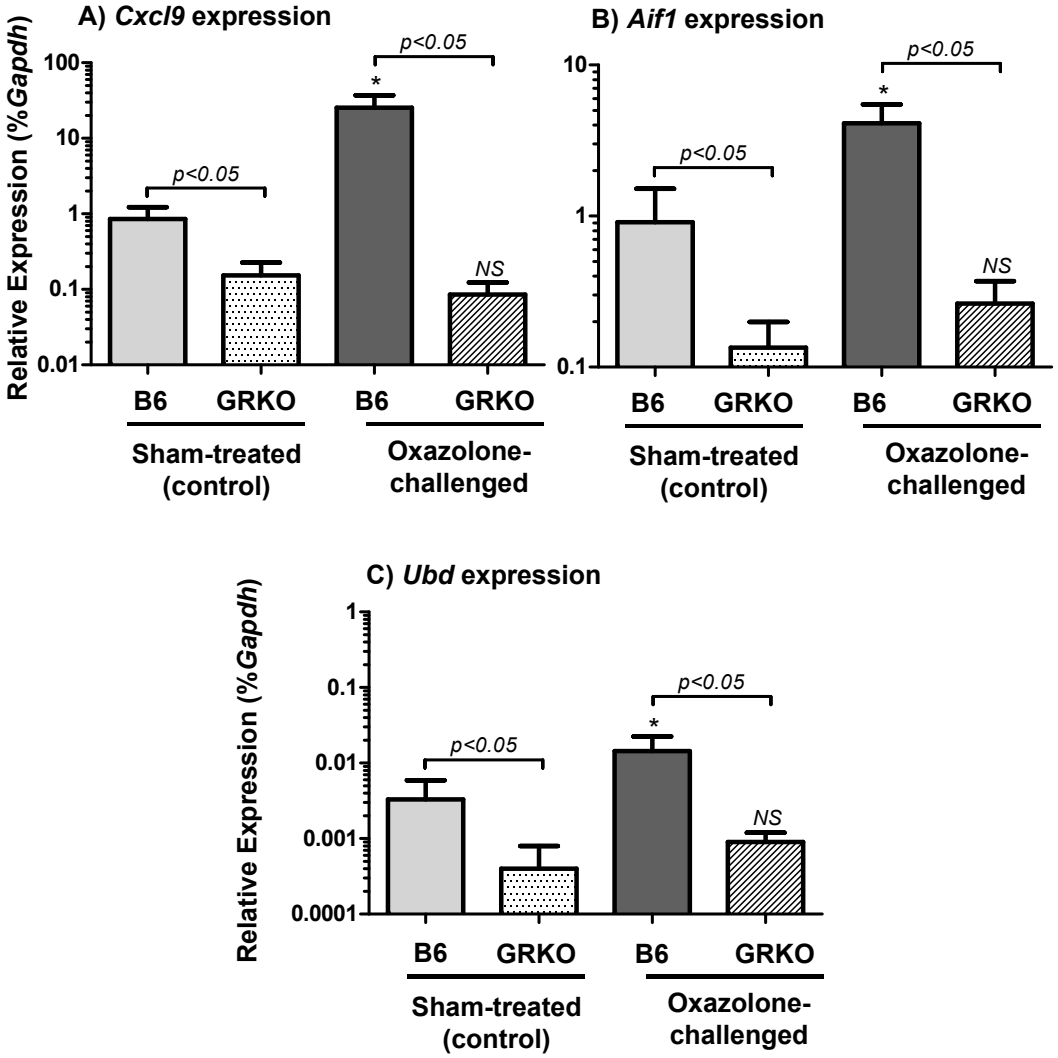

Figure 4.4: Transcript expression of the IFNG-induced transcripts, *Cxcl9*, *Aif* and *Ubd* within sham-treated and oxazolone-challenged B6 and GRKO mouse skin assessed by real time RT-PCR. Transcript expression is expressed as %*Gapdh* transcript expression using the dCt formula. Compared to the oxazolone-challenged B6 skin, transcript expression of: *Cxcl9* **(A)**; *Aif1* **(B)**; and, *Ubd* **(C)** decreased within the oxazolone-challenged B6.GRKO skin. Transcript expression is significantly different, as determined by an ANOVA and adjusted with Bonferroni correction: $p<0.05$ between oxazolone and respective (strain controlled) sham condition is indicated by *; horizontal bars indicate level of significance between B6 and GRKO mouse strains of the same treatment, oxazolone or sham (NS, not significant $p>0.05$).

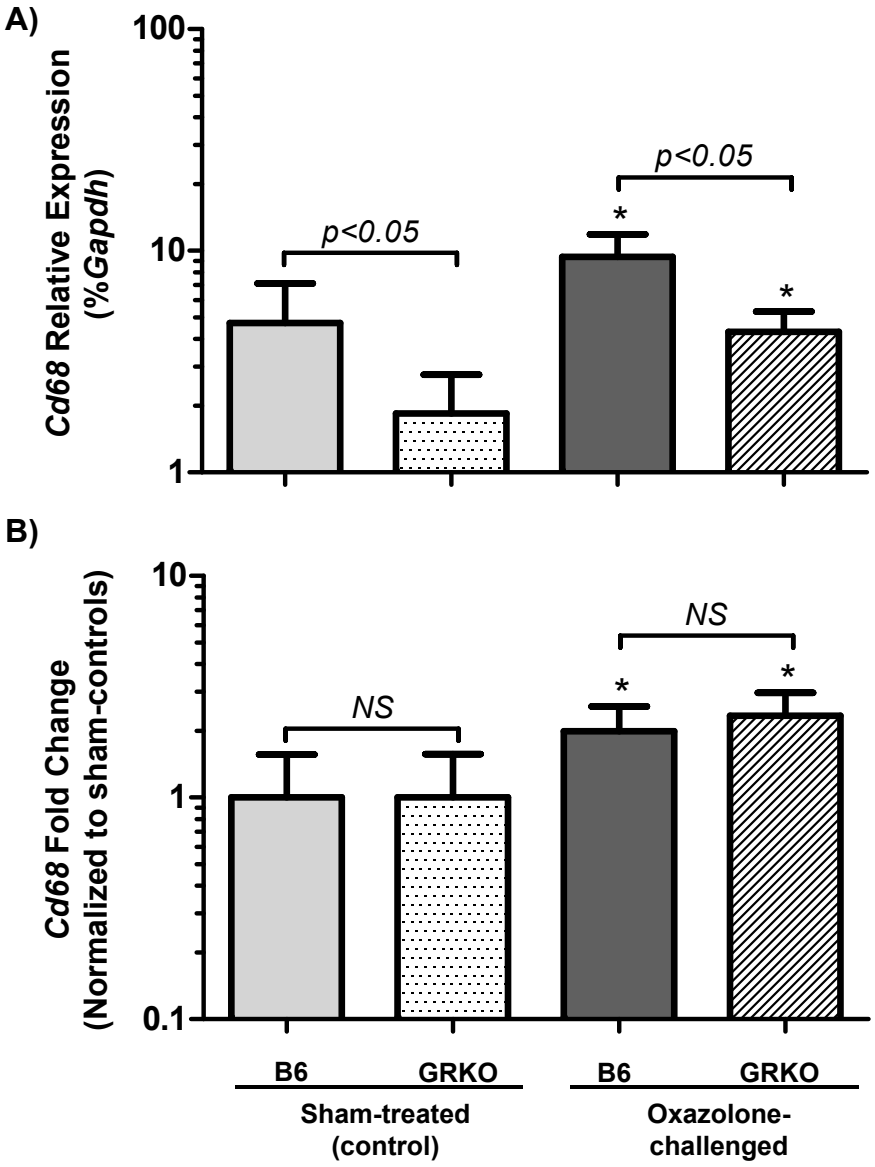

Figure 4.5: *Cd68* transcript expression within sham-treated and oxazolone-challenged B6 and GRKO mouse skin assessed by real time RT-PCR. *Cd68* transcript expression is expressed as: %*Gapdh* transcript expression using the dCt formula **(A)**; or is normalized as a fold change in the oxazolone-challenged mice to the sham-treated controls using the ddCt formula **(B)**. Transcript expression is significantly different, as determined by a two-way ANOVA and adjusted with Bonferroni correction using the dCt values **(A)** or the ddCt values **(B)**: $p<0.05$ between oxazolone and respective (strain controlled) sham condition is indicated by *; horizontal bars indicate level of significance between B6 and GRKO mouse strains of the same treatment, oxazolone or sham (NS, not significant $p>0.05$).

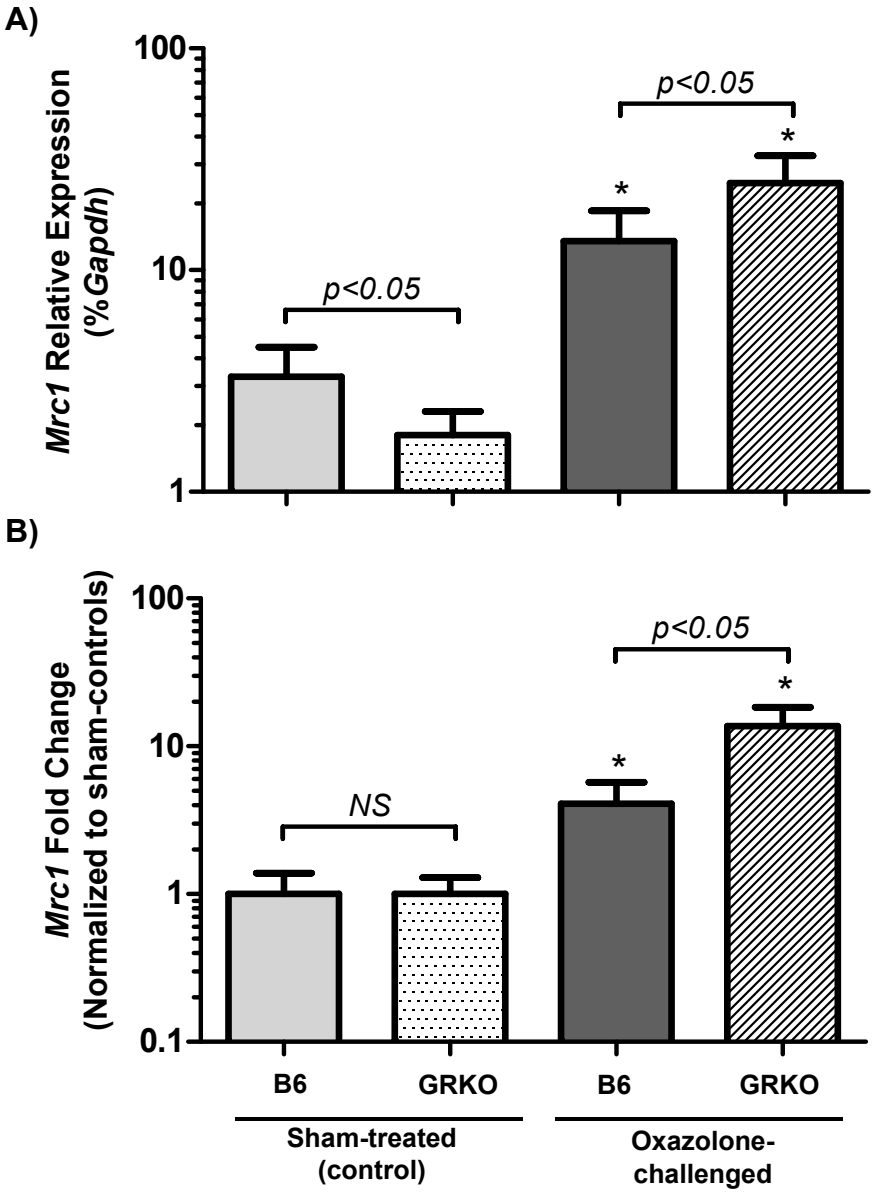

Figure 4.6: *Mrc1* transcript expression within sham-treated and oxazolone-challenged B6 and GRKO mouse skin assessed by real time RT-PCR. *Mrc1* transcript expression is expressed as: %*Gapdh* transcript expression using the dCt formula **(A)**; or is normalized as a fold change in the oxazolone-challenged mice to the sham-treated controls using the ddCt formula **(B)**. Transcript expression is significantly different, as determined by a two-way ANOVA and adjusted with Bonferroni correction using the dCt values **(A)** or the ddCt values **(B)**: $p<0.05$ between oxazolone and respective (strain controlled) sham condition is indicated by *; horizontal bars indicate level of significance between B6 and GRKO mouse strains of the same treatment, oxazolone or sham (NS, not significant $p>0.05$).

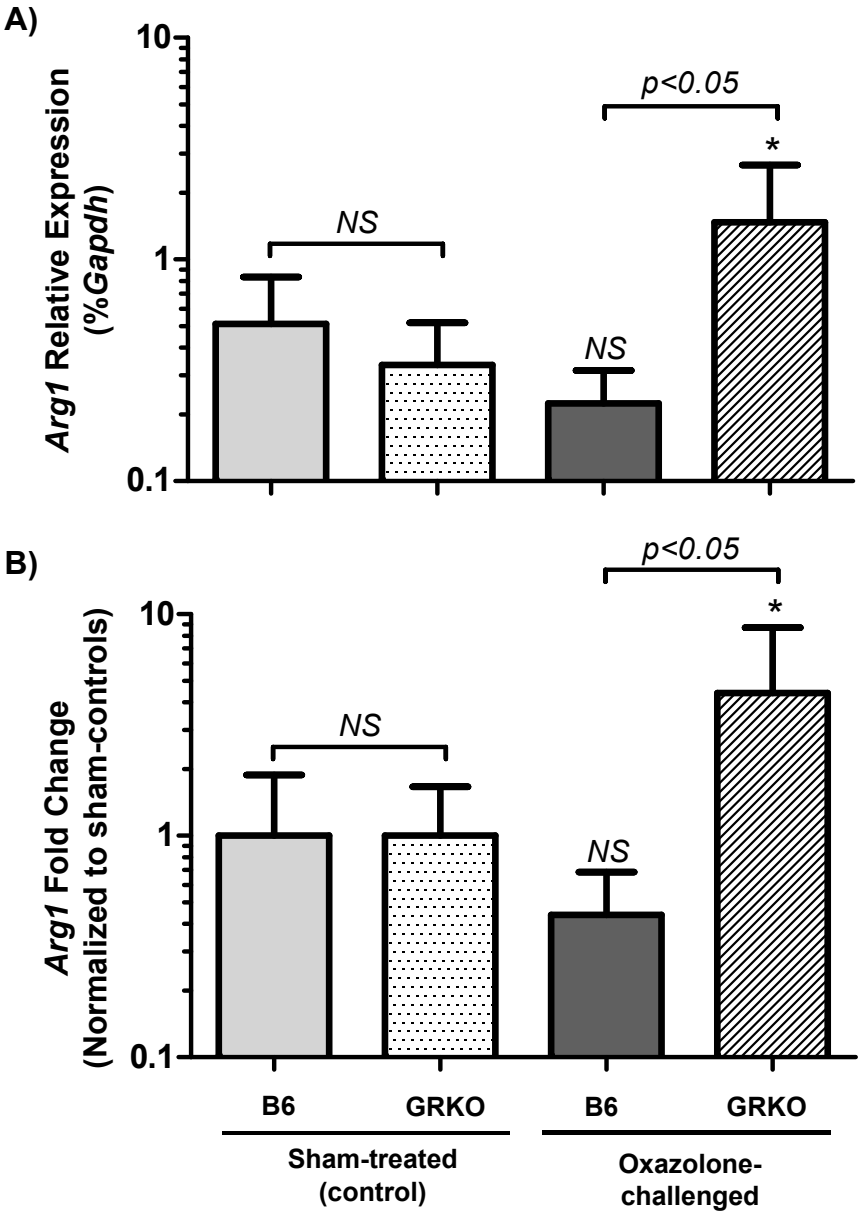

Figure 4.7: *Arg1* transcript expression within sham-treated and oxazolone-challenged B6 and GRKO mouse skin assessed by real time RT-PCR. *Arg1* transcript expression is expressed as: %*Gapdh* transcript expression using the dCt formula **(A)**; or is normalized as a fold change in the oxazolone-challenged mice to the sham-treated controls using the ddCt formula **(B)**. Transcript expression is significantly different, as determined by a two-way ANOVA and adjusted with Bonferroni correction using the dCt values **(A)** or the ddCt values **(B)**: $p<0.05$ between oxazolone and respective (strain controlled) sham condition is indicated by *; horizontal bars indicate level of significance between B6 and GRKO mouse strains of the same treatment, oxazolone or sham (NS, not significant $p>0.05$).

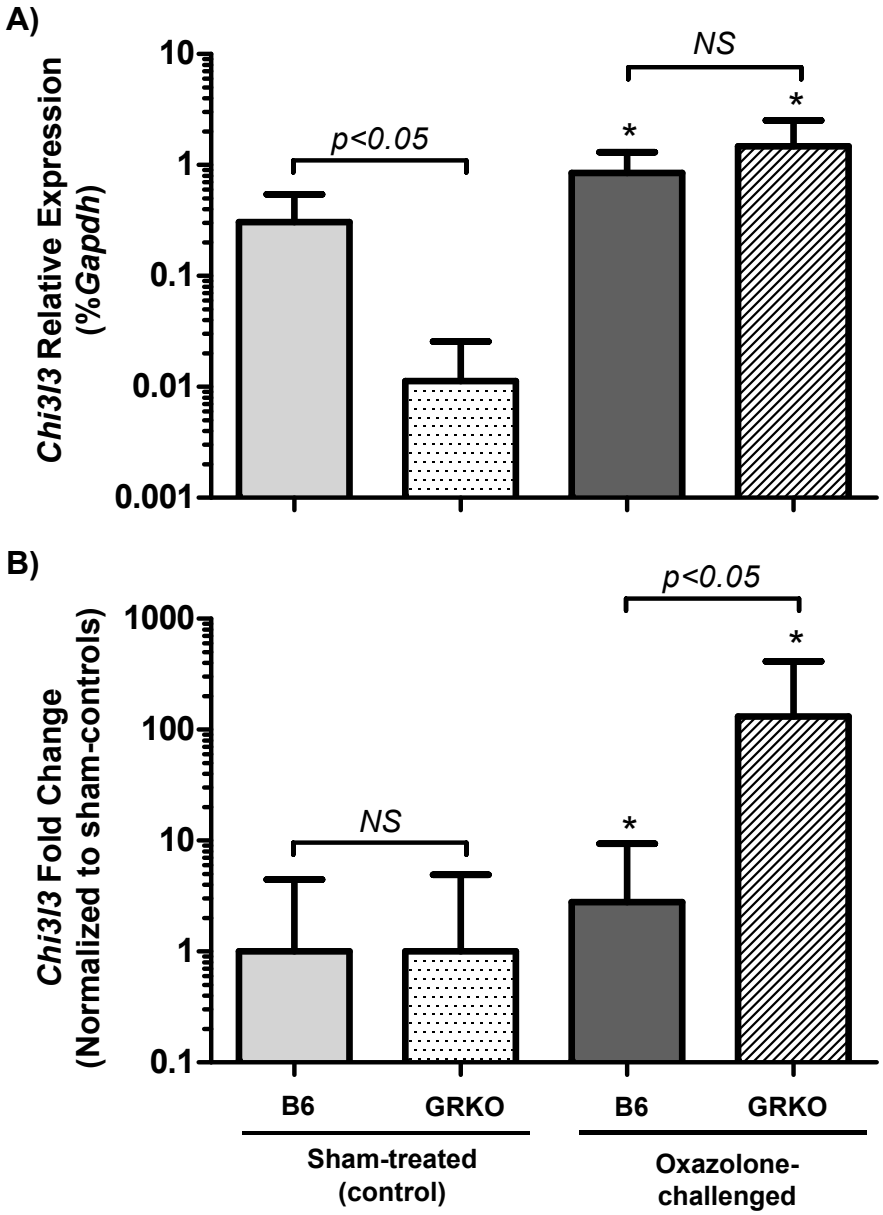

Figure 4.8: *Chi3l3* transcript expression within sham-treated and oxazolone-challenged B6 and GRKO mouse skin assessed by real time RT-PCR. *Chi3l3* transcript expression is expressed as: %*Gapdh* transcript expression using the dCt formula **(A)**; or is normalized as a fold change in the oxazolone-challenged mice to the sham-treated controls using the ddCt formula **(B)**. Transcript expression is significantly different, as determined by a two-way ANOVA and adjusted with Bonferroni correction using the dCt values **(A)** or the ddCt values **(B)**: $p<0.05$ between oxazolone and respective (strain controlled) sham condition is indicated by *; horizontal bars indicate level of significance between B6 and GRKO mouse strains of the same treatment, oxazolone or sham (NS, not significant $p>0.05$).

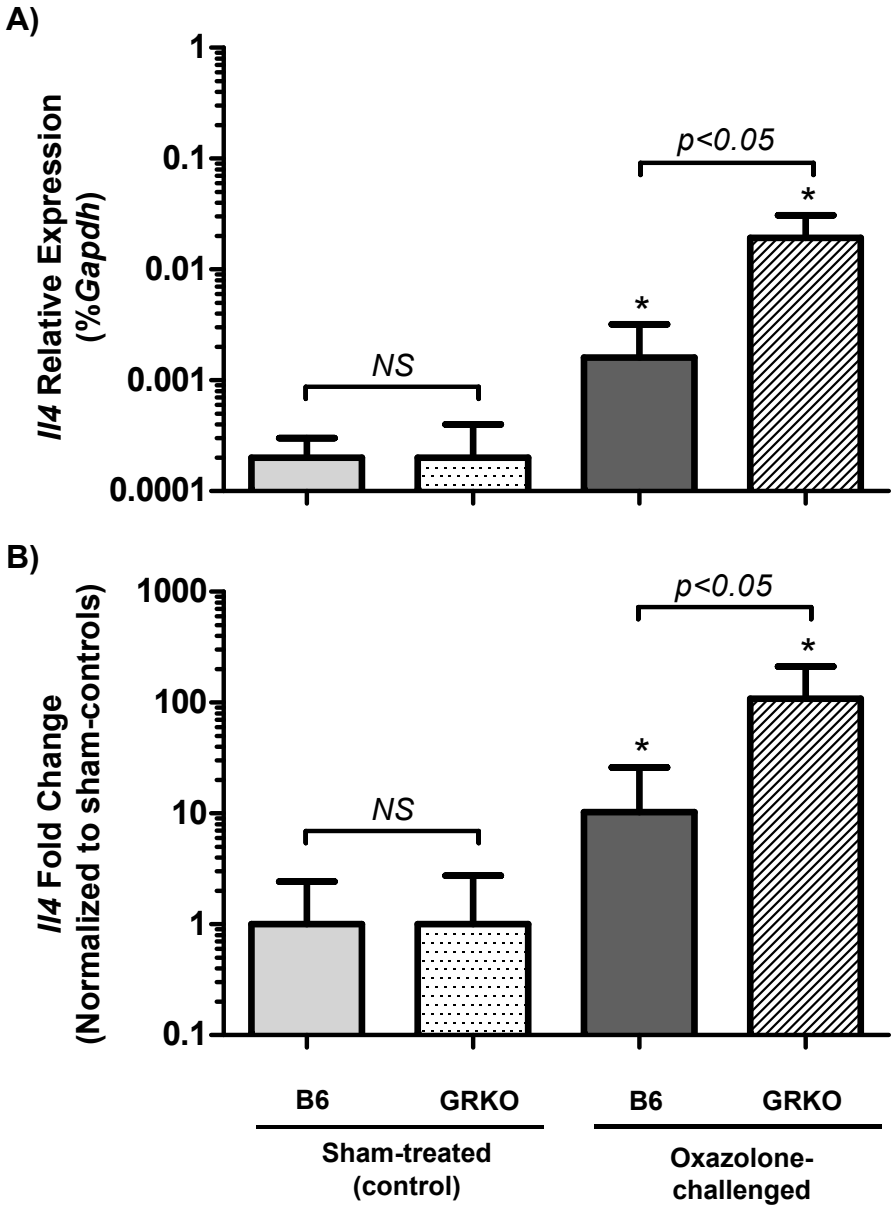

Figure 4.9: *Il4* transcript expression within sham-treated and oxazolone-challenged B6 and GRKO mouse skin assessed by real time RT-PCR. *Il4* transcript expression is expressed as: %*Gapdh* transcript expression using the dCt formula **(A)**; or is normalized as a fold change in the oxazolone-challenged mice to the sham-treated controls using the ddCt formula **(B)**. Transcript expression is significantly different, as determined by a two-way ANOVA and adjusted with Bonferroni correction using the dCt values **(A)** or the ddCt values **(B)**: $p<0.05$ between oxazolone and respective (strain controlled) sham condition is indicated by *; horizontal bars indicate level of significance between B6 and GRKO mouse strains of the same treatment, oxazolone or sham (NS, not significant $p>0.05$).

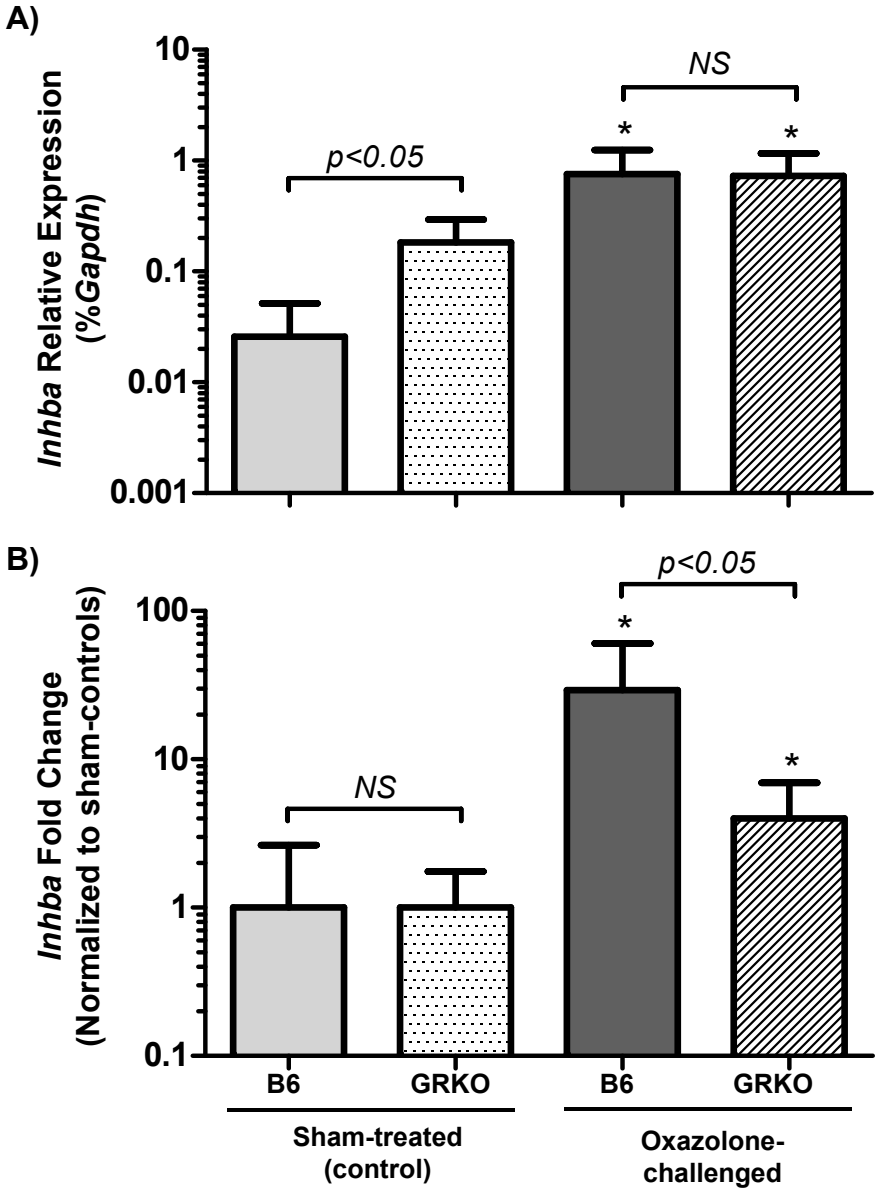

Figure 4.10: *Inhba* transcript expression within sham-treated and oxazolone-challenged B6 and GRKO mouse skin assessed by real time RT-PCR. *Inhba* transcript expression is expressed as: %*Gapdh* transcript expression using the dCt formula **(A)**; or is normalized as a fold change in the oxazolone-challenged mice to the sham-treated controls using the ddCt formula **(B)**. Transcript expression is significantly different, as determined by a two-way ANOVA and adjusted with Bonferroni correction using the dCt values **(A)** or the ddCt values **(B)**: $p<0.05$ between oxazolone and respective (strain controlled) sham condition is indicated by *; horizontal bars indicate level of significance between B6 and GRKO mouse strains of the same treatment, oxazolone or sham (NS, not significant $p>0.05$).

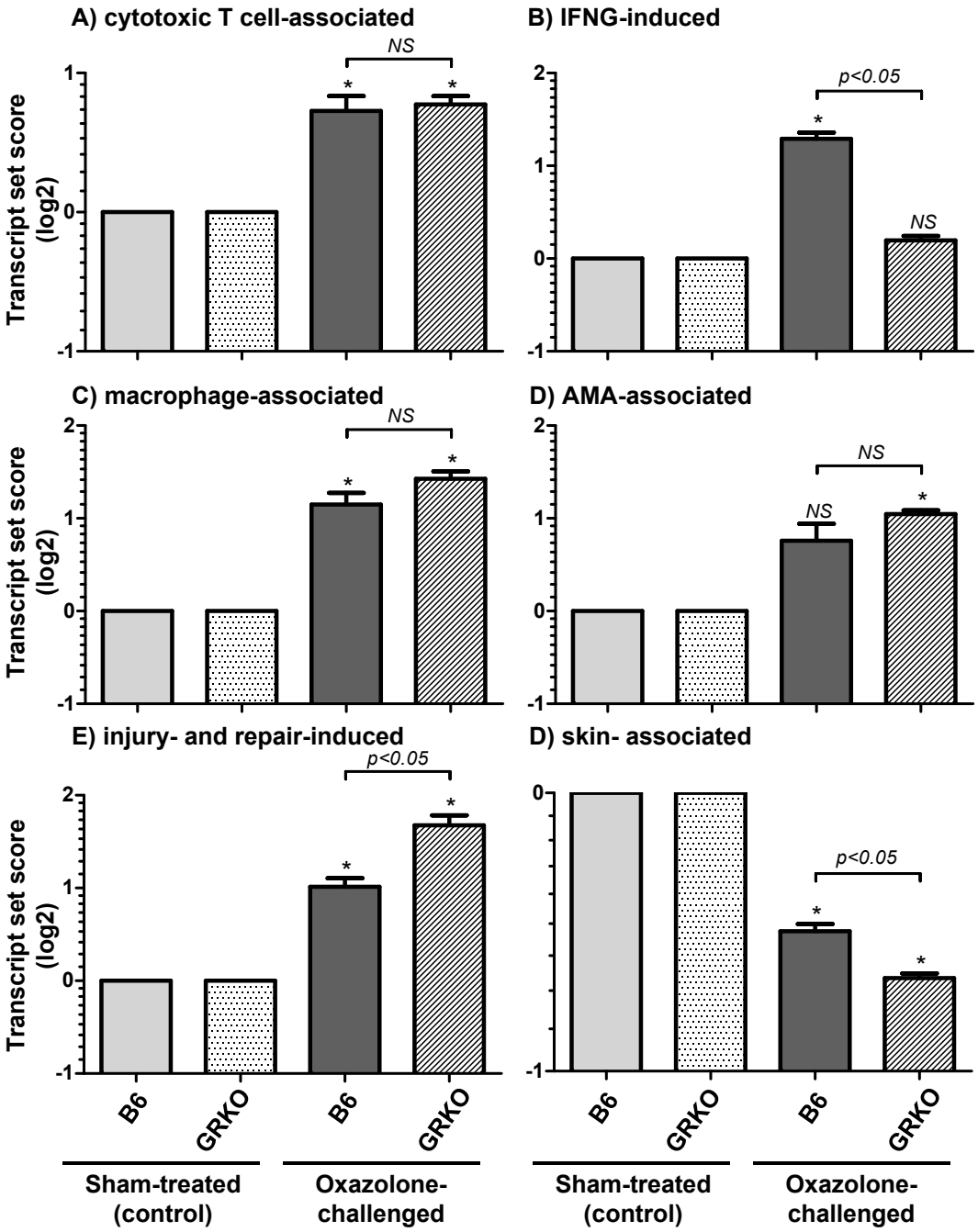

Figure 4.11: Transcript set scores of the inflammatory and injury-repair response PBTs in oxazolone-challenged B6 and GRKO skin. Cytotoxic T cell associated **(A)**; IFNG-induced **(B)**; macrophage associated **(C)**; and, AMA-associated **(D)**. Only expression of the IFNG-induced transcripts is grossly affected by the deficient *Ifngr1* **(B)**. Skin-selective injury- and repair-induced PBTs increase expression in the GRKO oxazolone-challenged skin over challenged B6 skin **(E)**. The opposite affect is seen in the skin-associated PBTs **(F)**. Values are mean ± SEM. Significance is determined by a student's T-test, $p<0.05$, sham-treated skin and oxazolone-challenged skin, or oxazolone-challenged skin of B6 and GRKO mice.

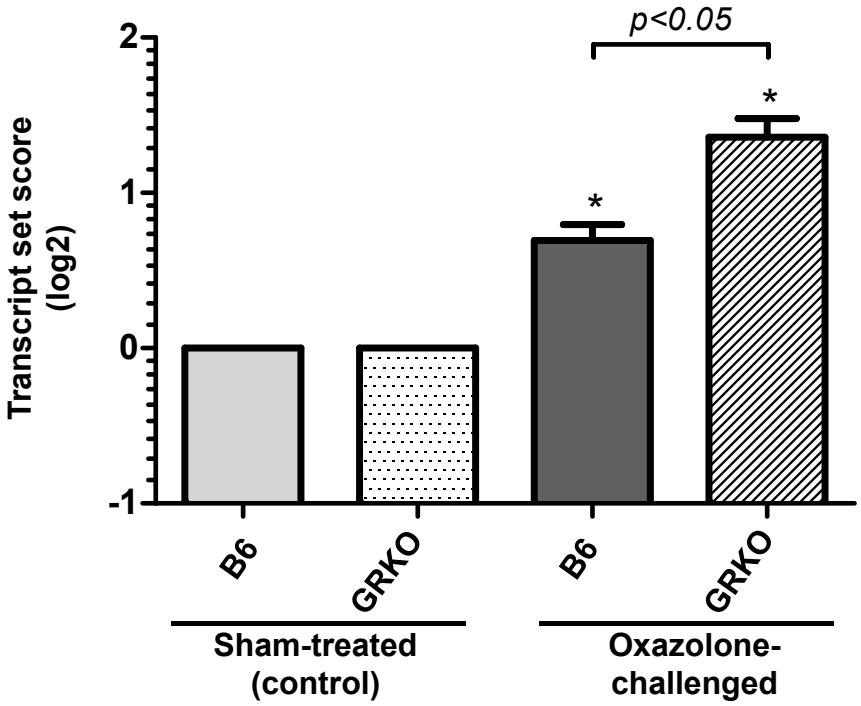

Figure 4.12: IFNG-suppressed transcript set score in oxazolone-challenged B6 and GRKO skin. IFNG-suppressed transcripts have increased expression when IFNG-signalling is deficient within Ifngr1 deficient (GRKO) oxazolone-challenged mice compared to sham-controls or B6 (wild type) oxazolone-challenged mice, which have the Ifngr. Values are mean ± SEM. Significance is determined by a student's T-test, $p<0.05$, sham-treated skin and oxazolone-challenged skin, or oxazolone-challenged skin of B6 and GRKO mice.

CHAPTER 5

DISCUSSION

5.1 STUDY SUMMARY PART 1: A COMPARISON OF DTH AND TCMR

The broad molecular changes that occur over the time course in TCMR of mouse renal allografts have been previously described (6). We sought to characterize the breadth of these changes in TCMR by qualitatively analyzing, and comparing them to the molecular changes that occur in another T cell mediated disease outside of a rejecting allograft. As such, the first aim of this study was to analyze whether DTH and TCMR experience the same molecular changes. Because the immunological mechanisms of TCMR are thought to be similar to that of DTH, we hypothesized that the histological changes, but especially the molecular changes in TCMR and DTH would be qualitatively similar.

We setup an experimental method for inducing CHS, a model of DTH, by challenging mice epicutaneously with oxazolone; and compared the histological and molecular phenotype of oxazolone-challenged skin to that of TCMR of mouse renal allografts. As in TCMR (8), the histology of CHS presents itself as mononuclear infiltration and epithelial injury (ulcer and necrosis in skin and tubulitis and necrosis in kidney). In combination with histological analysis, we utilized real time RT-PCR and gene expression microarrays to assess and compare molecular features in both CHS and TCMR involved in T cell and macrophage infiltration, AMA, IFNG-effects, and parenchymal injury-repair processes. While skin and kidney tissue are structurally and functionally very dissimilar; we found that CHS, induced by oxazolone, shows many molecular features that are shared with TCMR.

5.2 MOLECULAR CHANGES OF T CELL-MEDIATED INFLAMMATION

5.2.1 T cells. Nine cytotoxic T cell-associated transcripts were found in the oxazolone-challenged skin and rejecting renal allografts. Some of these transcripts included *Cxcr6*, *Tcra* and *Cd8a*, which are common markers associated with T cells (76). Additionally, these transcripts were previously annotated by our laboratory as typical rejection transcripts which robustly quantify TCMR in human and mouse allografts (31).

While some of T cell-associated transcripts, such as *Gzma* and *Gzmb*, are directly involved in cytotoxic mechanisms, we know these mechanisms are not necessarily employed despite their presence; because TCMR of mouse renal allografts progresses in *Gzma* and *Gzmb* deficient hosts as it would in wild type hosts (16). In other words, renal allografts in *Gzma* and *Gzmb* deficient hosts still develop the classic histological lesions of TCMR, including interstitial inflammation and tubulitis. It has been proposed in TCMR, within the rejecting allograft cognate T cells recognize specific antigen on antigen presenting cells and recruit noncognate T cells, which express transcripts for GZMA and GZMB, and macrophages(8); presumptively similar mechanisms exist in CHS. Naturally therefore, we looked for the overlapping macrophage-associated transcripts.

5.2.2 Macrophages. We found that 20 members of our macrophage-associated transcripts were found in both oxazolone-challenged skin and TCMR of renal allografts. Many of the differentially expressed macrophage-associated transcripts code for molecules that ultimately have a diverse array of functions; some of these include: *Cd300lf* and *Pirb* which code for immunoglobulin (Ig)-superfamily, immunoreceptor tyrosine-based inhibitory motifs (ITIM s) cell surface receptors (77,78). CD300LF is a recently described inhibitory receptor, and its ligand and biological function is yet to be determined (77). PIRB, binds to MHC class I molecules and plays a role in determining CMA or AMA lineage during development in the bone marrow (78). Another two

macrophage-associated transcripts included in the above lists were *Tlr2*/*8*. TLRs are pattern-recognition receptors, and the protein products of these two recognise beta-glucan and viral RNA particles, respectively (79). Another transcript that exemplifies the diverse functions of the macrophage-associated transcripts was *Emilin2*. EMILIN2 has been shown to putatively associate with platelets, and aid in thrombus formation (80).

The general macrophage marker *Cd68* was also increased in both oxazolone-challenged skin and TCMR of renal allografts. Our laboratory previously confirmed the increased macrophage presence through positive immunohistochemical stains for CD68 in TCMR of mouse renal allografts (46,81). Not surprisingly, when we stained the sham-treated and oxazolone-challenged skin for CD68, we also observed an increase in the number of $CD68^+$ cells within the oxazolone-challenged skin. Thus, these results would suggest there was a paralleled influx of macrophages into the inflamed skin and kidney tissues.

5.2.3 IFNG-effects. IFNG-induced transcripts were similar in both oxazolone-challenged skin and the rejecting renal allografts. In total there were 26 IFNG-induced transcripts that were shared in these two inflammatory states, and not surprisingly many of these transcripts included: the chemokine ligands for CXCR3 which is found on T cells, *Cxcl9* and *Cxcl10* (82); and the immunoproteasome subunits (*Psmb8* and *Psmb9*) and tapasin (*Tapbp*), which have a roles in antigen processing and presentation (83,84). Other shared transcripts included a number of IFNG-inducible GTPases, including *Tgtp* and *Iigp1*. Both of these molecules appear to play a direct role in the defense against the intracellular parasitic protozoa *Toxoplasma gondii* defense by rupturing intracellular vacuoles containing the protozoa (85,86). However, *Tgtp* and *Iigp* were still significantly expressed in the rejecting mouse kidneys and oxazolone-challenged skin. Thus, the effects of IFNG are broad, regardless of the inflammatory stimuli.

5.2.4 Alternative macrophage activation. Features of AMA that were revealed by the microarray analysis of the oxazolone-challenged skin and TCMR of renal allografts, included expression of: the chitinase like protein *Chi3l3*; the C-type lectin and beta-glucan pattern recognition receptor *Clec7a* (Dectin-1); and, *Thbs1* and *Adam8*, both of which play numerous roles in tissue (basement membrane) remodeling and are capable of releasing cytokines from their inactive form, such as TGF-beta and TNF-alpha (87,88).

The signature markers of AMA include IL-4/13 induced expression of *Chi3l3*, *Arg1* and *Mrc1* (89). While our microarray analysis only indicated a significant increase of *Chi3l3* transcript expression; *Mrc1* was not present because there is no probeset for *Mrc1* (*Cd206*) on the NimbleGen MMP_EXP_HX12 12x135K Arrays, and *Arg1* did not meet the statistical cut off (FDR<0.05) of the arrays. However, we were able to verify increased transcript expression of *Mrc1* in the oxazolone-challenged skin by real time RT-PCR. Furthermore, by immunohistochemical stains for MRC1, we verified increased protein expression of MRC1 within the oxazolone-challenge skin over sham-treated controls. This parallels our observed increase of $CD68^+$ macrophages, and our previous report of increased $MRC1^+$ cells within TCMR of mouse renal allografts (46). Real time RT-PCR analysis of *Arg1* expression indicated that there was no change in expression within the oxazolone-challenged skin; thus verifying the microarray results. In agreement with the above findings, the summarized burden of AMA depicted by the AMA-associated transcript set score was increased in the oxazolone-challenged skin compared to sham-treated controls; but the finding was not statistically significant.

It should be noted that in rejecting mouse allografts expression of *Arg1* (as detected by real time RT-PCR) is not significantly increased until after day 21 post-transplantation (46). Therefore, visualization of the complete AMA phenotype may be a feature of perpetual inflammation or injury; consequently we would not have seen a strong AMA presence in the skin only 6 days after the first sensitization, or 24 hours post-challenged. Indeed, hairless mice receiving repeated hapten treatments (up to 10) develop severe epidermal hyperplasia which has been associated with clinical chronic

atopic dermatitis in humans; a disease that has been associated with a Th2- and AMA-type dermal infiltrate (72,90).

5.2.5 Macrophage marker promiscuity. We have assumed that the macrophage- and AMA-associated transcripts are expressed in macrophages that have infiltrated the rejecting renal allografts and oxazolone-challenged skin. However, it is well known that other cell types express many of these markers, as they are shared between cells of the myeloid lineage which include macrophages and dendritic cells. Both CD68 and MRC1 can be found on subsets of Langerin$^-$ (CD207$^-$) epidermal-dendritic-like cells that are DC-SIGN$^+$ (CD209$^+$) (91). Moreover, this provides a hypothesis driven explanation of why the number of MRC1$^+$ cells in our oxazolone-challenged skin almost equaled the number of CD68$^+$ cells. Thus, some of the MRC1$^+$ cells in inflamed skin may have been epidermal-dendritic cells.

Nevertheless, the collective presence of the macrophage- and AMA-associated transcripts, along with the many IFNG-induced transcripts involved in antigen processing and presentation implies that TCMR and DTH involve myeloid cells which are involved in mediating the local adaptive, inflammatory response, and remodelling the injured tissue.

5.2.6 Conclusion. We summarized the burden of our inflammatory transcript sets within the oxazolone-challenged skin and rejecting renal allografts with TCMR by calculating the transcript set score, and comparing that score to their respective controls (sham-treated skin or normal kidneys). There were significant gains in the cytotoxic T cell-associated, IFNG-induced, and macrophage-associated transcript set scores in both the oxazolone-challenged skin and renal allografts with TCMR. As previously mentioned, there was also a nominal increase in the AMA-associated transcript set score within the oxazolone-challenged skin. This is in addition to increases in *Il4*, *Mrc1* and *Chi3l3* transcript expression, select markers of AMA, assessed by PCR. Our microarray data of oxazolone-induced CHS and TCMR of mouse renal allografts has revealed that changes

in transcript expression are stereotyped and therefore predictable, in a T cell-mediated inflammatory compartment.

5.3 THE ACTIVE INJURY-REPAIR RESPONSE REFLECTS A LARGE-SCALE ANTI-PARALLEL SHIFT IN THE EXPRESSION OF TRANSCRIPTS

While it could be expected that the molecules representing the inflammatory phenotype are widely shared in different diseases, we found that the molecules involved in injury and repair processes are more organ or tissue specific. Our original (kidney-selective) IRITs, which represented the injury-repair response's increased transcript expression (injury-up); and our KTs, which represented decreased (injury-down) parenchymal and stromal function were derived in mouse renal isografts (13,14). Moreover, these transcript sets were also validated to accurately assess the injury-repair response in human renal allografts after finding their human orthologs (6,7). However, neither of these transcript sets, the IRITs or KTs, could qualitatively assess the injury-repair response in oxazolone-challenged mouse skin. Consequently, using similar algorithms as we did in the kidney, we derived two transcript sets to assess the active injury-repair response in mouse skin: the skin-selective IRITs (injury-up); and the STs (injury-down). In suit with their independent derivations and tissue specificity, these transcript sets had very little overlap with the kidney-selective IRITs and KTs. Nevertheless, in both inflamed skin and kidney, the skin- and kidney-selective IRITs, and STs and KTs, were associated with a similar injury-repair response pattern: tissue remodelling, promotion of secondary inflammation and dedifferentiation (re-expression of transcripts related to embryonic development and loss of function.

5.3.1 Injury-up: the injury- and repair-induced transcripts (IRITs). Despite the relatively small number of transcripts that overlapped between our skin- and kidney-

selective IRITs, these transcript sets shared some common functionalities. GO analysis indicated both transcript sets were enriched in: response to stress related categories, including response to wounding and wound healing (examples include TLRs, TGF-beta, and epithelial derived *Cxcl5*); and, extracellular matrix remodelling, including matrix catabolism (examples include matrix metalloproteinase, and a disintegrin and metalloproteinase families) and synthesis of matrix components (examples include collagens, laminins, tanascin and versican).

Our laboratory also published that kidney-selective IRITs within isografts and allografts were overrepresented with transcripts involved in mesenchymal and embryonic kidney development (13); this suggested a de-differentiation event as the kidney tissue went through the repair processes. Interestingly, the skin- IRITs also contained a set of transcripts belonging to small proline-rich region (*Sprr*) proteins that were overrepresented in the GO epithelial development annotation. Although very little is known about SPRR functions, high *Sprr* transcript (and protein) expression is associated with developing ectoderm derived tissues and epithelial-mesenchymal transition (75,92).

In accordance with the above results, the transcript set scores for the skin- and kidney-selective IRITs indicated an overall increase in the injury-up in both the oxazolone-challenged skin and TCMR of renal allografts, respectively. Therefore, despite the moderate differential transcript representation, the presence of skin- and kidney-selective IRITs indicates a convergence of injury-repair response functional processes in these two tissues.

5.3.2 Injury-down: skin- and kidney-associated transcripts (STs and KTs). Akin to the skin- and kidney-selective IRITs, the STs and KTs had a relatively little overlapping transcripts; and as expected, GO analysis of these transcripts sets revealed their distinct, tissue-selective, molecular biology. The KTs were overrepresented with numerous transporter activities that were enriched with solute carrier (*Slc*) transcripts including *Slc5a1* and *Slc5a2*, which code for renal sodium-glucose cotransporters (93).

Conversely, the STs were overrepresented with filament synthesis, largely involving the keratin (*Krt*) keratin-associated (*Krtap*) proteins. Keratins are intermediate filaments, produced by keratinocytes in the epithelium, and help form an epithelial extracellular matrix (49). Notwithstanding these differences, both KTs and STs were enriched with many metabolic pathway annotations, such as fatty acid beta-oxidation, amino acid catabolic process, and hexose metabolic process. In suit of these observations, the ST and KT transcript set scores decreased in the oxazolone-challenged skin and TCMR of renal allografts, respectively. Hence, the loss of STs and KTs represent a large-scale epithelial response encompassing the loss of parenchymal and stromal function.

However, unlike TCMR, we observed extensive epithelial necrosis in our oxazolone-challenged skin; thus, this could have contributed to the loss of STs. Nevertheless, the enrichment of metabolic pathway annotations and the re-emergence of IRIT developmental transcripts, in both renal allografts with TCMR and oxazolone-challenged skin, suggest a decrease in ST expression is not purely the result of lost nuclei. Repeating these experiments and applying a repeated hapten-challenge protocol (as mentioned above) may result in epidermal hyperplasia (72), instead of necrosis.

5.4 CONCLUSIONS PART 1: MOLECULAR CHANGES ARE STEREOTYPED

Here we have shown that T cell-mediated inflammation induced from antigenic-challenge via the purportedly creation of hapten adducts, or through the reaction with alloantigen such as MHC, induces large-scale molecular changes. Gene expression microarrays revealed stereotyped biological processes involved in inflammation (T cell and general macrophage infiltration, AMA, and IFNG-effects), and active injury-repair response. We reason that the loss of function and dedifferentiation of the local parenchyma and stroma is the molecular equivalent of *functio laesa*; a necessary

response of the tissue while it mounts efforts towards repairing basement membranes and extracellular matrices.

5.5 STUDY SUMMARY PART 2: IFNG-DEPENDENT CHANGES

The second aim of this study was to analyze experimentally induced CHS within GRKO (*Ifngr1* deficient) mice. Our laboratory previously showed that IFNG plays a critical role in the stabilization of mouse renal allografts (41). When IFNG is unable to act on the donor renal allograft, either because of *Ifng* deficient hosts or *Ifngr1* deficient allografts, the grafts fail by day 5-7 post-transplant due to massive necrosis and collapse of the microcirculation (41). Gene expression microarray analysis of these allografts revealed increased expression of IFNG-suppressed transcripts enriched with AMA-associated transcripts and kidney-selective IRITs. In other words, during the normal (wild type) course of rejection IFNG directly suppresses the expression of transcripts that are IRIT or AMA annotated; or alternatively, IFNG stabilized the graft, ultimately preventing necrosis and subsequent increased injury-repair response from the adjacent viable cells. It is difficult to explain the increased AMA phenotype however; because AMA is still a feature of allografts lacking MHC class I (*Tap* or *B2m* deficient), but have functional IFNG-signalling (41).

Since the first part of our study indicated that oxazolone-challenged (wild type) mouse skin underwent similar molecular changes as wild type mouse renal allografts; we hypothesized that oxazolone-challenged GRKO skin would exhibit similar histological and molecular changes as previously reported in our GRKO renal allografts. While we found an analogous increase of IFNG-suppressed transcripts enriched with skin-selective IRITs, there was little enrichment of AMA-associated transcripts within the oxazolone-challenged GRKO skin compared to oxazolone-challenged B6 skin. However, the canonical AMA markers, *Arg1* and *Chi3l3*, were both increased in the oxazolone-

challenged GRKO skin, as assessed by real time RT-PCR. Thus, a robust increase of AMA in inflamed skin may be dampened by a high basal presence of AMA and myeloid cells in normal skin (described below), compared to a lower presence in kidneys.

5.5.1 IFNG-effects within GRKO skin. Real time RT-PCR analysis of the oxazolone-challenged GRKO skin revealed that, as expected, expression of the IFNG-inducible transcripts, *Cxcl9*, *Aif1* and *Ubd* was significantly reduced in the oxazolone-challenged GRKO skin compared to the oxazolone-challenged B6 skin. By the same comparison, these findings were mirrored by the microarrays: all IFNG-induced transcripts were decreased in the oxazolone-challenged GRKO skin compared to the oxazolone-challenged B6 skin. Interestingly, real time RT-PCR assayed expression of *Ifng* revealed slightly lower expression levels within the oxazolone-challenged GRKO skin than the oxazolone-challenged B6 skin; this is indicative of IFNG autoinduction. As previously reported, *Ifng* autoinduction has been implicated in mouse kidneys resulting from systemic effects of local T cell-mediated inflammation (69), and in *in vitro* experiments within PBMCs and T cell depleted PBMCs (94). The reduced levels of *Cxcl9*, Aif1 and *Ubd* within the sham-treated GRKO skin points towards basal effects of IFNG in uninflamed tissue. Similar basal effects have been reported in GKO (*Ifng* deficient) mice, which have reduced MHC class I expression within GKO kidneys compared to wild type (95).

5.5.2 GRKO kidney derived IFNG-suppressed transcripts are enriched with IRITs in GRKO skin. The IFNG-suppressed transcripts, which were derived from a series of GKO and GRKO renal allografts (48), were also found within the oxazolone-challenged GRKO skin: individual IFNG-suppressed transcripts and the summarized transcript set score were both increased in oxazolone-challenged GRKO skin over the oxazolone-challenged B6 skin. Moreover, over a third of the IFNG-suppressed transcripts differentially expressed in the oxazolone-challenged GRKO skin were annotated as skin-selective

IRITs; denoting the oxazolone-challenged GRKO skin was undergoing a greater active injury-repair response. Indeed, there were many individual skin-selective IRITs that were increased within the oxazolone-challenged GRKO skin compared to the oxazolone-challenged B6 skin. By the same comparison, the skin-selective IRIT set score was also increased in the GRKO skin. Literature review of the other non-IRIT IFNG-suppressed transcripts revealed these transcripts are largely involved in the acute-phase response and tissue remodelling. Contrasting with the increased presence of IRITs, the STs were reduced in the oxazolone-challenged GRKO skin. Despite these observations that imply a greater injury-repair response in the oxazolone-challenged skin, there was no histological evidence of increased injury. Another group has looked at CHS in GKO mice using the haptens, picryl chloride and fluorescein isothiocyanate (FITC) (96). While they found that an increase in ear thickness (swelling) zero to 24 hours post-FITC-challenge in GKO skin did not differ from FITC-challenged B6 skin; ear thickness increased significantly in picryl chloride-challenged skin over challenged B6 skin, zero to four hours post-challenge, but increased thickness was equivalent by 24 hours post-challenge (96). Therefore, the efficacy for haptens to covalently bind to proteins could vary; and/or different haptens might induce various MHC-restricted hapten-determinants that result in varied TCR binding affinity.

Our laboratory's previous analyses of rejecting GRKO renal allografts revealed a strong AMA phenotype and injury-repair response along with severe necrosis of the GRKO graft (41,48). However, unlike the injury-repair response, AMA was not dependent on the necrosis; as AMA was still present in GRKO allografts into *Prf1* and *Gzma*/*b* deficient hosts, where rejection progresses similar to wild type allografts (41). That is, these allografts develop interstitial infiltrate and tubulitis, not severe necrosis. Thus, the lack of increased AMA within the oxazolone-challenged GRKO skin was unexpected and puzzling. Markers associated with AMA may be such a robust feature of the skin microenvironment, that deficient IFNG-signaling is unable to grossly affect expression of AMA-associated markers. As described above, MRC1 (*Cd206*) and Dectin-1 (*Clec7a*)

can also be found on epidermal dendritic cells (91). There is also evidence that Langerhans ($CD207^+$) cells may exhibit features of AMA (97). However, a more preferred explanation is that AMA may be a more robust feature of repeated oxazolone challenges; similar to the inflammatory compartment of an allograft, where antigen is constitutively presently. Thus the level of immunogenic-challenge or injury was not great enough in our model to induce a strong AMA phenotype.

5.6 CONCLUSIONS PART 2: IFNG-DEPENDENT CHANGES IN CHS

Here we described the IFNG-dependent changes within CHS, a model of DTH. CHS in GRKO skin displayed stereotyped changes; decreased IFNG-effects with increased IFNG-suppressed transcripts. The IFNG-suppressed response was largely a representation of the skin-selective IRITs. Taking into consideration the results from the first study (CHS in wild type skin), we have shown that IFNG-dependent molecular changes are very robust, despite the disparate tissues and antigens, alloMHC versus haptenized self-proteins. In wild type inflamed skin and kidney allografts, IFNG-effects qualitatively manifest as antigen processing and presentation processes, and lymphocyte chemotaxis. Additionally, IFNG appears to ameliorate or stabilize the injury-repair response, as inflamed skin and kidneys with deficient IFNG-signalling manifest as increased expression of IFNG-suppressed transcripts, which are enriched with skin- or kidney-selective IRITs. Unlike rejecting renal allografts with IFNG-deficient signaling (host GKO or allograft GRKO), CHS in GRKO did not manifest robust features of AMA (assessed by microarrays) in addition to CHS in wild type skin. As described above, this is likely due: one, to the single sensitization and challenge with hapten, rather than the constitutive presence of antigen; and/or two, the different residential myeloid populations in normal skin and kidney.

5.7 ADDITIONAL CONCLUSIONS AND FUTURE DIRECTIONS

5.7.1 Real time RT-PCR and microarrays offer similar results. A previous report on the comparison of real time RT-PCR and microarray performance concluded that both platforms offer almost equivalent performance (98). Indeed, we observed similar results in our oxazolone experiments; changes in transcript expression *Cxcl9* were mirrored by both real time RT-PCR and microarrays. In both wild type and GRKO CHS studies, significant changes in *Ubd* transcript expression were only detected by real time RT-PCR, as it did not meet the FDR cut-off (FDR<0.05) within the microarray analysis. Real time RT-PCR is relatively more sensitive than microarrays, as real time RT-PCR has been shown to have a lower limit of detection (98). Nevertheless, microarrays are an efficient way of measuring large-scale transcript changes. Microarrays can conceal select outliers of the transcript set herd-movement: one, where a single probeset becomes a false negative, as was our case with *Ubd*; or two, where even real time RT-PCR fails to detect transcripts due to a poorly functioning primer/probe or an outlier in the sample population, such as a patient biopsy (98).

5.7.2 Versatility of pathogenesis based transcript sets (PBTs). Our transcript sets that assess the inflammatory burden such as T cells, macrophages, IFNG-effects and IFNG-suppressed-effects are not restricted to assessing inflammation within the one tissue compartment they were derived from. Here we have shown these transcript sets can qualitatively assess inflammation in a CHS reaction; in addition, many of these transcript sets can quantitatively assess allograft rejection of human renal allografts (9). Contrary to the versatility of our inflammatory PBTs, individual members of the IRITs and tissue-associated transcripts (STs and KTs) are more tissue- or organ-selective. For example, the kidney is enriched with solute carriers for ion transport, and the skin is enriched with keratins that constitute a barrier function against pathogens, toxins and

moisture loss. Nevertheless, these individual transcripts enrich overlapping functional annotations: upon injurious insult, tissues lose their primary function and dedifferentiate (*functio laesa*), enabling the damaged tissue to engage in concerted mechanisms that prevent further damage and infection, while undergoing injury-repair. Thus, even tissue-selective transcripts manifest a herd-movement through the sharing of common biological processes.

Above, we demonstrated the applicability of our PBTs to assess the active biological processes present in a CHS reaction at a single time point. In addition, our laboratory previously demonstrated that PBTs can robustly quantify TCMR and ABMR of renal allografts (6,7), as well as cardiac allografts (99), and ulcerative colitis (unpublished data), in human patients. With the development of our skin-selective injury-repair transcript sets, it would be pragmatic to apply our PBTs to human cutaneous diseases such as psoriasis, atopic eczema and allergic contact dermatitis; diseases that we understand very little of. These inflammatory diseases are prevalent and they grossly influence the quality of life of those affected; therefore, they also have economic implications (100,101).Revealing and quantifying the coordinated, large-scale biological processes (the herd-movement) involved in cutaneous diseases will undoubtedly lead to more precise diagnoses and therefore, improved treatment regimens.

REFERENCES

(1) Spencer WG. Celsus, De Medicina. [Volume I, Books 1-4]. 1935. Cambridge, Mass. and London, The Loeb Classical Library. On Medicine.

(2) Macartney J. A treatise of inflammation. British Library, Historical Print Editions; 2011.

(3) Subramanian A, Tamayo P, Mootha VK, Mukherjee S, Ebert BL, Gillette MA, et al. Gene set enrichment analysis: a knowledge-based approach for interpreting genome-wide expression profiles. Proc Natl Acad Sci U S A 2005;102(43):15545-50.

(4) Chang HY, Nuyten DS, Sneddon JB, Hastie T, Tibshirani R, Sorlie T, et al. Robustness, scalability, and integration of a wound-response gene expression signature in predicting breast cancer survival. Proc Natl Acad Sci U S A 2005;102(10):3738-43.

(5) Mueller TF, Einecke G, Reeve J, Sis B, Mengel M, Jhangri.G., et al. Microarray analysis of rejection in human kidney transplants using pathogenesis-based transcript sets. Am J Transplant 2007;7(12):2712-22.

(6) Halloran PF, de Freitas DG, Einecke G, Famulski KS, Hidalgo LG, Mengel M, et al. The molecular phenotype of kidney transplants. Am J Transplant 2010;10(10):2215-22.

(7) Halloran PF, de Freitas DG, Einecke G, Famulski KS, Hidalgo LG, Mengel M, et al. An integrated view of molecular changes, histopathology, and outcomes in kidney transplants. Am J Transplant 2010;10(10):2223-30.

(8) Halloran PF. T Cell Mediated Rejection of Kidney Transplants: A Personal Viewpoint. Am J Transplant 2010;10(5):1126-34.

(9) Famulski KS, Einecke G, Sis B, Mengel M, Hidalgo LG, Kaplan B, et al. Defining the Canonical Form of T-Cell-Mediated Rejection in Human Kidney Transplants. Am J Transplant 2010;10(4):810-20.

(10) Sis B, Jhangri G, Bunnag S, Allanach K, Kaplan B, Halloran PF. Endothelial gene expression in kidney transplants with alloantibody indicates antibody-mediated damage despite lack of C4d staining. Am J Transplant 2009;9(10):2312-23.

(11) Hidalgo LG, Sis B, Sellares J, Campbell PM, Mengel M, Einecke G, et al. NK cell transcripts and NK cells in kidney biopsies from patients with donor-specific antibodies: evidence for NK cell involvement in antibody-mediated rejection. Am J Transplant 2010;10(8):1812-22.

(12) Reeve J, Einecke G, Mengel M, Sis B, Kayser N, Kaplan B, et al. Diagnosing rejection in renal transplants: a comparison of molecular- and histopathology-based approaches. Am J Transplant 2009;9(8):1802-10.

(13) Famulski KS, Broderick G, Hay K, Cruz J, Sis B, Mengel M, et al. Transcriptome analysis reveals heterogeneity in the injury response of kidney transplants. Am J Transplant 2007;7(11):2483-95.

(14) Einecke G, Broderick G, Sis B, Halloran PF. Early loss of renal transcripts in kidney allografts: relationship to the development of histologic lesions and alloimmune effector mechanisms. Am J Transplant 2007;7(5):1121-30.

(15) Jabs WJ, Sedlmeyer A, Ramassar V, Hidalgo LG, Urmson J, Afrouzian M, et al. Heterogeneity in the evolution and mechanisms of the lesions of kidney allograft rejection in mice. Am J Transplant 2003;3(12):1501-9.

(16) Einecke G, Fairhead T, Hidalgo LG, Sis B, Turner P, Zhu LF, et al. Tubulitis and Epithelial Cell Alterations in Mouse Kidney Transplant Rejection Are Independent of CD103, Perforin or Granzymes A/B. Am J Transplant 2006;6(9):2109-20.

(17) Wynn JJ, Alexander CE. Increasing organ donation and transplantation: the U.S. experience over the past decade. Transplant Int 2011;24:324-32.

(18) Cozzi E, Seveso M, Hutabba S, Fabris S, Cavicchioli L, Ancona E. An update on Xenotransplantation. Veterinary Research Communications 2007;31:15-25.

(19) Fishman JA, Patience C. Xenotransplantation: infectious risk revisited. Am J Transplant 2004;4(9):1383-90.

(20) Chen GY, Nunez G. Sterile inflammation: sensing and reacting to damage. Nat Rev Immunol 2010;10:826-37.

(21) Medzhitov R, Horng T. Transcriptional control of the inflammatory response. Nat Rev Immunol 2009;9(10):692-703.

(22) Medzhitov R, Janeway CA, Jr. Innate immune recognition and control of adaptive immune responses. Semin Immunol 1998;10(5):351-3.

(23) Goes N, Urmson J, Ramassar V, Halloran PF. Ischemic acute tubular necrosis induces an extensive local cytokine response: evidence for induction of interferon-g, transforming growth factorb-1, granulocyte-macrophage colony-stimulating factor, interleukin-2 and interleukin-10. Transplant 1995;59:565-72.

(24) von Andrian UH, MacKay CR. T-cell function and migration. Two sides of the same coin. N Engl J Med 2000;343(14):1020-34.

(25) Halloran PF. Immunosuppressive drugs for kidney transplantation. N Engl J Med 2004;351(26):2715-29.

(26) Sallusto F, Lenig D, Forster R, Lipp M, Lanzavecchia A. Two subsets of memory T lymphocytes with distinct homing potentials and effector functions. Nature 1999;401(6754):708-12.

(27) Waiser J, Schreiber M, Budde K, Bohler T, Kraus W, Hauser I, et al. Prognostic value of the Banff classification. Transpl Int 2000;13 Suppl 1:S106-S111.

(28) Halloran PF, Urmson J, Ramassar V, Melk A, Zhu LF, Halloran BP, et al. Lesions of T-cell-mediated kidney allograft rejection in mice do not require perforin or granzymes A and B. Am J Transplant 2004;4(5):705-12.

(29) Hidalgo LG, Einecke G, Allanach K, Halloran PF. The transcriptome of human cytotoxic T cells: similarities and disparities among allostimulated CD4(+) CTL, CD8(+) CTL and NK cells. Am J Transplant 2008;8(3):627-36.

(30) Strehlau J, Pavlakis M, Lipman M, Maslinski W, Shapiro M, Strom TB. The intragraft gene activation of markers reflecting T-cell-activation and -cytotoxicity analyzed by quantitative RT-PCR in renal transplantation. Clin Nephrol 1996;46(1):30-3.

(31) Hidalgo LG, Einecke G, Allanach K, Mengel M, Sis B, Mueller TF, et al. The transcriptome of human cytotoxic T cells: measuring the burden of CTL-associated transcripts in human kidney transplants. Am J Transplant 2008;8(3):637-46.

(32) Du C, Jiang J, Guan Q, Yin Z, Masterson M, Parbtani A, et al. Renal tubular epithelial cell self-injury through Fas/Fas ligand interaction promotes renal allograft injury. Am J Transplant 2004;4(10):1583-94.

(33) Cerf-Bensussan N, Jarry A, Brousse N, Lisowska-Grospierre B, Guy-Grand D, Griscelli C. A monoclonal antibody (HML-1) defining a novel membrane molecule present on human intestinal lymphocytes. Eur J Immunol 1987;17(9):1279-85.

(34) Robertson H, Wong WK, Talbot D, Burt AD, Kirby JA. Tubulitis after renal transplantation: demonstration of an association between CD103+ T cells, transforming growth factor beta1 expression and rejection grade. Transplant 2001;71(2):306-13.

(35) Voskoboinik I, Dunstone MA, Baran K, Whisstock JC, Trapani JA. Perforin: structure, function, and role in human immunopathology. Immunol Rev 2010;235:35-54.

(36) Choy JC. Granzymes and perforin in solid organ transplant rejection. Cell Death Differ 2010;17:567-76.

(37) Strasser A, Jost PJ, Nagata S. The Many Roles of FAS Receptor Signaling in the Immune System. Immunity 2009;30(2):180-92.

(38) Kayser D, Einecke G, Famulski KS, Mengel M, Sis B, Zhu LF, et al. Donor Fas is not necessary for T-cell-mediated rejection of mouse kidney allografts. Am J Transplant 2008;8(10):2049-55.

(39) Lefrancois L, Parker CM, Olson S, Muller W, Wagner N, Puddington L. The role of beta 7 integrins in CD8 T cell trafficking during an antiviral immune response. J Exp Med 1999;189(10):1631-8.

(40) Jose MD, Ikezumi Y, van Rooijen N, Atkins RC, Chadban SJ. Macrophages act as effectors of tissue damage in acute renal allograft rejection. Transplant 2003;76(7):1015-22.

(41) Sis B, Famulski KS, Allanach K, Zhu L-F, Halloran PF. IFN-g prevents early perforin-granzyme-mediated destruction of kidney allografts by inducing donor class I products in the kidney. Am J Transplant 2007;7(10):2301-10.

(42) Yang J, Riella LV, Chock S, Liu T, Zhao X, Yuan X, et al. The novel costimulatory programmed death ligand 1/b7.1 pathway is functional in inhibiting alloimmune responses in vivo. Journal of Immunology 2011;187(3):1113-9.

(43) Sis B, Halloran PF. Endothelial transcripts uncover a previously unknown phenotype: C4d-negative antibody-mediated rejection. Curr Opin Organ Transplant 2010;15(1):42-8.

(44) Mauiyyedi S, Pelle PD, Saidman S, Collins AB, Pascual M, Tolkoff-Rubin NE, et al. Chronic humoral rejection: identification of antibody-mediated chronic renal allograft rejection by C4d deposits in peritubular capillaries. J Am Soc Nephrol 2001;12(3):574-82.

(45) Colvin RB, Smith RN. Antibody-mediated organ-allograft rejection. Nat Rev Immunol 2005;5(10):807-17.

(46) Famulski KS, Kayser D, Einecke G, Allanach K, Badr D, Venner J, et al. Alternative macrophage activation-associated transcripts in T-cell-mediated rejection of mouse kidney allografts. Am J Transplant 2010;10(3):490-7.

(47) Famulski KS, Einecke G, Reeve J, Ramassar V, Allanach K, Mueller T, et al. Changes in the transcriptome in allograft rejection: IFN-g induced transcripts in mouse kidney allografts. Am J Transplant 2006;6(6):1342-54.

(48) Famulski KS, Sis B, Billesberger L, Halloran PF. Interferon-gamma and donor MHC class I control alternative macrophage activation and activin expression in rejecting kidney allografts: a shift in the Th1-Th2 paradigm. Am J Transplant 2008;8(3):547-56.

(49) Nestle FO, Meglio PD, Qin J, Nickoloff BJ. Skin immune sentinels in health and disease. Nat Rev Immunol 2009;9:679-91.

(50) Gordon S. Alternative activation of macrophages. Nat Rev Immunol 2003;3(1):23-35.

(51) Gocinski BL, Tigelaar RE. Roles of CD4+ and CD8+ T cells in murine contact sensitivity revealed by in vivo monoclonal antibody depletion. Journal of Immunology 1990;144(11):4121-8.

(52) Wang B, Fujisawa H, Zhuang L, Freed I, Howell BG, Shahid S, et al. CD4+ Th1 and CD8+ type 1 cytotoxic T cells both play a crucial role in the full development of contact hypersensitivity. Journal of Immunology 2000;165:6783-90.

(53) Taube M, Carlsten H. Cutaneous delayed type hypersensitivity in SCID mice adoptively transferred with lymphocytes is B cell independent and H-2 restricted. Scand J Immunol 1997;45(5):515-20.

(54) Grabbe S, Schwarz T. Immunoregulatory mechanisms involved in elicitation of allergic contact hypersensitivity. Immunol Today 1998;19(1):37-44.

(55) Koch R. Die aetiologie der tuberculose. Berl Klin Wsch 1882;19:221-30.

(56) Weltzien HU, Moulon C, Martin S, Padovan E, Harmann U, Kohler J. T cell immune responses to haptens. Structural models for allergic and autoimmune reactions. Toxicology 1996;107:141-51.

(57) Black CA. Delayed Type Hypersensitivity: Current Theories with an Historic Perspective. Dermatol Online J 1999;5(1):7.

(58) Martin SF, Dudda JC, Delattre V, Bachtanian E, Leicht C, Burger B, et al. Fas-mediated inhibition of CD4+ T cell priming results in dominance of type 1 CD8+ T cells in the immune response to the contact sensitizer trinitrophenyl. Journal of Immunology 2004;173(5):3178-85.

(59) Itano AA, McSorley SJ, Reinhardt RL, Ehst BD, Ingulli E, Rudensky AY, et al. Distinct dendritic cell populations sequentially present antigen to CD4 T cells and stimulate different aspects of cell-mediated immunity. Immunity 2003;19(1):47-57.

(60) Merad M, Ginhoux F, Collin M. Origin, homeostasis and function of Langerhans cells and other langerinexpressing dendritic cells. Nat Rev Immunol 2008;8:935-47.

(61) Kimber I, Cumberbatch M. Stimulation of Langerhans cell migration by tumor necrosis factor alpha (TNF-alpha). J Invest Dermatol 1992;99:48S-50S.

(62) McLachlan JB, Catron DM, Moon JJ, Jenkins MK. Dendritic cell antigen presentation drives simultaneous cytokine production by effector and regulatory T cells in inflamed skin. Immunity 2008;30(2):277-88.

(63) Girardi M. Immunosurveillance and Immunoregulation by gammdelta T Cells. J Invest Dermatol 2006;126(1):25-31.

(64) Conrad C, Boyman O, Tonel G, Tun-Kyi A, Laggner U, de Fougerolles A, et al. a1b1 integrin is crucial for accumulation of epidermal T cells and the development of psoriasis. Nature Medicine 2011;13(7):836-42.

(65) Eardley KS, Zehnder D, Quinkler M, Lepenies J, Bates RL, Savage CO, et al. The relationship between albuminuria, MCP-1/CCL2, and interstitial macrophages in chronic kidney disease. Kidney Int 2006;69(7):1189-97.

(66) Girlanda R, Kleiner DE, Duan Z, Ford EAS, Wright EC, Mannon RB, et al. Monocyte infiltration and kidney allograft dysfunction during acute rejection. Am J Transplant 2008;8(3):600-7.

(67) Yawalkar N, Nunger RE, Buri C, Schmid S, Egli F, Brand CU, et al. A comparative study of the expression of cytotoxic proteins in allergic contact dermatitis and psoriasis: spongiotic skin lesions in allergic contact dermatitis are highly infiltrated by T cells expressing perforin and granzyme B. Am J Pathol 2001;158(3):803-8.

(68) Gaspari A, Katz SI. Contact Hypersensitivity. Current Protocols in Immunology 1991;1:4.2.1-4.2.5.

(69) Halloran PF, Autenried P, Ramassar V, Urmson J, Cockfield S. Local T cell responses induce widespread MHC expression. Evidence that IFN-g induces its own expression in remote sites. Journal of Immunology 1992;148:3837-46.

(70) Billingham RE, Medawar PB. The technique of free skin grafting in mammals. J Exp Med 1951;28(3):385-402.

(71) Sis B, Mengel M, Haas M, Colvin RB, Halloran PF, Racusen L, et al. Banff '09 Meeting Report: Antibody Mediated Graft Deterioration and Implementation of Banff Working Groups. Am J Transplant 2010;10(3):464-71.

(72) Man M-Q, Hatano Y, Lee SH, Man M, Chang S, Feingold KR, et al. Characterization of a hapten-induced, murine model with multiple features of atopic dermatitis: structural, immunologic, and biochemical changes following single versus multiple oxazolone challenges. J Invest Dermatol 2008;128:79-86.

(73) Jeong JK, Kim HR, Hwang SM, Park JW, Lee BJ. Region- and neuronal phenotype-specific expression of NELL2 in the adult brain. Mol Cell 2008;26(2):186-92.

(74) Kamsteeg M, Bergers M, de Boer R, Zeeuwen PL, Hato SV, Schalkwijk J, et al. Type 2 helper T-cell cytokines induce morphologic and molecular characteristics of atopic dermatitis in human skin equivalent. Am J Pathol 2011;178(5):2091-9.

(75) Demetris A, Specht S, Nozaki I, Lunz JG, Stolz DB, Murase N, et al. Small proline-rich proteins (SPRR) function as SH3 domain ligands, increase resistance to injury and are associated with epithelial–mesenchymal transition (EMT) in cholangiocytes. J Hepatol 2008;48:276-88.

(76) Kim CH, Kunkel EJ, Boisvert J, Johnston B, Campbell JJ, Genovese MC, et al. Bonzo/CXCR6 expression defines type 1-polarized T-cell subsets with extralymphoid tissue homing potential. J Clin Invest 2001;107(5):595-601.

(77) Can I, Tahara-Hanaoka S, Hitomi K, Nakano T, Nakahashi-Oda C, Kurita N, et al. Caspase-independent cell death by CD300LF (MAIR-V), an inhibitory immunoglobulin-like receptor on myeloid cells. Journal of Immunology 2008;180(1):207-13.

(78) Ma G, Pan P, Eisenstein S, Divino CM, Lowell CA, Takai T. Paired Immunoglobin-like Receptor-B Regulates the Suppressive Function and Fate of Myeloid-Derived Suppressor Cells. Immunity 2011;34(3):385-95.

(79) Kawai T, Akira S. Toll-like receptors and their crosstalk with other innate receptors in infection and immunity. Immunity 2011;34(5):637-50.

(80) Sa Q, Hoover-Plow JL. EMILIN2 (Elastin microfibril interface located protein), potential modifier of thrombosis. Thromb J 2011;11(9):1-8.

(81) Einecke G, Mengel M, Hidalgo LG, Allanach K, Famulski KS, Halloran PF. The early course of renal allograft rejection: Defining the time when rejection begins. Am J Transplant 2009;9(3):483-93.

(82) Qin S, Rottman JB, Myers P, Kassam N, Weinblatt M, Loetscher M, et al. The chemokine receptors CXCR3 and CCR5 mark subsets of T cells associated with certain inflammatory reactions. J Clin Invest 1998;101(4):746-54.

(83) Driscoll J, Brown MG, Finley D, Monaco JJ. MHC-linked LMP gene products specifically alter peptidase activities of the proteasome. Nature 1993;365:262-4.

(84) Van Kaer L, Ashton-Rickardt PG, Ploegh HL, Tonegawa S. TAP1 mutant mice are deficient in antigen presentation, surface class I molecules, and CD4-8+ T cells. Cell 1992;71:1205-14.

(85) Zhao Y, Ferguson DJ, Wilson DC, Howard JC, Sibley LD, Yap GS. Virulent Toxoplasma gondii evade immunity-related GTPase-mediated parasite vacuole disruption within primed macrophages. Journal of Immunology 2009;182(6):3775-81.

(86) Pawlowski N, Khaminets A, Hunn JP, Papic N, Schmidt A, Uthaiah RC, et al. The activation mechanism of Irga6, an interferoninducible GTPase contributing to mouse resistance against Toxoplasma gondii. BMC Biology 2011;9(7):1-15.

(87) Lee HS, Song CY. Differential role of mesangial cells and podocytes in TGF-beta-induced mesangial matrix synthesis in chronic glomerular disease. Histol Histopathol 2009;24(7):901-8.

(88) Yamamoto S, Yasunori H, Yoshiyama K, Shimizu E, Kataoka M, Hijiya N, et al. ADAM family proteins in the immune system. Immunol Today 2011;20(6):278-84.

(89) Gordon S, Martinez FO. Alternative Activation of Macrophages: Mechanism and Functions. Immunity 2007;32:593-604.

(90) Jin J, He R, Oyoshi M, Geha RS. Animal Models of Atopic Dermatitis. J Invest Dermatol 2009;129:31-40.

(91) Ochoa MT, Loncaric A, Krutzik SR, Becker TC, Modlin RL. "Dermal dendritic cells" comprise two distinct populations: CD1+ dendritic cells and CD209+ macrophages. J Invest Dermatol 2008;128(9):2225-31.

(92) Kalluri R, Neilson EG. Epithelial-mesenchymal transition and its implications for fibrosis. J Clin Invest 2003;112(12):1776-84.

(93) Wright EM. Renal Na+-glucose cotransporters. Am J Physiol Renal Physiol 2001;280:F10-F18.

(94) Hardy KJ, Sawada T. Human g interferon strongly upregulates its own gene expression in peripheral blood lymphocytes. J Exp Med 1989;170:1021-6.

(95) Goes N, Sims T, Urmson J, Vincent D, Ramassar V, Halloran PF. Disturbed MHC regulation in the interferon-g knockout mouse. Journal of Immunology 1995;155:4559-66.

(96) Mori T, Kabashima K, Yoshiki R, Sugita K, Shiraishi N, Onoue A, et al. Cutaneous hypersensitivities to hapten are controlled by IFN-gamma-

upregulated keratinocyte Th1 chemokines and IFN-gamma-downregulated langerhans cell Th2 chemokines. J Invest Derm 2008;128:1719-27.

(97) Dupasquier M, Stoitzner P, Wan H, Cerqueira D, Van Oudenaren A, Voerman JS, et al. The dermal microenvironment induces the expression of the alternative activation marker CD301/mMGL in mononuclear phagocytes, independent of IL-4/IL-13 signaling. J Leukoc Biol 2006;80(4):838-49.

(98) Allanach K, Mengel M, Einecke G, Sis B, Hidalgo LG, Mueller T, et al. Comparing microarray versus RT-PCR assessment of renal allograft biopsies: similar performance despite different dynamic ranges. Am J Transplant 2008;8(5):1006-15.

(99) Mengel M, Sis B, Kim D, Chang J, Famulski K, Hidalgo L, et al. The molecular phenotype of heart transplant biopsies: relationship to histopathological and clinical variables. Am J Transplant 2010;10(9):2105-15.

(100) Nestle FO, Kaplan D, Barker J. Mechanisms of disease: psoriasis. N Engl J Med 2009;361(15):496-509.

(101) Eyerich S, Onken AT, Weidinger S, Franke A, Nasorri F, Pennino D, et al. Mutual antagonism of T cells causing psoriasis and atopic eczema. N Engl J Med 2011;365(3):231-8.